Canadian Journal of Infectious Diseases and Medical Microbiology

# Climate and Vector Borne Pathogens: Challenges of the Present and of the Future

Lead Guest Editor: Dimosthenis Chochlakis
Guest Editors: Snezana Tomanovic and Emmanouil Angelakis

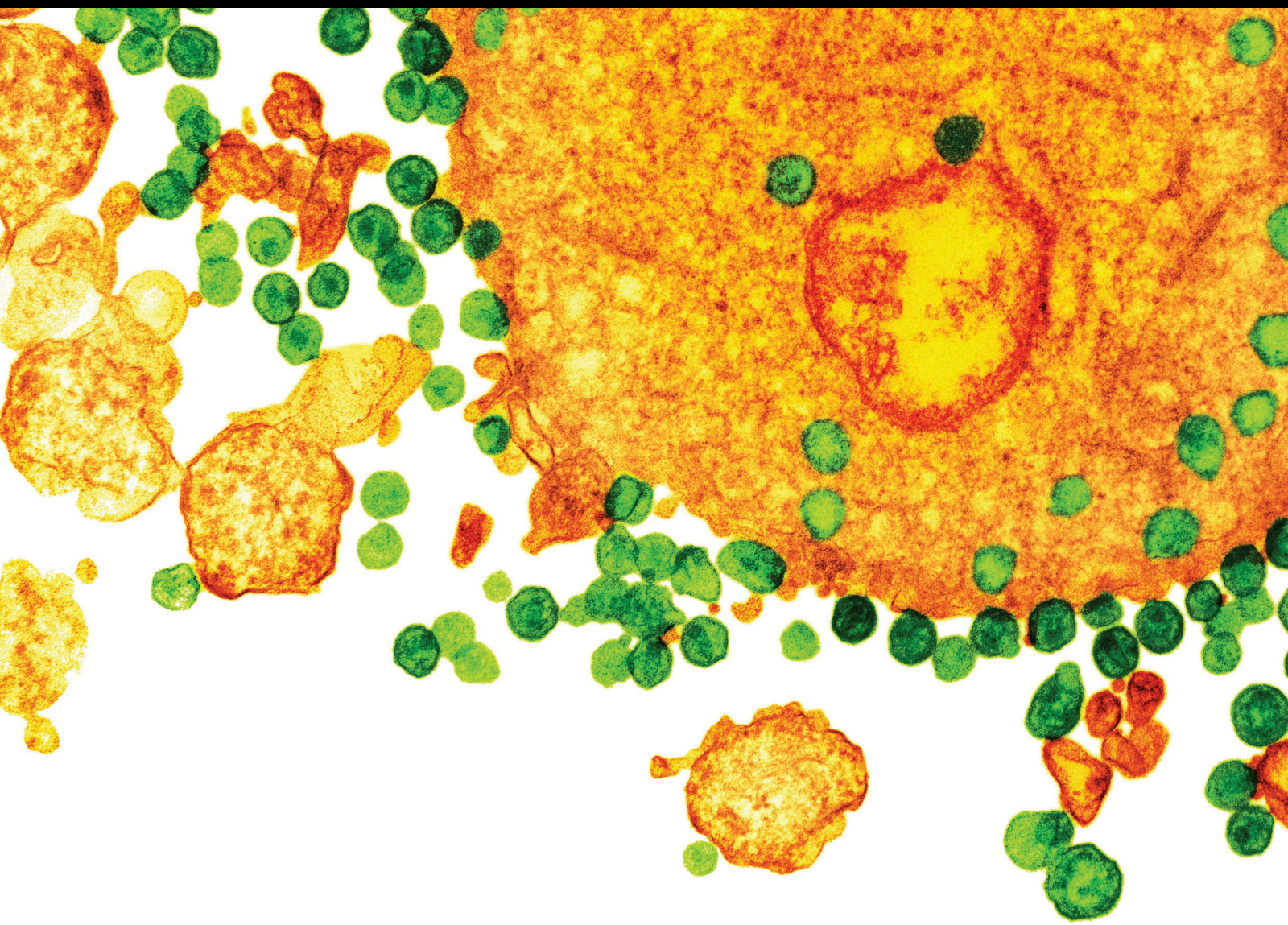

# Climate and Vector Borne Pathogens: Challenges of the Present and of the Future

Canadian Journal of Infectious Diseases and Medical Microbiology

# Climate and Vector Borne Pathogens: Challenges of the Present and of the Future

Lead Guest Editor: Dimosthenis Chochlakis
Guest Editors: Snezana Tomanovic and Emmanouil Angelakis

# Editorial Board

# Contents

Hindawi
Canadian Journal of Infectious Diseases and Medical Microbiology
Volume 2019, Article ID 4298716, 2 pages
https://doi.org/10.1155/2019/4298716

*Editorial*

# Climate and Vector Borne Pathogens: Challenges of the Present and of the Future

**Dimosthenis Chochlakis**,[1] **Snežana Tomanović**,[2] **and Emmanouil Angelakis**[3]

[1]*Laboratory of Clinical Microbiology and Microbial Pathogenesis, Unit of Zoonoses, School of Medicine, University of Crete, Heraklion, Greece*
[2]*Department for Medical Entomology, Institute for Medical Research, University of Belgrade, Belgrade, Serbia*
[3]*Aix-Marseille University, Institut de Recherche pour le Développement (IRD), Assistance Publique Hôpitaux de Marseille (APHM), Microbes, Evolution, Phylogénie et Infections, IHU (Institut Hospitalo-Universitaire)-Méditerranée Infection, Marseille, France*

Correspondence should be addressed to Dimosthenis Chochlakis; surreydimos@hotmail.com

Received 22 August 2019; Accepted 24 August 2019; Published 1 October 2019



It is thought that 75% of emerging diseases are related to zoonotic diseases; therefore, any change in the ecology that can affect wildlife can also affect human health [1]. The transmission of infectious diseases should be considered through an ecological context. As regards those which are indirectly spread through a vector (mosquito, tick, flea, etc.), they and their respective vectors depend, to a large extent, on local microclimates, the so-called climatic shell (temperature, rainfall, rising sea levels, wind, sunshine, etc.) [2]. Climate changes may affect the vector itself and its ability to come into contact with humans or may lead to a prolongation of the transmission period. Vectors can adapt to changes in climate by altering their geographical distribution or by undergoing an evolutionary "response" to external changes. Furthermore, human activity (migrations, vector control practices (deparasitization, spraying, etc.), deforestation, land use change, the development of intensive crops, water storage, and the expansion of cities in suburban areas) may also affect transmission.

To understand the linkage among multiple factors and predict, to a certain extent, the distribution of vector-borne pathogens, several models are currently used. Experimental models contain a multitude of meteorological data and have been developed to describe the "bioclimatic envelope" for various vector-borne pathogens. Moreover, there is an ever-growing dynamic of the combination of climatic models with the field study which uses spatial analysis methods with the ultimate goal of studying various meteorological and environmental factors. Data are retrieved either from land or remote sensors or from satellites (GIS) and used for the analysis of the complex pathways involved [3].

Further to the above-mentioned, mathematical models and neural networks are now used to understand various parameters/factors/events in several areas of everyday life such as economy, environment, behaviors, migration (of humans and of animals), diseases (infectious or not), etc [4]. The goal is to move from ex post recording of events to their ex ante view, by processing existing and past data in order to make, as much as possible, the forecasting of future events (whether long-term, either short-term) feasible [5]. In vector-borne diseases, the information gathered daily is enormous and the need to exploit it in order to study not only their current behavior (spreading, distribution to the population of humans and animals, etc.) but also their future development. To do so, the need to introduce different approaches such as climatic and mathematical models, classical statistics, and Artificial Neural Networks seems to be unavoidable.

The purpose of current special issue was to put one more stone in the understanding of the link between climate and vector-borne diseases, as well as, to the tools that should be used to achieve this goal. The issue contains collection of five papers covering different aspects that one way or another,

directly or indirectly cause a turn in the distribution of vector-borne diseases.

The paper "Application of kDNA Minicircle PCR-RFLP to Characterize *Leishmania donovani* Clinical Isolates Obtained from Post-Kala-Azar Dermal Leishmaniasis in Eastern Nepal" by O. Pokherel and coauthors focuses on molecular-epidemiology approach as a tool in revealing the transmission dynamics of visceral leishmaniasis (VL), vector-borne diseases transmitted by sandflies. Post-kala-azar dermal leishmaniasis (PKDL) is a skin manifestation of VL, and both forms of the disease are still considered as a major public health problem in South Asian countries such as Nepal. Using highly efficient molecular assays, the authors performed genotyping of VL and PKDL parasite isolates from Nepal. Both methods, with different resolution, showed separation of isolates in two groups. One group comprises isolates originating from hill districts and VL patients, while isolates clustered to the other group originate from low-land districts and both VL and PKDL patients. Based on these results, the authors propose the need for further study with large number of samples for systematic characterization of the clinical isolates to track the molecular-epidemiology of the *L. donovani* causing VL and the role of PKDL as a reservoir.

One of the emerging pathogens, widely distributed in aquatic environment, is *Shewanella algae*. Bacteremia is a major manifestation of *S. algae* infections, and there are increasing reports of antibiotic-resistant strains. However, little is known about the genomic characteristics of human bacteremic *S. algae*. In the paper "Genome Sequence of Colistin-Resistant Bacteremic *Shewanella algae* Carrying the Beta-Lactamase Gene $bla_{OXA-55}$," Y.-J. Chen and coauthors determined the whole genome sequence of a colistin-resistant *S. algae* strain isolated from blood. The authors proposed continuous surveillance for the emergence of *S. algae* and noted that the widespread environmental nature of the pathogen raises the concern for its role as a resistance reservoir.

Mosquitoes are the most important vectors of diseases on the global scale. The paper "Seasonal and Gender Differences in Presence of *Rickettsia felis* and Blood Meals Provide Additional Evidence of a Vector Role for Mosquitoes" by J. Zhang and coauthors indicates possible role of these vectors in transmission of rickettsial species vectored predominantly by fleas. While recent evidence has suggested mosquitoes could be infected with *R. felis*, there is little information about the exact role. For the purpose of this study, mosquitoes were collected monthly between 2013 and 2014 from the same residential dwelling at Yangzhou, China. Prevalence of *Rickettsia* and blood meal in mosquitoes were detected by PCR. Observed seasonal and gender differences of *R. felis* and blood-meal presence suggest the possible transstadial and transovarial transmission of the pathogen. The authors point to the need for further research of *R. felis* infection model within the full life cycle of mosquitoes to unambiguously prove the potential vector role of mosquitoes in transmission of this organism.

Moving on to the yellow fever virus, it has been responsible for thousands of deaths in the last decades. The article entitled "The Importance of Coordinated Actions in Preventing the Spread of Yellow Fever to Human Populations: The Experience from the 2016-2017 Yellow Fever Outbreak in the Northeastern Region of São Paulo State" by M. J. L. Siconelli and coauthors reports the features of the recent yellow fever (YF) outbreak in nonhuman primates (NHPs) in Brazil, the molecular characterization of a YF virus isolated during this period, and the importance of these findings to initiate coordinated measures among all public health services to prevent the occurrence of human cases. Yellow fever is a zoonotic arthropod-borne viral disease characterized by a sylvatic and urban cycle. The YF virus sylvatic cycle occurred in the peri-urban areas of the northeastern region of São Paulo state, but no human cases were reported during this period, showing that integrated actions between human, animal, and environmental health professionals were critical to restrain the virus to the sylvatic cycle.

We, as the guest editors, would like to thank all the authors of this special issue for contributing the high-quality papers. We would also like to thank the referees who have critically evaluated the papers and significantly influenced the quality standards of our special issue. Finally, we hope that the readers will find this special issue useful and informative.

## Conflicts of Interest

The guest editors declare that they have no conflicts of interest regarding the publication of this special issue.

*Dimosthenis Chochlakis*
*Snežana Tomanović*
*Emmanouil Angelakis*

## References

[1] L. Akil and H. A. Ahmad, "Salmonella infections modelling in Mississippi using neural network and geographical information system (GIS)," *BMJ Open*, vol. 6, no. 3, Article ID e009255, 2016.

[2] J. A. Patz, A. K. Githeko, J. P. McCarty, S. Hussein, U. Confalonieri, and N. de Wet, "Climate change and infectious diseases," in *Climate Change and Human Health, Chapter 6*, WHO, Geneva, Switzerland, 2003.

[3] D. A. Relman, M. A. Hamburg, E. R. Choffnes, and A. Mack, "Global climate change and extreme weather events: understanding the contributions to infectious disease emergence: workshop summary," Rapporteurs, Forum on Global Health, The National Academies Press, Washington, DC, USA, 2008.

[4] S. Haykin, *Neural Networks: A Comprehensive Foundation*, Macmillan College Publishing, New York, NY, USA, 2nd edition, 1998.

[5] B. D. Ripley, *Pattern Recognition and Neural Networks*, Cambridge University Press, Cambridge, UK, 1996.

Hindawi
Canadian Journal of Infectious Diseases and Medical Microbiology
Volume 2019, Article ID 9817930, 15 pages
https://doi.org/10.1155/2019/9817930

*Research Article*

# Effect of Rising Temperature on Lyme Disease: *Ixodes scapularis* Population Dynamics and *Borrelia burgdorferi* Transmission and Prevalence

**Dorothy Wallace, Vardayani Ratti, Anita Kodali, Jonathan M. Winter, Matthew P. Ayres, Jonathan W. Chipman, Carissa F. Aoki, Erich C. Osterberg, Clara Silvanic, Trevor F. Partridge, and Mariana J. Webb**

*Dartmouth College, Hanover, NH 03755, USA*

Correspondence should be addressed to Dorothy Wallace; dwallace@math.dartmouth.edu

Received 17 April 2019; Revised 11 June 2019; Accepted 7 July 2019; Published 16 September 2019

Guest Editor: Dimosthenis Chochlakis



Warmer temperatures are expected to increase the incidence of Lyme disease through enhanced tick maturation rates and a longer season of transmission. In addition, there could be an increased risk of disease export because of infected mobile hosts, usually birds. A temperature-driven seasonal model of *Borrelia burgdorferi* (Lyme disease) transmission among four host types is constructed as a system of nonlinear ordinary differential equations. The model is developed and parametrized based on a collection of lab and field studies. The model is shown to produce biologically reasonable results for both the tick vector (*Ixodes scapularis*) and the hosts when compared to a different set of studies. The model is used to predict the response of Lyme disease risk to a mean annual temperature increase, based on current temperature cycles in Hanover, NH. Many of the risk measures suggested by the literature are shown to change with increased mean annual temperature. The most straightforward measure of disease risk is the abundance of infected questing ticks, averaged over a year. Compared to this measure, which is difficult and resource-intensive to track in the field, all other risk measures considered underestimate the rise of risk with rise in mean annual temperature. The measure coming closest was "degree days above zero." Disease prevalence in ticks and hosts showed less increase with rising temperature. Single field measurements at the height of transmission season did not show much change at all with rising temperature.

## 1. Introduction

Lyme disease is the most common vector-borne disease in the US and accounts for 82% of reported tick-borne cases [1]. It is characterized by an initial infection by the spirochete *B. burgdorferi* which, if left untreated, can lead to severe consequences later [1, 2]. Lyme disease has two primary vectors: the black-legged tick (*I. scapularis*), found throughout the Eastern and North Central United States, with infectious ticks most abundant in the Northeast [3] and the western black-legged tick (*Ixodes pacificus*), found along the Pacific coast. Here, we focus on *I. scapularis*.

Because temperature controls many aspects of the tick life cycle, many efforts have been made to understand the dependence of *I. scapularis* life cycle on temperature [4–9] and to link climate to the potential range of this vector [10–16]. The mechanisms underlying the link between temperature and tick abundance can be approached via models such as the one developed here, as well as others [5, 7–9]. It is widely claimed that an increase in overall temperature will affect tick-borne diseases in general [17–21] and Lyme disease in particular has been the subject of a few models based on various measures of risk [10, 11, 16, 22–24].

Only a few dynamic models of Lyme disease transmission exist. Ogden et al. use their temperature-dependent

life cycle model to model transmission between ticks and mice [25]. A model by Gaff and Gross for a different tick-borne disease combines all hosts into one population and does not track the full vector lifecycle. It does incorporate a version of seasonality and extends the model to multiple patches [26].

This study introduces a model of both tick life cycle and Lyme disease transmission based on the work of Ogden et al. [5, 6]. In Ogden et al.'s [5] study, a model of the tick life cycle is presented in which temperature is incorporated via a time delay and host densities are not modeled directly but represented by varying the probability that a questing tick finds a host. No disease is modeled. In [25], this model was extended to include disease transmission and a single host, *Peromyscus leucopus*, whose life cycle was modeled in some detail. In this study, we simplify the *P. leucopus* life cycle but extend the model to multiple host classes with different transmission dynamics, tick removal capacities, and population densities.

The most straightforward measure of disease risk to humans is the number of infected ticks questing for a blood meal in a given area. An increase in this abundance translates directly to an increased probability of contact with humans [3]. However, tick abundance is difficult to measure outright in the field and an estimate must be provided through a model such as the one developed here.

The most commonly used measure of risk is the number of degree days above 0 Celsius, which is an indicator of temperature suitability for *I. scapularis*, both at present [10] and under conditions of rising temperature [22, 27–31]. Other factors besides temperature have been used to indicate habitat suitability as well [24]. Neither habitat nor climatological suitability alone provides a robust estimate of the density of ticks present, as this depends also on host distribution and whether ticks are recently introduced or long established, as well as the effect of temperature on maturation rates of larvae and nymphs.

A common field measurement is the prevalence of infection in questing ticks [21, 32, 33], which varies depending on location and time of year. Although useful, it is an incomplete measure of risk without accompanying tick population data.

A useful proxy for risk to humans could be disease prevalence in host animals. A rise in this prevalence would indicate either more ticks or higher infection rates in ticks, and either way could be an indicator of increased disease risk to humans. *B. burgdorferi* rates in mice have been measured in some studies, which also observe a seasonal trend [34, 35].

Some species of birds are competent and highly mobile hosts for Lyme disease and have been considered a source of introduction of the disease to new areas [10]. Disease prevalence in this host represents a different type of risk: the risk of exporting the disease elsewhere.

The model developed here represents a synthetic ecosystem with disease dynamics present that is complete enough to consider all of the risk measures mentioned, not only for a single example but also under conditions of rising temperature. Taken together, these risk measures give a picture of the likely effect of a rise in mean annual temperature on risk of Lyme disease in regions similar to the Northeastern United States.

## 2. Materials and Methods

This study is based on the work of Ogden et al. which includes laboratory and field experiments as well as models [5, 6]. Compartment models of ordinary differential equations describe both the *I. scapularis* population, at various life stages, and the host populations to model the disease dynamics within a one-square kilometer area. The model of Ogden et al. was revised to be implemented using the Matlab ODE solver [36] and extended to include more host categories than the original model. Laboratory experiments have shown a clear temperature dependence of maturation periods for *I. scapularis* [5]. These temperature-sensitive rates are incorporated into this model to produce recognizable seasonal patterns of questing activity, based on the seasonal cycle of 2-meter air temperature for Hanover, NH. Humidity also plays a role in measured tick abundance [37, 38], but given the relatively high levels of warm season precipitation in Hanover, NH, we assume humidity is not limiting.

Ticks feed on a wide range of mammal hosts, from mice and other rodents to larger mammals such as raccoons and deer, as well as nonmammal hosts such as birds and reptiles. Some of these tick hosts such as *P. leucopus* [4, 25] are competent hosts for *B. burgdorferi* and serve as a reservoir from which uninfected ticks can pick up the disease, while others are incompetent hosts that play a role in propagation of the *I. scapularis* population [39, 40] through providing blood meals but are incapable of transmitting the disease. Although mice have been strongly implicated in the prevalence of both the black-legged tick and the transmission of the Lyme disease spirochete, it is acknowledged that other hosts play a role in Lyme disease transmission [2, 39, 41, 42]. In particular, mobile hosts, such as birds and deer, can carry both the vector and the disease to new locations, where it can become endemic [10]. Consequently, in this study, we have six classes of host: incompetent mobile, incompetent stationary, competent mobile (infected and uninfected), and competent immobile (infected and uninfected). The full six-host model enables us to compare the model output with a wide range of field observations.

Although the various species of host in a given category may vary in competence, we assume the hosts in the incompetent categories could not transmit disease at all. The probability of transmission upon contact with an infected tick was calculated as a weighted average over all the species in a competent host category, based on rates reported in Levi et al. [39].

Birth, death, and maturation rates are based on measurements in both the laboratory and field. Densities of host populations and ticks per host are based on published studies, with references provided in Table 1. In particular, our single patch model includes six host populations categorized by competence, infectious versus uninfected, and mobile versus immobile. However, no published data set includes complete information on all stages of the tick

Table 1: Default parameters used in model.

| Parameter | Meaning | Value | Source |
|---|---|---|---|
| $w$ | Increase in mean annual temperature relative to historical | 0- to 5-degree Celsius | Arbitrary |
| $b$ | Per capita egg production per day | 300 | [5, 6] |
| $d_e$ | Daily death rate for eggs | 0.015 | [43] |
| $d_1$ | Daily death rate of young hardening larvae | 0.01 | [44] |
| $d_{n1}$, $d_{A1}$ | Daily death rate of engorged larvae and engorged nymphs | 0.001 | [45] |
| $d_2$, $d_{n2}$, $d_{A2}$ | Daily death rate of questing larvae, nymphs, and adults | 0.094 | [44] |
| $d_{3a} = d_{fna} = d_{A3a}$ | Daily death rate of feeding larva, nymphs, and adults on host type $a$ (IM) | 0.51 | [39] |
| $d_{3b} = d_{fnb} = d_{A3b}$ | Daily death rate of feeding larva, nymphs, and adults on host type $b$ (IS) | 0.89 | [39] |
| $d_{3c} = d_{fnc} = d_{A3c} = d_{3e} = d_{fne} = d_{A3e}$ | Daily death rate of feeding larva, nymphs, and adults on host types $c$ and $e$ (CUM, CIM) | 0.73 | [39] |
| $d_{3d} = d_{fnd} = d_{A3d} = d_{3f} = d_{fnf} = d_{A3f}$ | Daily death rate of feeding larva, nymphs, and adults on host types $c$ and $e$ (CUS, CIS) | 0.72 | [39] |
| $d_{A4}$ | Daily death rate of engorged adults | 0.5 | [5, 6] |
| $m_e(T)$ | Egg to larvae maturation rate | $m_e(T) = 0.0552 * \exp(-((T - 25.83)/4.946)^2) * \mathrm{HS}(T - 15)$ | [6] |
| $m_1$ | Young hardening larvae to questing larvae maturation rate | 0.033 | [43] |
| $m_2$, $m_{n2}$, $m_{A2}$ | Questing tick to feeding tick maturation (all stages) | 0.5 | Estimated questing period of 5–6 days |
| $m_3$, $m_{fn}$, $m_{A3}$ | Feeding tick maturation rate, all stages, all hosts | 0.5 | [46] |
| $m_{n1}(T)$ | Engorged larvae maturation rate | $m_{n1}(T) = 0.04001 * \exp(-((T - 26.68)/9.533)^2) * \mathrm{HS}(T - 15)$ | [6] |
| $m_{A1}(T)$ | Engorged nymph maturation rate | $m_{A1}(T) = 0.03173 * \exp(-((T - 23.85)/9.042)^2) * \mathrm{HS}(T - 15)$ | [6] |
| $r$ | A numerical feature to ensure you never divide by 0 | 0.001 | |
| $p_L$ | Probability of larvae infection | 0.1 | Estimated |
| $p_N$ | Probability of nymph infection | 0.1 | Estimated |
| $C_a$ | Per host tick carrying capacity of host type $a$, incompetent mobile | 239 | [39] |
| $C_b$ | Per host tick carrying capacity of incompetent stationary hosts | 176.75 | [39] |
| $C_c = C_e$ | Per host tick carrying capacity of CUM and CIM hosts | 11.4 | [39] |

Table 1: Continued.

| Parameter | Meaning | Value | Source |
|---|---|---|---|
| $C_d = C_f$ | Per host tick carrying capacity of CUS and CIS hosts | 46.84 | [39] |
| $b_{IM}$ | Birth rate of incompetent mobile hosts | 0.00261 | [39, 40, 47] |
| $b_{IS}$ | Birth rate of incompetent stationary hosts | 0.0102 | [39, 40, 47] |
| $b_{CUM}$ | Birth rate of competent uninfected mobile hosts | 0.00753 | [39, 40, 48] |
| $b_{CUS}$ | Birth rate of competent uninfected stationary host | 0.0176 | [39, 40, 47] |
| $d_{IM}$ | Death rate of IM hosts | 0.000609 | [39, 40, 47] |
| $d_{IS}$ | Death rate of IS hosts | 0.00129 | [39, 40, 47] |
| $d_{CUM} = d_{CIM}$ | Death rate of competent uninfected mobile hosts | 0.00157 | [39, 40, 48] |
| $d_{CUS} = d_{CIS}$ | Death rate of competent uninfected stationary hosts | 0.00345 | [39, 40, 47] |
| $K_{IM}$ | Cell carrying capacity of IM host | 25 | [39] |
| $K_{IS}$ | Cell carrying capacity of IS hosts | 45 | [39] |
| $K_{CM}$ | Cell carrying capacity of CUM + CIS hosts | 3100 | [39] |
| $K_{CS}$ | Cell carrying capacity of CUS + CIS hosts | 9,335 | [39] |
| $p_{CUM}$ | Probability of CUM host infection (per infective tick per day × number of hosts of that type) | 0.117 | [39] |
| $p_{CUS}$ | Probability of competent uninfected stationary host infection (per infective tick per day × number of hosts of that type) | 0.6635 | [39] |
| $E(0)$ | Initial number of eggs | 10,000,000 | |
| $NU_1(0)$ | Initial uninfected engorged larvae | 5,000,000 | |
| $AU_1(0)$ | Initial uninfected engorged nymphs | 300,000 | |
| IM(0) | Initial incompetent mobile hosts | 25 | |
| IS(0) | Initial incompetent stationary hosts | 45 | |
| CUM(0) | Initial competent mobile hosts | 3,100 | |
| CUS(0) | Initial competent stationary hosts | 9,335 | |
| All other initial conditions | | 0 | |

lifecycle throughout a season, tick densities on various hosts, and host densities in the landscape.

Many sources were used to estimate parameters in the model, summarized in Table 1 [5, 6, 39, 40, 43–48]. Any information from a study in the Northeastern US that was not used to estimate a parameter directly was used instead to compare with model outputs to make sure the model was producing reasonable seasonal patterns of tick populations, on-host tick distributions, and host densities. Seasonal effects produced by the model could be compared to the range observed in multiple studies. The range of hosts considered allows us to compare model predictions with measured tick burdens and disease prevalence on a variety of hosts in several published field studies in the Northeast [21, 32–35, 49–53]. Across all of these measures, the model produces results that are biologically reasonable compared to what are observed. The model produces a synthetic ecosystem and epidemiology that is the basis for numerical experiments.

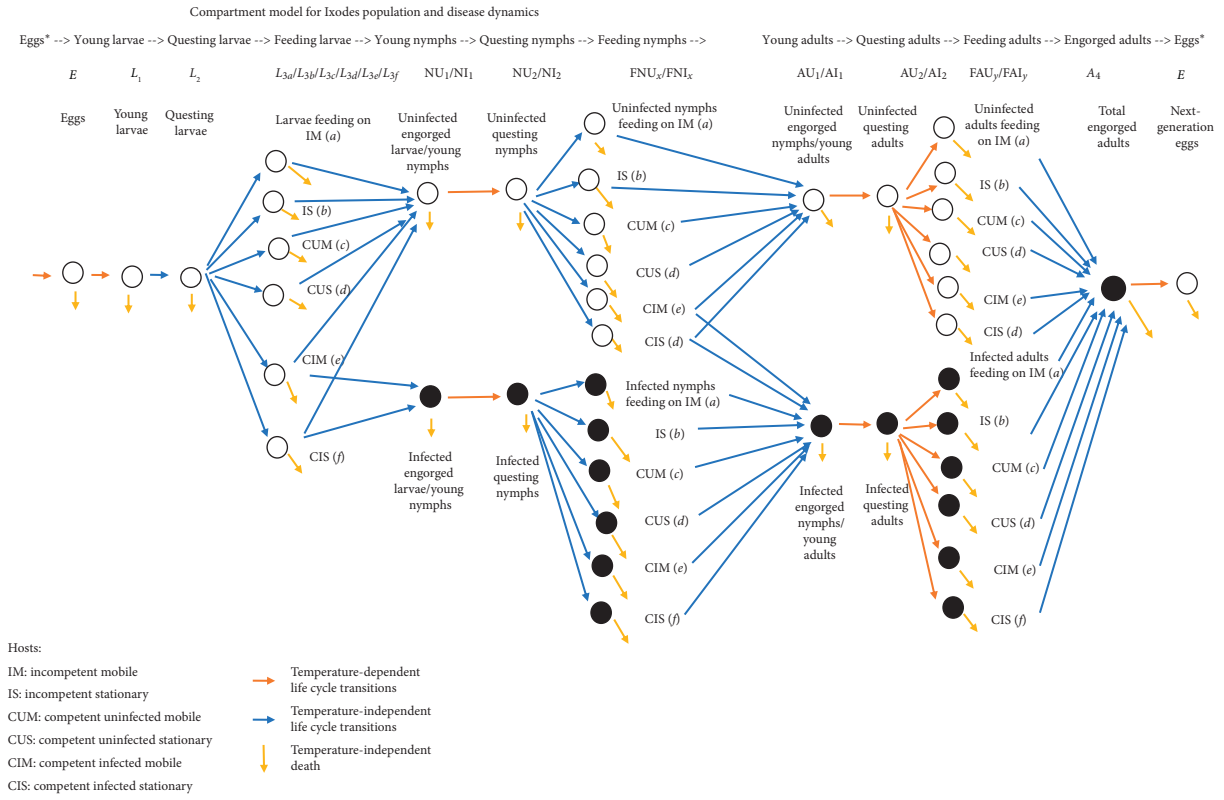


(a)

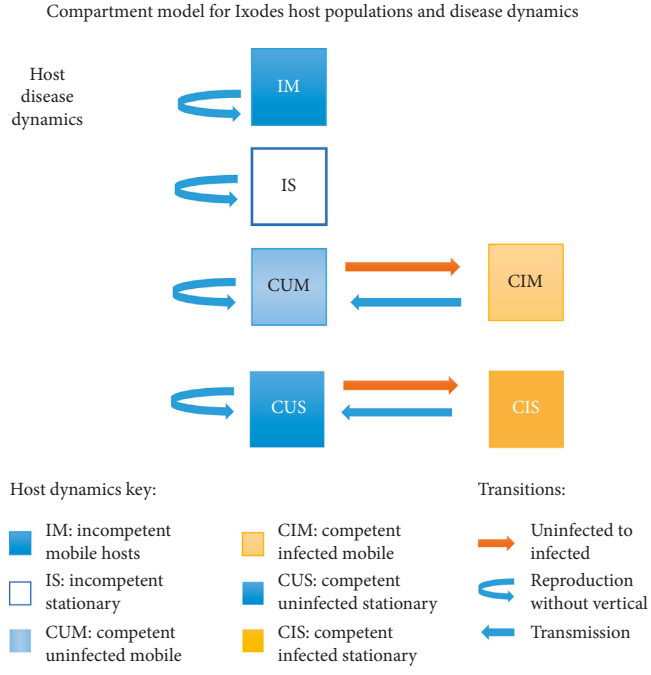


(b)

Figure 1: Compartment model for *I. scapularis* and host population and disease dynamics. (a) The life cycle of *I. scapularis* as described by equations (1)–(17). Feeding populations are split according to host type. Temperature-dependent maturation transitions are indicated in orange. (b) Host population and disease dynamics. Disease transitions require vector populations shown in this figure.

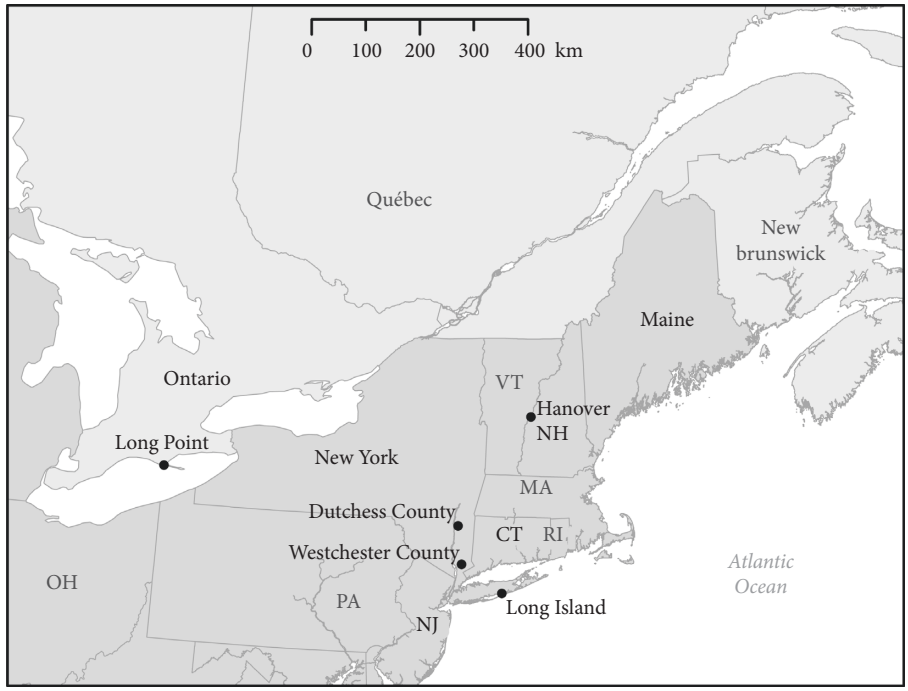


Figure 2: Map of Northeastern United States. Most field studies considered are from this region. Locations referenced in the text are labelled in black.

To study the role of increased mean annual temperature on vector dynamics and disease prevalence, a daily seasonal cycle for Hanover, NH, was fitted by a truncated Fourier series and the constant term in that series was increased. It is assumed that other variables such as host distribution remained constant.

Figures 1(a) (ticks) and 1(b) (hosts) offer an overview of the relationships modeled in this study. Figure 1(a) tracks the tick life cycle. During periods of feeding, the populations are split into six categories depending on the host. The potential of contracting disease from an infected host leads to twelve tick categories at the "feeding nymph" and "feeding adult" stages. Figure 1(b) tracks transitions in the six host compartments. We assume there is no vertical transmission in either the tick or host life cycle.

Host species listed in Levi et al. [39] were categorized based on their reservoir competencies and whether or not a species was (relatively) mobile. All species listed in Levi et al. were categorized as follows:

(1) Competent stationary hosts: white footed mouse, eastern chipmunk, masked shrew, short tailed shrew, eastern gray squirrel

(2) Competent mobile hosts: ground foraging birds

(3) Incompetent stationary hosts: striped skunk, raccoon, Virginia opossum

(4) Incompetent mobile hosts: white-tailed deer

The ability of hosts to actively remove ticks is reflected in the per host carrying capacities. For simplicity, the model embraces a form of the null hypothesis, by assuming that tick-host contact rates depend on population densities of hosts and ticks irrespective of life stage and that all on-host ticks taken together are subject to a single on-host carrying capacity.

Simulations were run on a 2015 MacBook Pro using Matlab ode45 solver [36], with run times of approximately 8 seconds. Figure 2 shows a map of the Northeastern United States, where most of the field studies cited were done.

*2.1. Equations.* The two-year life cycle for *I. scapularis* was broken into differential equations based on behaviorally distinguishable life stages as follows: eggs, young larvae, questing larvae, feeding larvae, engorged larvae, questing nymphs, feeding nymphs, engorged nymphs, questing adults, feeding adults, and engorged adults.

*2.1.1. Temperature (T).* The mean seasonal temperature cycle for Hanover, NH, was calculated from daily maximum and minimum temperature data obtained from the National Centers for Environmental Information (NCEI) Global Historical Climatology Network (GHCN) dataset.

GHCND data from both the Hanover and the Storrs, CT stations were used to create a seasonal average (1990–2015, Patch_Lyme) [54–56]. The data are modeled by a continuous function for temperature based on the day of the year for the model using a five-term Fourier series:

$$T = 10.5 + w + 1 * ((-10.79)\cos(t * 0.0172) + (-7.53)\sin(t * 0.0172) + (-1.212)\cos(2 * t * 0.0172) + (-0.07472)\sin(2 * t * 0.0172)). \quad (1)$$

The default value for $w$ is zero, corresponding to current temperature data from Hanover. In numerical experiments, $w$ is increased in increments of 1°C, which effectively increases the temperature at every time step and therefore the annually averaged mean temperature. While the actual seasonal pattern of anthropogenic temperature change will be different from the simple additive shift used in this study, the magnitude of warming is consistent with the anticipated range of increasing temperatures for the Northeast projected by global climate models: 2.2°C for midcentury and intermediate greenhouse gas emissions to 6.4°C for late-century and high greenhouse gas emissions [57].

The maturation of eggs to larvae is based on the laboratory studies by Ogden et al. [6]. In this study, maturation times are given for a selection of warm temperatures. These maturation times were converted to rates and fit with a Gaussian distribution. To ensure diapause at low enough temperatures, a Heaviside function was incorporated that reduces maturation rates to zero when the temperature is below 15-degree Celsius. Combining these gives the temperature-dependent egg maturation function, $m_e(T)$, where HS is the Heaviside function:

$$m_e(T) = 0.0552 * \exp\left(-\left(\frac{T-25.83}{4.946}\right)^2\right) * \mathrm{HS}(T-15). \tag{2a}$$

Based on [6] and using the same method as for $m_e(T)$, engorged larva matures with a temperature-dependent rate:

$$m_{n1}(T) = m_{n1} * 0.04001 * \exp\left(-\left(\frac{T-26.68}{9.533}\right)^2\right) * \mathrm{HS}(T-15). \tag{2b}$$

Based on [6] and using the same method as for $m_e(T)$, engorged nymphs have a temperature-dependent maturation rate:

$$m_{A1}(T) = 0.03173 * \exp\left(-\left(\frac{T-25.83}{9.042}\right)^2\right) * \mathrm{HS}(T-15). \tag{2c}$$

These temperature dependencies give rise to the changing tick and disease dynamics in this study.

*2.1.2. Tick Dynamics.* Tick dynamics include maturation into and out of each stage as well as a death rate. On host, stages are divided according to the disease status of both hosts and ticks. Quantities tracked include eggs ($E$), young hardening larvae ($L_1$), questing larvae ($L_2$), larvae feeding on host type $x$ ($L_{3x}$), as there are six types of host (IM, IS, CUM, CUS, CIM, and CIS) which for convenience we relabel ($U_a$, $U_b$, . . ., $U_f$) and set $x$ as an index for $a$–$f$. Equations for uninfected engorged larvae ($NU_1$) and infected engorged larvae ($NI_1$) include disease transmission terms based on tick/host interactions. Uninfected and infected questing nymphs ($NU_2$ and $NI_2$) and feeding nymphs ($FNU_x$ and $FNI_x$) are tracked similar to larvae. Uninfected and infected engorged nymphs ($AU_1$ and $AI_1$) include disease transmission terms similar to those for engorged larvae. The equations for uninfected and infected questing and feeding adults ($AU_2$, $AI_2$, $AU_{3x}$, and $AI_{3x}$) are constructed similarly to those for nymphs and larvae. Engorged adults ($A_4$) complete the life cycle:

$$E' = b * A_4 - d_e * E - m_e(T) * E, \tag{3}$$

$$L_1' = m_e(T) * E - d_1 * L_1 - m_1 * L_1, \tag{4}$$

$$L_2' = m_1 * L_1 - d_2 * L_2 - m_2 * L_2, \tag{5}$$

$$L_{3x}' = m_2 * Q_x * L_2 * F_x - d_{3x} * L_{3x} - m_3 * L_{3x}. \tag{6}$$

The first term represents attachment to a host where the parameter $m_2$ is a constant rate based on the estimated number of days spent questing, $Q_x$ is the probability that the host is of type $x$ (described in equation 21), and $L_2$ the population of questing larvae. The index $F_x$ (described in equation 22) is a function of total number of hosts of type $x$, the per host carrying capacity for ticks, and the amount of that capacity already occupied by ticks. $F_x$ is nonlinear and caps the feeding larvae population in terms of hosts:

$$\begin{aligned}\mathrm{NU}_1' = {} & m_{3a}L_{3a} + m_{3b}L_{3b} + m_{3c}L_{3c} + m_{3d}L_{3d} \\ & + (1-p_L)\left(m_{3e}L_{3e} + m_{3f}L_{3f}\right) - d_{n1}\mathrm{NU}_1 \\ & - m_{n1}(T)\mathrm{NU}_1,\end{aligned} \tag{7}$$

$$\mathrm{NI}_1' = p_L\left(m_{3e}L_{3e} + m_{3f}L_{3f}\right) - d_{n1}\mathrm{NI}_1 - m_{n1}(T)\mathrm{NI}_1, \tag{8}$$

$$\mathrm{NU}_2' = m_{n1}(T)\mathrm{NU}_1 - d_{n2}\mathrm{NU}_2 - m_{n2}\mathrm{NU}_2, \tag{9}$$

$$\mathrm{NI}_2' = m_{n1}(T)\mathrm{NI}_1 - d_{n2}\mathrm{NI}_2 - m_{n2}\mathrm{NI}_2, \tag{10}$$

$$\mathrm{FNU}_x' = m_{n2}\mathrm{NU}_2F_xQ_x - d_{fnx}\mathrm{FNU}_x - m_{fn}\mathrm{FNU}_x, \tag{11}$$

$$\mathrm{FNI}_x' = m_{n2}\mathrm{NI}_2F_xQ_x - d_{fnx}\mathrm{FNI}_x - m_{fn}\mathrm{FNI}_x, \tag{12}$$

$$\begin{aligned}\mathrm{AU}_1' = {} & m_{fn}\left(\mathrm{FNU}_a + \mathrm{FNU}_b + \mathrm{FNU}_c + \mathrm{FNU}_d\right) \\ & + m_{n3}(1-p_n)\left(\mathrm{FNU}_e + \mathrm{FNU}_f\right) - d_{A1}\mathrm{AU}_1 \\ & - m_{A1}(T)\mathrm{AU}_1,\end{aligned} \tag{13}$$

$$\begin{aligned}\mathrm{AI}_1' = {} & m_{fn}\left(\mathrm{FNI}_a + \mathrm{FNI}_b + \mathrm{FNI}_c + \mathrm{FNI}_d\right) \\ & + m_{n3}(p_n)\left(\mathrm{FNU}_e + \mathrm{FNU}_f\right) - d_{A1}\mathrm{AI}_1 - m_{A1}(T)\mathrm{AI}_1,\end{aligned} \tag{14}$$

$$\mathrm{AU}_2' = m_{A1}(T)\mathrm{AU}_1 - d_{A2}\mathrm{AU}_2 - m_{A2}\mathrm{AI}_2, \tag{15}$$

$$\mathrm{AI}_2' = m_{A1}(T)\mathrm{AI}_1 - d_{A2}\mathrm{AI}_2 - m_{A2}\mathrm{AI}_2, \tag{16}$$

$$\mathrm{AU}_{3x}' = m_{A2}\mathrm{AU}_2F_xQ_x - d_{A3x}\mathrm{AU}_{3x} - m_{A3}\mathrm{AU}_{3x}, \tag{17}$$

$$\mathrm{AI}_{3x}' = m_{A2}\mathrm{AI}_2F_xQ_x - d_{A3}\mathrm{AI}_{3x} - m_{A3}\mathrm{AI}_{3x}, \tag{18}$$

$$A_4' = m_{A3}\mathrm{AU}_{3\mathrm{total}} + m_{A3}\mathrm{AI}_{3\mathrm{total}} - d_{A4}A_4. \quad (19)$$

*2.1.3. Host Dynamics.* Host population dynamics are represented by logistic growth with observed per km$^2$ densities and death rates. Disease dynamics are given in terms of encounter rates with infected feeding ticks. Quantities tracked are incompetent mobile hosts (IM), incompetent stationary hosts (IS), competent mobile hosts both uninfected and infected (CUM and CIM), and competent stationary hosts both uninfected and infected (CUS and CIS):

$$\mathrm{IM}' = b_{\mathrm{IM}}\mathrm{IM}\left(1 - \frac{\mathrm{IM}}{K_{\mathrm{IM}}}\right) - d_{\mathrm{IM}}\mathrm{IM}, \quad (20)$$

$$\mathrm{IS}' = b_{\mathrm{IS}}\mathrm{IS}\left(1 - \frac{\mathrm{IS}}{K_{\mathrm{IS}}}\right) - d_{\mathrm{IS}}\mathrm{IS}, \quad (21)$$

$$\mathrm{CUM}' = b_{\mathrm{CUM}}(\mathrm{CUM} + \mathrm{CIM})\left(1 - \frac{\mathrm{CUM} + \mathrm{CIM}}{K_{\mathrm{CM}}}\right) - d_{\mathrm{CUM}}\mathrm{CUM} - p_{\mathrm{CUM}}(\mathrm{FNI}_c + \mathrm{AI3}_c) * \mathrm{CUM}, \quad (22)$$

$$\mathrm{CUS}' = b_{\mathrm{CUS}}(\mathrm{CUS} + \mathrm{CIS})\left(1 - \frac{\mathrm{CUS} + \mathrm{CIS}}{K_{\mathrm{CS}}}\right) - d_{\mathrm{CUS}}\mathrm{CUS} - p_{\mathrm{CUS}}(\mathrm{FNI}_d + \mathrm{AI3}_d) * \mathrm{CUS}, \quad (23)$$

$$\mathrm{CIM}' = p_{\mathrm{CUM}}(\mathrm{FNI}_c + \mathrm{AI3}_c) * \mathrm{CUM} - d_{\mathrm{CIM}}\mathrm{CIM}, \quad (24)$$

$$\mathrm{CIS}' = p_{\mathrm{CUS}}(\mathrm{FNI}_d + \mathrm{AI3}_d) * \mathrm{CUS} - d_{\mathrm{CIS}}\mathrm{CIS}. \quad (25)$$

*2.1.4. Auxiliary Equations.* Recall that there are six types of host (IM, IS, CUM, CUS, CIM, CIS) which for convenience we relabel ($U_a$, $U_b$,. . ., $U_f$) and set $x$ as an index for $a$–$f$.

To count total ticks on a given type of host, we have:

(i) Larvae $L_{3x}$ where $x = a, b, c, d, e, f$, feeding on hosts of type $x$

(ii) Uninfected nymphs feeding on hosts of type $x$, denoted $\mathrm{FNU}_x$

(iii) Infected nymphs feeding on hosts of type $x$, denoted $\mathrm{FNI}_x$

(iv) Uninfected adults feeding on hosts of type $x$, denoted $\mathrm{AU}_{3x}$

(v) Infected adults feeding on hosts of type $x$, denoted $\mathrm{AI}_{3x}$ where $x = a, b, c, d, e, f$

Let $T_x$ be the total ticks on hosts of type $x$, so $T_x = L_{3x} + \mathrm{FNU}_x + \mathrm{FNI}_x + \mathrm{AU}_{3x} + \mathrm{AI}_{3x}$.

Let $C_x$ be the per host carrying capacity for ticks on a host of type $x$.

Let $S = \mathrm{IM} + \mathrm{IS} + \mathrm{CUM} + \mathrm{CUS} + \mathrm{CIM} + \mathrm{CIS}$ be the total number of hosts of all types.

For each respective host type we have the following equations:

$$Q_x = \frac{U_x}{(S + r)}. \quad (26)$$

Equation (26) expresses the approximate fraction of hosts that are of type $x$. The parameter $r$ is set to a small number to avoid numerical issues if the number of hosts is set close to zero:

$$F_x = \max\left(\frac{C_x * U_x - T_x}{C_x * U_x + r}, 0\right). \quad (27)$$

Equation (27) describes the available on-host space for ticks on hosts that are of type $x$. $T_x$ counts the number of ticks on hosts of type $x$. The term $C_x * U_x$ is the per host tick capacity times the total number of hosts of type $x$, giving the per host tick capacity for hosts of type $x$. The difference between these two is the available space for ticks on all hosts of type $x$.

*2.2. Numerical Simulations.* Simulations were run on Matlab software [36] using the ODE45 solver for a ten-year simulated time period. The model achieved a periodic steady state before the last year, which is the year used for all figures and calculations. Parameters and initial conditions are listed in Table 1.

## 3. Results

Overall model performance is compared with field observations from the Northeastern US, showing the model produces reasonable results. The results of numerical experiments increasing mean annual temperature are shown Figures 3–7 and discussed.

*3.1. Overall Model Performance.* Counts of questing larva in Dutchess County, NY, 1992–1994, were observed to sometimes have unimodal distributions peaking anywhere from early July to early August and bimodal distributions with peaks in June and again in August. Questing nymphs were observed to have a unimodal peak during June/July. Adults were more likely to have a bimodal distribution, peaking as early as May and as late as November. Years with unimodal questing adult distributions peaked late, in October [50, 51]. Estimates of average questing larva density varied from 1.45 to 3.20 per square meter depending upon study site. Estimates of average nymph density ranged from 0.07 to 0.32 per square meter. The model predicts peak questing larva counts of 1.46 per m$^2$ near Aug 19 and peak questing nymph counts of 0.146 per m$^2$ near Aug 30, reasonably close to the field observations described above, although no attempt was made to match those data.

Studies also report an average tick burden for mice, *P. leucopus*, as 10–15 in a Dutchess County, NY, study for 1991–1993 [50]. A subsequent study in the same region in 1995, 1997, and 1998 reports a larva burden of 6 on mice and 17 on chipmunks, and a nymph burden of 5 on mice and 2 on chipmunks [52]. The annual mean maximum larva per

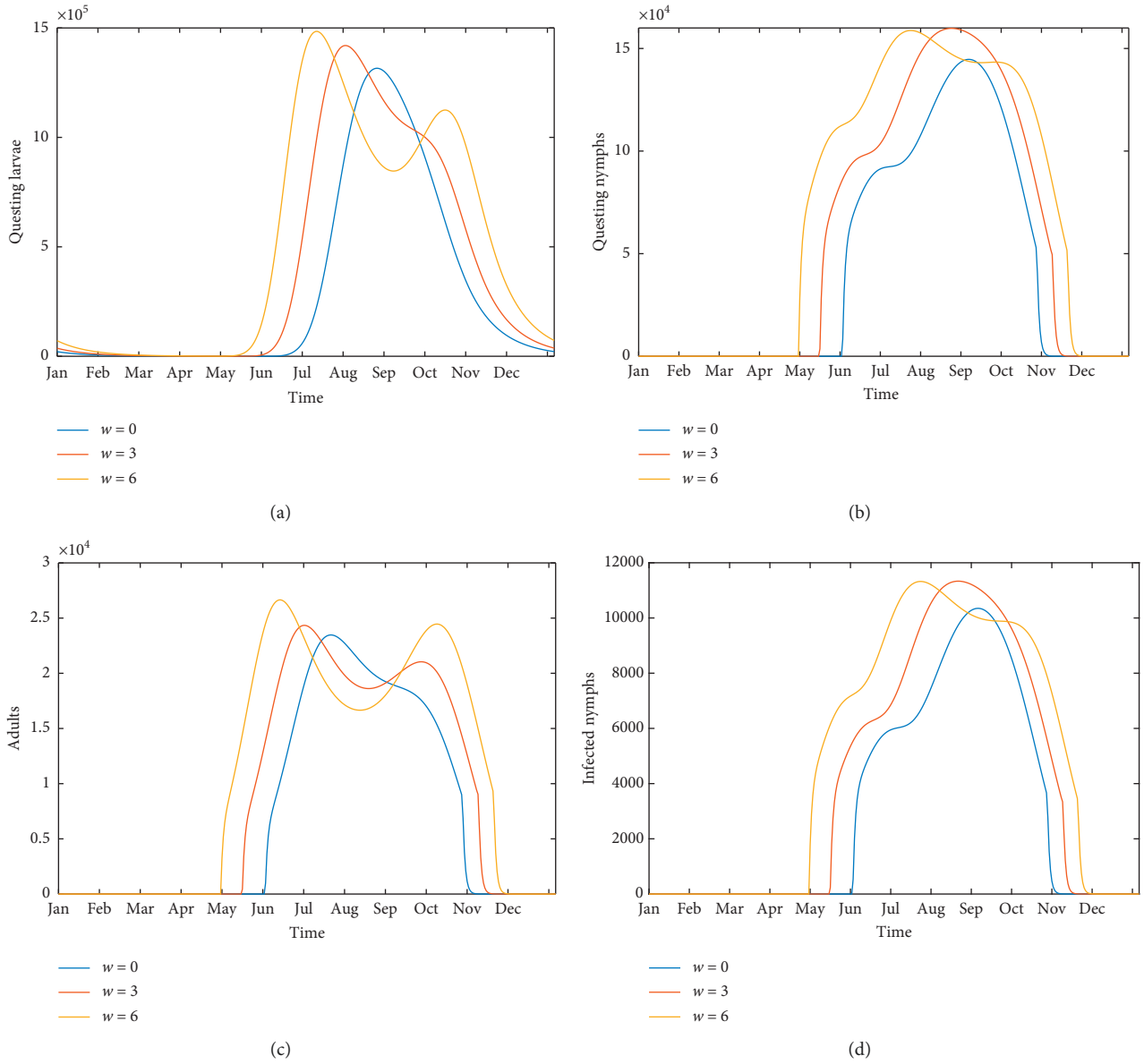


FIGURE 3: Temporal dynamics of tick populations and selected stages at steady state for historical temperature, 3°C above historical, and 6°C above historical. (a) Seasonal pattern of questing larvae ($L_2$), (b) questing nymphs ($NU_2 + NI_2$), (c) adults ($AU_2 + AI_2$), and (d) infected nymphs ($NI_2$) per km$^2$. The time axis represents the final year of the run from Jan 1 to Dec 31. Note the difference in scale of the four panels.

rodent was reported in the Long Point Ontario data for 1990 and 1992 as 10–32, with feeding nymph to feeding larva ratio of 0.15 [53]. The Levi et al. study from which we derived many of the model parameters presents a synopsis of 19 years of data from Dutchess County, NY, showing that peak larva to mouse ratios can range from less than 10 to over 40, while peak nymph to mouse ratios range from 1 to 4 [39]. In our model, chipmunks, mice, shrews, and squirrels are all grouped together as "competent stationary hosts," for which it predicts a maximum tick to host ratio of around 26 as seen in Figure 3(d), in reasonable agreement with these studies.

Long Point, Ontario, data for 1989–1992 also report average total tick per deer between 170 and 249 [53]. The model here gives a maximum of about 55 ticks per deer, which is lower than numbers reported in this study. However, the peak tick per competent mobile host is about 10, very close to the per host carrying capacity for that category. The ratio for incompetent stationary hosts, 40, was also close to the per host carrying capacity for that category of host. Discrepancies could be explained by differing host distributions.

The field data present a range of observations that reflect uncertainty in the expected timing of emergence and on-host tick burdens. In addition, no data set has complete information on host populations. The conclusion from these comparisons is that, although there appear to be some discrepancies in the timing of peak questing nymphs and

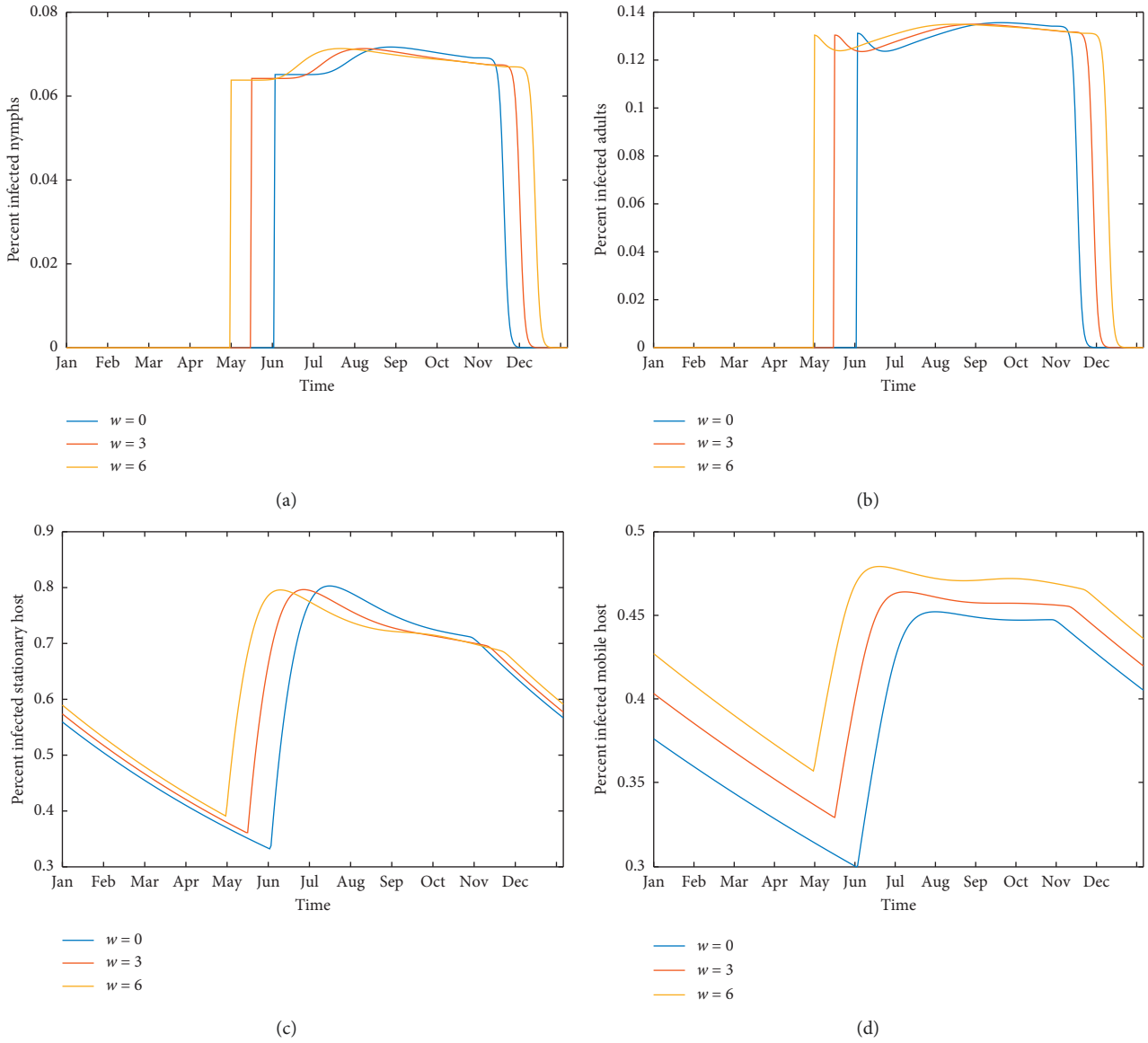


Figure 4: Temporal dynamics of Lyme disease. Temporal dynamics of *Borrelia burgdorferi* infection at steady state for historical temperature, 3°C above historical, and 6°C above historical. (a) *B. burgdorferi* prevalence in questing nymphs ($NI_2/(NI_2 + NU_2)$) (b) *B. burgdorferi* presence in questing adult ticks ($AI_2/(AI_2 + AU_2)$). (c) *B. burgdorferi* prevalence in competent stationary hosts (CIS/(CIS + CUS)) (d) *B. burgdorferi* presence in competent mobile hosts (CIM/(CIM + CUM)). Note the difference in scale of the four panels.

peak tick burden on deer, the overall results of the model are within the ranges observed across the field studies considered and the model is good enough to test the progression of disease and the impact of changes in host populations on both tick populations and disease.

The literature includes studies of disease prevalence in both ticks and hosts. Prevalence changes greatly from location to location and over time. In earlier studies measuring disease prevalence in ticks, the range goes from 3% infected [21] to 24% [32] and to 33% [33]. The Stafford study [32] indicates a seasonal trend with prevalence varying from 8% to 24%. Studies of *B. burgdorferi* in mice also report a seasonal trend, from 33% to 75% [34] to 57% to 93% [35]. Disease prevalence in the model has a seasonal trend similar to these.

*3.2. Results of Numerical Simulations.* The model presented here produces a periodic seasonal cycle of tick prevalence, as observed in many locations, while host populations all arrive and remain at equilibrium. As the temperature input is strictly periodic, there is no variation from year to year after an initial transient period. The behavior of questing tick populations over a typical steady state year is shown in Figures 3(a) (historical temperature), 3(b) (3°C above historical), and 3(c) (6°C above historical). Similarly, the model produces seasonal patterns of infected questing nymphs, shown in Figure 3(d), for the same three temperature patterns. Both the length of the questing season and the number of infected questing ticks are seen to increase with temperature. Figures 4(a) and 4(b) show changes in disease prevalence in questing nymphs and adults, showing a longer

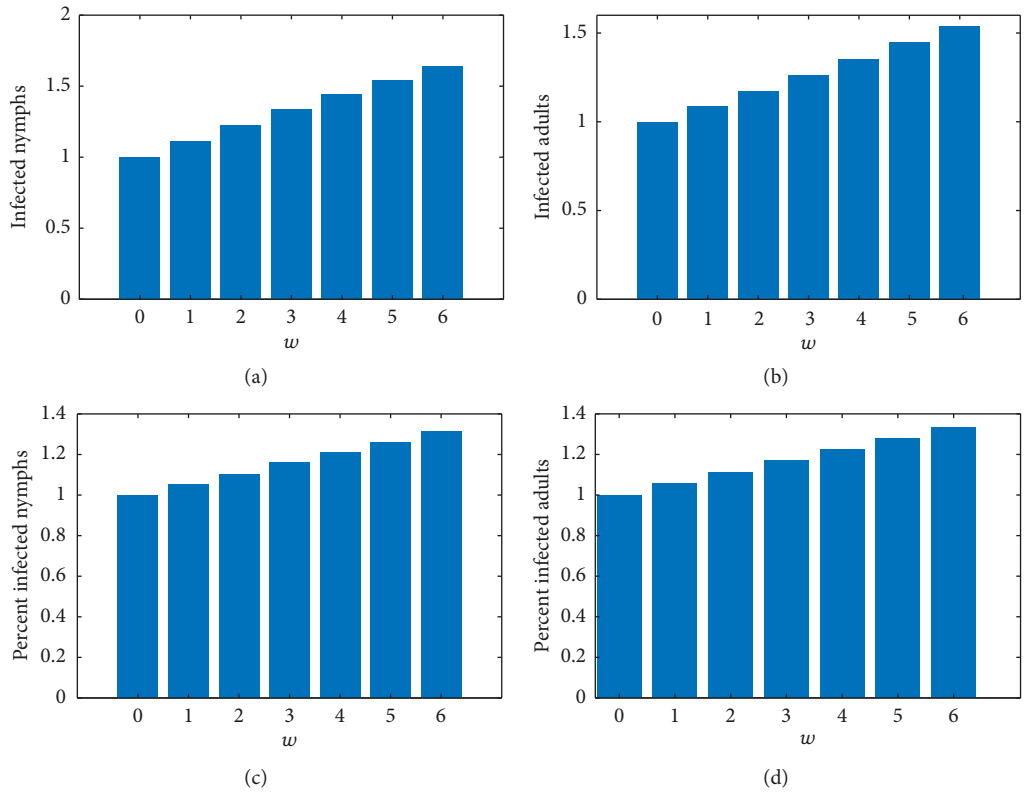


FIGURE 5: Response of tick-based risk measures to increasing temperature, as percent of control ($w = 0$, historical temperature). (a) Number of infected nymphs per day averaged over the last year of the simulation, scaled by the same quantity for $w = 0$ (no temperature rise), i.e., $\text{av}(\text{NI}_2)_{w=i}/\text{av}(\text{NI}_2)_{w=0}$, $i = 0, 1, \ldots, 6$. (b) Number of infected adults per day (averaged and scaled to $w = 0$), i.e., $\text{av}(\text{NA}_2)_{w=i}/\text{av}(\text{NA}_2)_{w=0}$, $i = 0, 1, \ldots, 6$. (c) Percent nymphs infected (averaged and scaled to $w = 0$), i.e., $\text{av}(\text{NI}_2/(\text{NU}_2 + \text{NI}_2))_{w=i}/\text{av}(\text{NI}_2/(\text{NU}_2 + \text{NI}_2))_{w=0}$, $i = 0, 1, \ldots, 6$. (d) Percent adults infected (averaged and scaled to $w = 0$), i.e., $\text{av}(\text{AI}_2/(\text{AU}_2 + \text{AI}_2))_{w=i}/\text{av}(\text{AI}_2/(\text{AU}_2 + \text{AI}_2))_{w=0}$, $i = 0, 1, \ldots, 6$.

season of potential transmission to humans with rising temperature. Figures 4(c) and 4(d) show changes in disease prevalence in host populations. Although a seasonal trend is still visible, the absolute change in numbers of infected hosts is small due to longer lifespans.

The response of tick-based risk measures to increasing temperature, as percent of control under temperature increases from 1°C to 6°C by increments of 1°C, is shown in Figure 5. Comparing Figures 5(a) and 5(b) show that the number of infected questing nymphs rises faster with increased temperature than the number of infected questing adults. Figures 5(c) and 5(d) show the disease prevalence in nymphs also rises faster than in adults. The model predicts over five times as many questing nymphs as adults, as seen in Figure 3. Together, these explain why the number of infected questing nymphs is close to the total number of infected questing ticks with rising temperature, as shown in Figure 7.

Risk measures based on disease prevalence in hosts are shown in Figure 6. Average annual prevalence in stationary hosts barely rises at all (Figure 6(a)). From Figure 4(c), one can see that the small rise that is visible is due to the longer season of transmission rather than to a larger percentage of infected hosts. Figure 6(b) shows a slightly higher effect on competent mobile hosts, due to both a longer season and slightly higher prevalence, shown in Figure 4(d). These hosts are birds, which can transmit the disease across long distances.

Risk based on degree days is not shown in Figure 6 but is included in Figure 7, which compares the measures of risk against each other for a given rise in temperature. Figure 7 compares each possible measure of risk against its value at $w = 0$. Bar c in each chart represents how the average number of infected questing ticks changes with rising temperature. Each bar may be compared to bar c to gauge how well that measure tracks the average number of infected questing ticks.

## 4. Discussion

While it is unreasonable to expect a model of a hypothetical but biologically reasonable scenario to match any particular study, we highlight places where the model could potentially be improved. The increase in mean annual temperature as a driver of increased risk of Lyme disease is discussed. The many possible measures of risk are compared to the intuitively solid criterion of average infected questing tick prevalence.

*4.1. Potential Model Improvements.* One explanation for the discrepancy between observed and predicted tick burden on

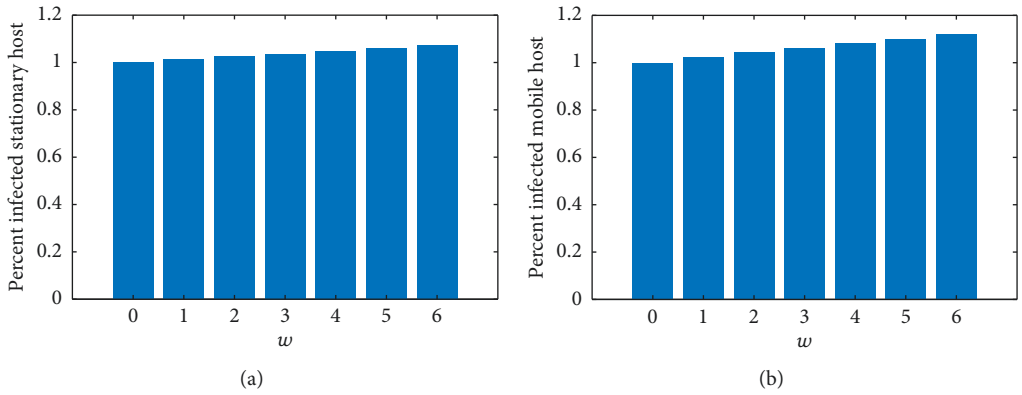


Figure 6: Response of host-based risk measures to increasing temperature, as percent of control (no temperature rise). (a) Percent infected competent stationary hosts per day averaged over the last year of the simulation, scaled by the same quantity for $w = 0$ (no temperature rise), i.e., av $(\mathrm{CIS}/(\mathrm{CUS} + \mathrm{CIS}))_{w=i}/\mathrm{av}(\mathrm{CIS}/(\mathrm{CUS} + \mathrm{CIS}))_{w=0}$, $i = 0, 1, \ldots, 6$ (b) Percent infected competent mobile hosts per day averaged over the last year of the simulation, scaled by the same quantity for $w = 0$ (no temperature rise), i.e., av $(\mathrm{CIM}/(\mathrm{CUM} + \mathrm{CIM}))_{w=i}/\mathrm{av}(\mathrm{CIM}/(\mathrm{CUM} + \mathrm{CIM}))_{w=0}$, $i = 0, 1, \ldots, 6$.

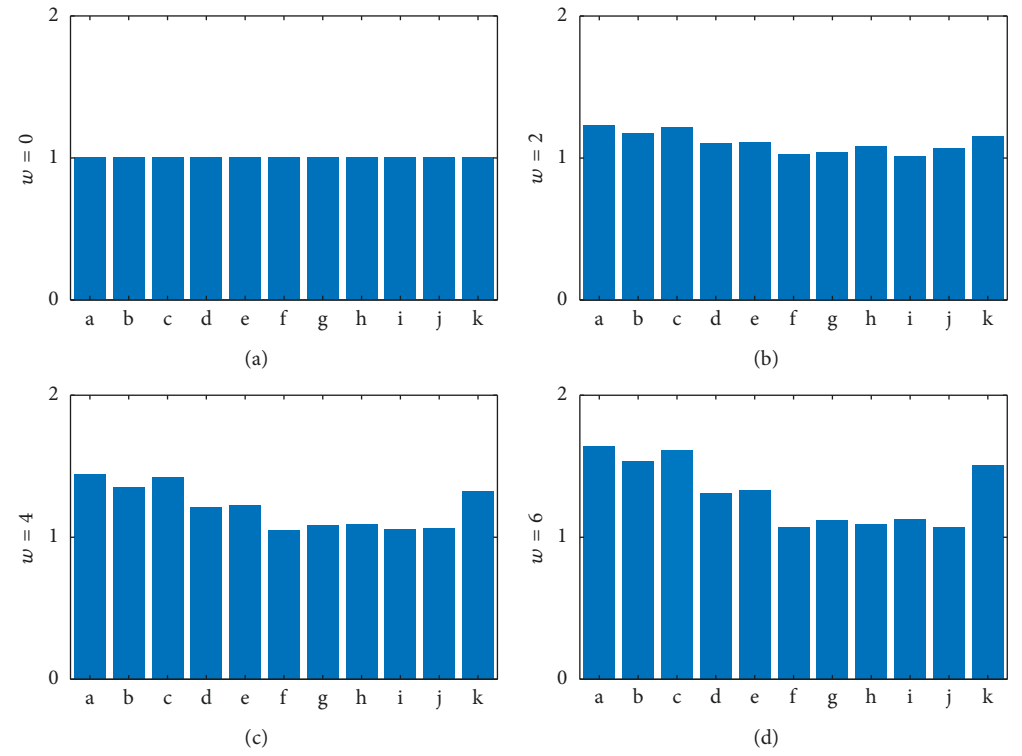


Figure 7: Response of various risk measures to increasing temperatures (relative to historical temperature, $w = 0$) for 0, 2, 4, and 6°C temperature increase. Each risk measure is scaled against its own value at $w = 0$. In this figure, a, b, c, d, e, f, g, h, i, j, and k represent the following: (a) annual average of number of questing nymphs ($\mathrm{NI}_2$) at steady state, (b) annual average of infected questing adult ticks ($\mathrm{AI}_2$) at steady state, (c) annual average of infected questing ticks ($\mathrm{AI}_2 + \mathrm{NI}_2$) at steady state, (d) annual average of disease prevalence in questing nymphs ($\mathrm{NI}_2/(\mathrm{NI}_2 + \mathrm{NU}_2)$) at steady state, (e) annual average of disease prevalence in questing adult ticks ($\mathrm{AI}_2/(\mathrm{AI}_2 + \mathrm{AU}_2)$) at steady state, (f) annual average of disease prevalence in competent stationary hosts ($\mathrm{CIS}/(\mathrm{CIS} + \mathrm{CUS})$) at steady state, (g) annual average of disease prevalence in competent mobile hosts ($\mathrm{CIM}/(\mathrm{CIM} + \mathrm{CUM})$) at steady state, (h) maximum daily number of infected nymphs ($\mathrm{NI}_2$) at steady state, (i) maximum daily number of infected adult ticks ($\mathrm{AI}_2$) at steady state, (j) maximum daily number of infected ticks ($\mathrm{AI}_2 + \mathrm{NI}_2$) at steady state, and (k) degree days at steady state.

deer is that the model allocates questing ticks according to the fraction of hosts in a category, and the number of incompetent mobile hosts (deer) is very low compared to the other categories. A questing tick is thus far more likely to find a different host. Those other hosts are effectively decoys. Another possibility is that deer are more prevalent in Dutchess County, NY, than estimates from [39] suggest, increasing the probability of encounter. The model currently

assumes that ticks choose a host based on the probability of encounter measured by relative density of a particular host type, but perhaps, this is not entirely true. It is possible that larvae are in locations where small mammals are more likely to be present, and are more likely to be on these, while adult ticks are higher in the brush and more likely to encounter deer. A survey of feeding ticks on hosts of various types according to their life stage could shed light on this question and possibly offer an electivity index [58, 59] for each stage of questing tick, as has been done for other organisms [60].

*4.2. Effect of Rising Mean Annual Temperature.* We find that increasing temperatures result in a higher risk of Lyme disease. Figure 3 shows that an overall increase in the number of ticks is due more to the longer season of activity, as peak counts do not differ much from one temperature to the next. Similarly, Figures 4(a) and 4(b) show similar peak prevalence of disease in questing ticks regardless of temperature increase, with an overall increase of average prevalence with warmer temperatures due to the extended season.

Figure 5 supports this, showing an average increase in disease prevalence in questing adults and nymphs of 30% for a 6°C temperature increase (Figures 5(c) and 5(d)). The rise in overall numbers of infected ticks is greater, an almost 50% increase for a 6°C temperature increase (Figures 5(a) and 5(b)). However, a field measurement taken at midsummer would show approximately the same population density of infected questing ticks for all mean annual temperatures. The model suggests that increased risk from warmer temperatures comes from somewhat higher tick populations (seen in Figure 4) coupled with a longer season of transmission (seen in Figures 5(a) and 5(b)).

Figure 6 shows a small increase in prevalence among host populations. Figure 4(b) indicates that for the competent stationary hosts, the transmission cycle starts earlier in the season but the peak does not increase much. The dynamics are somewhat different for the competent mobile hosts. For these, the season is longer and the peak is a bit higher (Figure 4(c)). Host prevalence measures show only around 10% increase over the 6-degree rise in temperature (Figures 6(a) and 6(b)).

*4.3. Comparing Risk Measures.* Figure 7 summarizes the relative performance of these various measures of risk compared to the intuitively clear measure of abundance of infected questing ticks ($NI_2 + AI_2$) integrated over the course of the year. Figure 7 shows that overall abundance of infected ticks (bar a in the figure) rises with temperature more quickly than the usual field measurements would indicate. Increased risk of disease for humans is likely to depend on this abundance, which increases with temperature more than disease prevalence in hosts or ticks alone would indicate. Figure 7 in particular indicates that the response of degree days to rising temperature tracks the rising abundance of infected questing ticks better than prevalence measures.

This study does not include human behavior that affects the likelihood of encounter with infected ticks. Overall abundance is a reasonable measure for humans spending time outdoors over a long season, for example, through-hikers on the Appalachian Trail or rural populations. Overall abundance of infected ticks increases by about 50% for this period (Figures 5(a) and 5(b)), largely due to the extended tick season. It is less important for children on a short summer vacation in the country during high tick season, where maximum abundance of infected ticks describes local contact during that period, and which does not vary much with rising temperature (Figure 7).

## 5. Conclusions

The model of tick populations and Lyme disease developed in this study, based on earlier work by Ogden et al. [5, 6], incorporates temperature-dependent maturation rates and six categories of tick host populations based on whether they are incompetent or competent Lyme disease hosts, whether they are infected or uninfected, and whether they are relatively mobile or stationary. The results of the model were compared with field data taken from a variety of studies in the Northeast US. The model produces, on the whole, biologically reasonable results, including the seasonality of tick populations, observed on-host tick burdens, and disease prevalence at steady state.

The model predicts rising risk of Lyme disease with increasing temperature although not all risk measures give the same enhanced increased risk for a given temperature change. Compared to the intuitively clear measure of infected tick abundance, more easily measured quantities such as overall disease prevalence in ticks or hosts rise relatively slowly. Measures of disease prevalence in ticks or hosts at a single time point barely change at all with rising temperature during the high transmission season. These measures are therefore likely to give a lower estimate of increased risk to humans than is the case. Other than absolute measures of infected tick abundance, the best measure of overall risk was degree days greater than zero. For shorter visits to tick-infested areas during the high transmission season, risk would be measured by maximum abundance of infected ticks, which does not change much with temperature.

## Data Availability

All data used in this study came from published, cited sources. The data used to support the findings of this study are available from the corresponding author upon request.

## Conflicts of Interest

The authors declare that there are no conflicts of interest.

## Acknowledgments

The authors wish to acknowledge the generosity of the Neukom Institute for Computational Science and Dartmouth College for supporting both graduate and undergraduate researchers on this project. In addition, the

authors would like to thank Dominic Carrese for his field work.

## References


[1] R. Rosenberg, N. P. Lindsey, M. Fischer et al., "Vital signs: trends in reported vectorborne disease cases—United States and Territories, 2004–2016," *Morbidity and Mortality Weekly Report*, vol. 67, no. 17, pp. 496–501, 2018.

[2] R. Ostfeld, *Lyme Disease: The Ecology of a Complex System*, Oxford University Press, New York, NY, USA, 2010.

[3] K. M. Pepin, M. A. Diuk-Wasser, R. J. Eisen et al., "Geographic variation in the relationship between human Lyme disease incidence and density of infected host-seeking *Ixodes scapularis* nymphs in the eastern United States," *American Journal of Tropical Medicine and Hygiene*, vol. 86, no. 6, pp. 1062–1071, 2012.

[4] T. C. Porco, "A mathematical model of the ecology of Lyme disease," *Mathematical Medicine and Biology*, vol. 16, no. 3, pp. 261–296, 1999.

[5] N. H. Ogden, M. Bigras-Poulin, C. J. O'Callaghan et al., "A dynamic population model to investigate effects of climate on geographic range and seasonality of the tick *Ixodes scapularis*," *International Journal for Parasitology*, vol. 35, no. 4, pp. 375–389, 2005.

[6] N. H. Ogden, L. R. Lindsay, G. Beauchamp et al., "Investigation of relationships between temperature and developmental rates of Tick *Ixodes scapularis* (Acari: ixodidae) in the laboratory and field," *Journal of Medical Entomology*, vol. 41, no. 4, pp. 622–633, 2004.

[7] X. Wu, V. R. S. K. Duvvuri, and J. Wu, "Modeling dynamical temperature influence on tick *Ixodes scapularis* population," in *Proceedings of the 5th International Congress on Environmental Modelling and Software*, Ottawa, ON, Canada, July 2010, https://scholarsarchive.byu.edu/cgi/viewcontent.cgi?article=2268&context=iemssconference.

[8] A. D. M. Dobson, T. J. R. Finnie, and S. E. Randolph, "A modified matrix model to describe the seasonal population ecology of the European tick *Ixodes ricinus*," *Journal of Applied Ecology*, vol. 48, no. 4, pp. 1017–1028, 2011.

[9] M. A. Diuk-Wasser, G. Vourc'h, P. Cislo et al., "Field and climate-based model for predicting the density of host-seeking nymphal *Ixodes scapularis*, an important vector of tick-borne disease agents in the eastern United States," *Global Ecology and Biogeography*, vol. 19, no. 4, pp. 504–514, 2010.

[10] N. H. Ogden, A. Maarouf, I. K. Barker et al., "Climate change and the potential for range expansion of the Lyme disease vector *Ixodes scapularis* in Canada," *International Journal for Parasitology*, vol. 36, no. 1, pp. 63–70, 2006.

[11] N. H. Ogden, L. St-Onge, I. K. Barker et al., "Risk maps for range expansion of the Lyme disease vector, *Ixodes scapularis*, in Canada now and with climate change," *International Journal of Health Geographics*, vol. 7, no. 1, p. 24, 2008.

[12] N. H. Ogden, M. Bigras-Poulin, K. Hanincová, A. Maarouf, C. J. O'Callaghan, and K. Kurtenbach, "Projected effects of climate change on tick phenology and fitness of pathogens transmitted by the North American tick *Ixodes scapularis*," *Journal of Theoretical Biology*, vol. 254, no. 3, pp. 621–632, 2008.

[13] N. H. Ogden, M. Radojević, X. Wu, V. R. Duvvuri, P. A. Leighton, and J. Wu, "Estimated effects of projected climate change on the basic reproductive number of the Lyme disease vector *Ixodes scapularis*," *Environmental Health Perspectives*, vol. 122, no. 6, pp. 631–638, 2014.

[14] J. A. Simon, R. R. Marrotte, N. Desrosiers et al., "Climate change and habitat fragmentation drive the occurrence of *Borrelia burgdorferi*, the agent of Lyme disease, at the northeastern limit of its distribution," *Evolutionary Applications*, vol. 7, no. 7, pp. 750–764, 2014.

[15] P. A. Leighton, J. K. Koffi, Y. Pelcat, L. R. Lindsay, and N. H. Ogden, "Predicting the speed of tick invasion: an empirical model of range expansion for the Lyme disease vector *Ixodes scapularisin* Canada," *Journal of Applied Ecology*, vol. 49, no. 2, pp. 457–464, 2012.

[16] J. S. Brownstein, T. R. Holford, and D. Fish, "A climate-based model predicts the spatial distribution of the Lyme disease vector *Ixodes scapularis* in the United States," *Environmental Health Perspectives*, vol. 111, no. 9, pp. 1152–1157, 2003.

[17] K. L. Gage, T. R. Burkot, R. J. Eisen, and E. B. Hayes, "Climate and vectorborne diseases," *American Journal of Preventive Medicine*, vol. 35, no. 5, pp. 436–450, 2008.

[18] J. J. Hess, J. N. Malilay, and A. J. Parkinson, "Climate change," *American Journal of Preventive Medicine*, vol. 35, no. 5, pp. 468–478, 2008.

[19] A. Greer, V. Ng, and D. Fisman, "Climate change and infectious diseases in North America: the road ahead," *Canadian Medical Association Journal*, vol. 178, no. 6, pp. 715–722, 2008.

[20] R. Shope, "Global climate change and infectious diseases," *Environmental Health Perspectives*, vol. 96, pp. 171–174, 1991.

[21] D. A. Jobe, S. D. Lovrich, J. A. Nelson et al., "*Borrelia burgdorferiin Ixodes scapularis* ticks, Chicago area," *Emerging Infectious Diseases*, vol. 12, no. 6, pp. 1039–1041, 2006.

[22] N. H. Ogden and L. R. Lindsay, "Effects of climate and climate change on vectors and vector-borne diseases: ticks are different," *Trends in Parasitology*, vol. 32, no. 8, pp. 646–656, 2016.

[23] N. H. Ogden, L. R. Lindsay, M. Morshed, P. N. Sockett, and H. Artsob, "The emergence of Lyme disease in Canada," *Canadian Medical Association Journal*, vol. 180, no. 12, pp. 1221–1224, 2009.

[24] J. S. Brownstein, T. R. Holford, and D. Fish, "Effect of climate change on Lyme disease risk in North America," *EcoHealth*, vol. 2, no. 1, pp. 38–46, 2005.

[25] N. H. Ogden, M. Bigras-Poulin, C. J. O'callaghan et al., "Vector seasonality, host infection dynamics and fitness of pathogens transmitted by the tick *Ixodes scapularis*," *Parasitology*, vol. 134, no. 2, pp. 209–227, 2007.

[26] H. D. Gaff and L. J. Gross, "Modeling tick-borne disease: a metapopulation model," *Bulletin of Mathematical Biology*, vol. 69, no. 1, pp. 265–288, 2007.

[27] M. McPherson, A. García-García, F. J. Cuesta-Valero et al., "Expansion of the Lyme disease vector *Ixodes scapularis* in Canada inferred from CMIP5 climate projections," *Environmental Health Perspectives*, vol. 125, no. 5, article 057008, 2017.

[28] D. J. Lieske and V. K. Lloyd, "Combining public participatory surveillance and occupancy modelling to predict the distributional response of *Ixodes scapularis* to climate change," *Ticks and Tick-Borne Diseases*, vol. 9, no. 3, pp. 695–706, 2018.

[29] R. S. Ostfeld and J. L. Brunner, "Climate change and *Ixodes* tick-borne diseases of humans," *Philosophical Transactions of the Royal Society B: Biological Sciences*, vol. 370, no. 1665, p. 20140051, 2015.

[30] T. L. Johnson, K. A. Boegler, R. J. Clark et al., "An acarological risk model predicting the density and distribution of host-seeking *Ixodes scapularis* nymphs in Minnesota," *American*

*Journal of Tropical Medicine and Hygiene*, vol. 98, no. 6, pp. 1671–1682, 2018.

[31] K. M. Clow, N. H. Ogden, L. R. Lindsay, P. Michel, D. L. Pearl, and C. M. Jardine, "The influence of abiotic and biotic factors on the invasion of *Ixodes scapularis* in Ontario, Canada," *Ticks and Tick-Borne Diseases*, vol. 8, no. 4, pp. 554–563, 2017.

[32] K. C. Stafford, M. L. Cartter, L. A. Magnarelli, S. H. Ertel, and P. A. Mshar, "Temporal correlations between tick abundance and prevalence of ticks infected with *Borrelia burgdorferi* and increasing incidence of Lyme disease," *Journal of Clinical Microbiology*, vol. 36, no. 5, pp. 1240–1244, 1998.

[33] M. E. Adelson, R.-V. S. Rao, R. C. Tilton et al., "Prevalence of *Borrelia burgdorferi*, *Bartonella* spp., *Babesia microti*, and *Anaplasma phagocytophila* in *Ixodes scapularis* ticks collected in Northern New Jersey," *Journal of Clinical Microbiology*, vol. 42, no. 6, pp. 2799–2801, 2004.

[34] J. F. Anderson, R. C. Johnson, and L. A. Magnarelli, "Seasonal prevalence of *Borrelia burgdorferi* in natural populations of white-footed mice, *Peromyscus leucopus*," *Journal of Clinical Microbiology*, vol. 25, no. 8, pp. 1564–1566, 1987.

[35] J. Bunikis, J. Tsao, C. J. Luke, M. G. Luna, D. Fish, and A. G. Barbour, "*Borrelia burgdorferi* infection in a natural population of *Peromyscus Leucopus* mice: a longitudinal study in an area where Lyme borreliosis is highly endemic," *Journal of Infectious Diseases*, vol. 189, no. 8, pp. 1515–1523, 2004.

[36] The Mathworks. Inc., "USG Matlab," *The Mathworks. Inc.,* Natick, MA, USA, 1992.

[37] K. A. Berger, H. S. Ginsberg, L. Gonzalez, and T. N. Mather, "Relative humidity and activity patterns of *Ixodes scapularis* (Acari: ixodidae)," *Journal of Medical Entomology*, vol. 51, no. 4, pp. 769–776, 2014.

[38] L. Bennet, A. Halling, and J. Berglund, "Increased incidence of Lyme borreliosis in southern Sweden following mild winters and during warm, humid summers," *European Journal of Clinical Microbiology & Infectious Diseases*, vol. 25, no. 7, pp. 426–432, 2006.

[39] T. Levi, F. Keesing, R. D. Holt, M. Barfield, and R. S. Ostfeld, "Quantifying dilution and amplification in a community of hosts for tick-borne pathogens," *Ecological Applications*, vol. 26, no. 2, pp. 484–498, 2016.

[40] K. LoGiudice, R. S. Ostfeld, K. A. Schmidt, and F. Keesing, "The ecology of infectious disease: effects of host diversity and community composition on Lyme disease risk," *Proceedings of the National Academy of Sciences*, vol. 100, no. 2, pp. 567–571, 2003.

[41] S. A. Hamer, J. I. Tsao, E. D. Walker, and G. J. Hickling, "Invasion of the Lyme disease vector *Ixodes Scapularis*: implications for *Borrelia burgdorferi* endemicity," *EcoHealth*, vol. 7, no. 1, pp. 47–63, 2010.

[42] P. W. Rand, C. Lubelczyk, G. R. Lavigne et al., "Deer density and the abundance of *Ixodes scapularis* (Acari: ixodidae)," *Journal of Medical Entomology*, vol. 40, no. 2, pp. 179–184, 2003.

[43] T. J. Daniels, R. C. Falco, K. L. Curran, and D. Fish, "Timing of *Ixodes scapularis* (Acari: ixodidae) oviposition and arval activity in southern New York," *Journal of Medical Entomology*, vol. 33, no. 1, pp. 140–147, 1996.

[44] M. R. Bertrand and M. L. Wilson, "Microclimate-dependent survival of unfed adult *Ixodes scapularis* (Acari: ixodidae) in nature: life cycle and study design implications," *Journal of Medical Entomology*, vol. 33, no. 4, pp. 619–627, 1996.

[45] J. L. Brunner, M. Killilea, and R. S. Ostfeld, "Overwintering survival of nymphal *Ixodes scapularis* (Acari: ixodidae) under natural conditions," *Journal of Medical Entomology*, vol. 49, no. 5, pp. 981–987, 2012.

[46] A. Hojgaard, R. J. Eisen, and J. Piesman, "Transmission dynamics of *Borrelia burgdorferis*.s. During the key third day of feeding by nymphal *Ixodes scapularis* (Acari: ixodidae)," *Journal of Medical Entomology*, vol. 45, no. 4, pp. 732–736, 2008.

[47] J. O. Whitaker and W. J. Hamilton, *Mammals of the Eastern United States*, Cornell University Press, Ithaca, NY, USA, 1998.

[48] P. Porneluzi, M. A. Van Horn, and T. M. Donovan, *The Birds of North America Online*, P. G. Rodewald, Ed., Cornell Lab of Ornithology, Ithaca, NY, USA, 2011, https://birdsna.org/.

[49] R. S. Ostfeld, K. R. Hazler, and O. M. Cepeda, "Temporal and spatial dynamics of *Ixodes scapularis* (Acari: ixodidae) in a rural landscape," *Journal of Medical Entomology*, vol. 33, no. 1, pp. 90–95, 1996.

[50] R. S. Ostfeld, O. M. Cepeda, K. R. Hazler, and M. C. Miller, "Ecology of Lyme disease: habitat associations of ticks (*Ixodes scapularis*) in a rural landscape," *Ecological Applications*, vol. 5, no. 2, pp. 353–361, 1995.

[51] L. R. Lindsay, S. W. Mathison, I. K. Barker, S. A. McEwen, T. J. Gillespie, and G. A. Surgeoner, "Microclimate and habitat in relation to *Ixodes scapularis* (Acari: ixodidae) populations on long point, Ontario, Canada," *Journal of Medical Entomology*, vol. 36, no. 3, pp. 255–262, 1999.

[52] K. A. Schmidt, R. S. Ostfeld, and E. M. Schauber, "Infestation of *Peromyscus leucopus* and *Tamias striatus* by *Ixodes scapularis* (Acari: ixodidae) in relation to the abundance of hosts and parasites," *Journal of Medical Entomology*, vol. 36, no. 6, pp. 749–757, 1999.

[53] L. R. Lindsay, S. W. Mathison, I. K. Barker, S. A. McEwen, and G. A. Surgeoner, "Abundance of *Ixodes scapularis* (Acari: ixodidae) larvae and nymphs in relation to host density and habitat on long point, Ontario," *Journal of Medical Entomology*, vol. 36, no. 3, pp. 243–254, 1999.

[54] M. J. Menne, I. Durre, R. S. Vose, B. E. Gleason, and T. G. Houston, "An overview of the global historical climatology network-daily database," *Journal of Atmospheric and Oceanic Technology*, vol. 29, no. 7, pp. 897–910, 2012.

[55] M. J. Menne, I. Durre, B. Korzeniewski et al., *Global Historical Climatology Network—Daily. Version 3.22*, NOAA National Climatic Data Center, Asheville, NC, USA, ftp://ftp.ncdc.noaa.gov/pub/data/ghcn/daily, 2012.

[56] NOAA National Centers for Environmental Information, *Local Climatological Dataset, Lebanon Municipal Airport*, NOAA National Centers for Environmental Information, Asheville, NC, USA, 2018, https://www.ncdc.noaa.gov/cdo-web/datasets/LCD/stations/WBAN:94765/detail.

[57] R. S. Vose, D. R. Easterling, K. E. Kunkel, A. N. LeGrande, and M. F. Wehner, "Temperature changes in the United States," in *Climate Science Special Report: Fourth National Climate Assessment, Volume I*, D. J. Wuebbles, D. W. Fahey, K. A. Hibbard, D. J. Dokken, B. C. Stewart, and T. K. Maycock, Eds., U.S. Global Change Research Program, Washington, DC, USA, pp. 185–206, 2017.

[58] J. Jacobs, "Quantitative measurement of food selection," *Oecologia*, vol. 14, no. 4, pp. 413–417, 1974.

[59] J. Chesson, "The estimation and analysis of preference and its relatioship to foraging models," *Ecology*, vol. 64, no. 5, pp. 1297–1304, 1983.

[60] M. J. Lechowicz, "The sampling characteristics of electivity indices," *Oecologia*, vol. 52, no. 1, pp. 22–30, 1982.

Hindawi
Canadian Journal of Infectious Diseases and Medical Microbiology
Volume 2019, Article ID 9392414, 8 pages
https://doi.org/10.1155/2019/9392414

*Research Article*

# Application of kDNA Minicircle PCR-RFLP to Characterize *Leishmania donovani* Clinical Isolates Obtained from Post-Kala-Azar Dermal Leishmaniasis in Eastern Nepal

**Ojesh Pokhrel,[1] Keshav Rai,[1] Narayan Raj Bhattarai,[1] Suman Rijal,[2] Arpana Rijal,[3] and Basudha Khanal[1]**

[1]*Department of Microbiology, B. P. Koirala Institute of Health Sciences, Dharan, Nepal*
[2]*Department of Internal Medicine, B. P. Koirala Institute of Health Sciences, Dharan, Nepal*
[3]*Department of Dermatology, B. P. Koirala Institute of Health Sciences, Dharan, Nepal*

Correspondence should be addressed to Keshav Rai; raikeshav@hotmail.com

Received 19 April 2019; Accepted 8 July 2019; Published 30 July 2019

Guest Editor: Dimosthenis Chochlakis



Post-kala-azar dermal leishmaniasis (PKDL) is a skin manifestation of visceral leishmaniasis (VL) which develops after apparent cure in some patients. PKDL is considered as the potential reservoir for the VL infection. Molecular epidemiological characterization of *L. donovani* isolates obtained from VL and PKDL isolates is essentially required in order to understand the transmission dynamics of the VL infection. To date, genetic variation among the VL and PKDL *L. donovani* isolates was not fully elucidated. Therefore, 14 clinical isolates from VL and 4 clinical isolates from PKDL were speciated by *hsp70* and rDNA genes. Further characterization of *L. donovani* by *haspB* PCR demonstrates two different genotypes. All PKDL isolates have the same genetic structure. kDNA PCR-RFLP assay revealed 18 different genotypes; however, structural analysis showed the two distinct kDNA genotype population ($k = 2$). The kDNA fingerprint patterns of parasites from hilly districts were clustered separately from low-land districts. Therefore, further study with a large number of samples is urgently required for systematic characterization of the clinical isolates to track the molecular epidemiology of the *Leishmania donovani* causing VL and the role of PKDL as a reservoir.

## 1. Introduction

Post-kala-azar dermal leishmaniasis (PKDL) is a progression of visceral leishmaniasis (VL) that demonstrates lesions or hypopigmented skin rashes in patients even after successful treatment of VL [1]. This cryptic PKDL is characterised by papular, macular, and/or nodular lesions throughout the body, mainly demonstrated on the face, trunk, legs, arms, and genitals. About 5–10% of patients infected with VL develop PKDL in the Indian subcontinent [2]. In Nepal, PKDL occurs in 2.4% of previously treated cases of VL with 1.4% estimated to be at risk within 2 years of treatment [3] whereas in case of India, the interval ranges between 2 and 7 years [4].

The PKDL skin lesion has a tendency to become chronic and harbours the parasite, hence considered as a reservoir, especially challenging the elimination programme of VL from the Indian subcontinent [5, 6]. The clinical, epidemiological, parasitological, and immunological development of PKDL is not yet fully understood [7]. In fact, the eradication of PKDL could be an essential factor for the current VL elimination programme. Moreover, the asymptomatic VL infection is also considered as the reservoir for VL transmission that threatens for VL elimination in the Indian subcontinent [8]. The immunological responses are also found to be different in patients with VL and PKDL [2]. Hence, the molecular epidemiology of *L. donovani* causing different clinical manifestations is required to understand in order to minimize the risk of VL elimination in the Indian subcontinent. The genetic analysis has shown the significant heterogeneity among the Indian *L. donovani* isolates that cause different clinical presentations such as VL and PKDL [9, 10]. But no such data on genetic characterization of *L.*

*donovani* isolates from Nepal were available yet. Therefore, we focused on the study of the genetic characterization of VL and PKDL parasite isolates from Nepal using available highly efficient molecular assay kDNA minicircles PCR-RFLP together with *haspB* PCR assay.

## 2. Materials and Methods

*2.1. Sample Collection and Parasite Isolation.* The sample collection consisted of *L. donovani* clinical isolates from 14 VL and 4 PKDL patients who were presented between January 2013 and June 2014 at B. P. Koirala Institute of Health Sciences (BPKIHS), a tertiary care hospital in Dharan, Nepal. Ethical clearance was obtained from Institutional Ethical Review Board (IERB), BPKIHS, Nepal. Written consent was obtained from all patients or from parents or guardians in case of children. Promastigote forms of *L. donovani* were isolated from bone marrow aspirates of VL patients and skin punch biopsy of PKDL patients. Parasite culture was performed by inoculating the clinical specimens in Tobie's blood agar medium with Locke's overlay, with 200 IU/ml penicillin and 200 $\mu$g/ml streptomycin [11]. Once the parasites were fully grown from the clinical material, they were transferred to M199 (Sigma-Aldrich, cat. no. 2520) with 20% fetal calf serum (Invitrogen, cat. no. 10270) + adenosine + haemin.

*2.2. Parasite DNA Extraction and Species Identification.* DNA was extracted from parasite cultures using the QIAamp DNA mini kit (Qiagen, http://www.qiagen.com). Parasites in late logarithmic growth phase were washed thrice with sterile PBS solution, and DNA was eluted in 200 $\mu$L AE buffer. DNA concentration and purity were verified by spectrophotometric measurement with the BioPhotometer plus (Eppendorf). The *Leishmania donovani* species was confirmed using PCR-RFLP analysis of the heat-shock protein 70 gene (*hsp70*). The fragments referred to as HSP70-N [12, 13] were digested with restriction enzymes HincII [14] (Promega, cat. no. R6031) and MluI (Promega, cat. no. R6381).

In addition, the *Leishmania* genus screening was also done by rRNA-specific PCR with the forward primer 18S-L-F (5′-CGTAGTTGAACTGTGGGCTGTGC-3′) and the reverse primer 18S-L-R (5′-ACTCCCGTGTTTCTTGTTTCTTT-GAA-3′) [15]. We followed the methods described by Ostyn et al. [16]. The PCR were done in 25 $\mu$l containing 1X PCR buffer, 2.5 mM $MgCl_2$, 200 $\mu$M of each dNTP (Eurogentec), 0.1 mg/ml of bovine serum albumin (Promega), 0.8 $\mu$M of each primer (Sigma-Aldrich), and 0.5 unit of HotStar Taq DNA polymerase (Qiagen, cat. no. 203605). Finally, 100 pg of template DNA was added. The thermocycling program was (i) initial denaturation at 94°C for 5 minutes; (ii) 40 cycles of denaturation at 94°C for 30 seconds and 60°C for 30 seconds and extension at 72°C for 45 seconds; and (iii) final extension at 72°C for 5 minutes. In addition, *L. donovani* isolate DNA (BPK282/0 cl4) as a positive control and two no-template controls were included in each experiment. The amplified PCR products were visualised on 2% agarose gel after electrophoresis at 5 V/cm and ethidium bromide staining. Hence, the positive PCR results show DNA band at 115 bp. In order to rule out the false-negative PCR results, plasmid DNA cloned with oligonucleotide (236 bp) was used as an internal control [17].

*2.3. L. donovani Genotyping Assay*

*2.3.1. haspB PCR.* The *haspB* PCR for K26 antigen detection was used as species screening for *L. donovani* by primers K26f (5′-ACGAAGGACTCCGCAAAG-3′) and K26r (5′-TTCCCATCGTTTTGCTG-3′) [18]. The PCR master mix was prepared in 50 $\mu$l containing 1X Qiagen PCR buffer, 1.5 mM $MgCl_2$, 200 $\mu$m of each dNTP (Eurogentec), 0.5 $\mu$M of each primer (Sigma-Aldrich), and 1 U of HotStar Taq polymerase. Amplification was done with (i) initial denaturation step of 95°C for 5 minutes; (ii) 35 cycles of denaturation at 94°C for 30 seconds, annealing at 50°C for 30 seconds, and extension at 72°C for 60 seconds; and (iii) a final extension at 72°C for 10 minutes. Out of two *haspB* genotypes identified, genotype A has amplicon size of 640 bp and genotype B has amplicon size of 320 bp.

*2.3.2. kDNA PCR-RFLP.* Genotyping of *L. donovani* clinical isolates was also done by kDNA PCR-RFLP assay. First, the kDNA minicircle is amplified by PCR using the primer pairs BPKMINFOR (5′-CTGGGGGTTGGTGTAAAATAGGGC-3′) and BPKDNAMINREV (5′-CCCGATTTTTGGCATTTTTGG-3′). The PCR master mix was prepared in 50 $\mu$l containing 1X PCR buffer, 2 mM $MgCl_2$, 200 $\mu$M of each dNTP (Eurogentec), 0.5 $\mu$M of each primer (Sigma-Aldrich), 1 U of HotStar Taq polymerase, and about 1 ng of template DNA. Amplification was done with (i) initial denaturation step of 95°C for 5 minutes; (ii) 40 cycles of denaturation at 94°C for 1 minute, annealing at 60°C for 1 minute, and extension at 72°C for 1 minute; and (iii) a final extension at 72°C for 10 minutes. The PCR amplicon verified at 800 bp was precipitated with 0.3 M sodium acetate and 100% ethanol at −20°C overnight. The pellets were washed with 70% ethanol, and restriction digestion was done on precipitated PCR amplicons. Restriction digestion was done in a total of 20 $\mu$l of the buffer with 10 units of HaeIII and incubated at 37°C overnight. The reaction was stopped by heating to 80°C for 20 minutes, and then the fragments were analysed by electrophoresis in 3.75 V/cm in a 3% metaphor agarose gel (Lonza, USA), after staining with ethidium bromide.

The patterns of fingerprint bands were analysed using Gel Compare II 6.6 (Applied Maths, Ghent, Belgium) software. The spectral analysis was used to remove the background noise using the gel picture without signal saturation. Other gel artefacts were filtered out using the DNA ladder at both sides and middle part of each gel. Only the region between 200 and 600 bp was considered for fingerprint analysis, following the digested fragments demonstrated by Bhattarai et al. Similarity matrix was made and UPGMA dendrogram was built. The validity of each branch was evaluated using Pearson's correlation coefficient between the dendrogram derived and the original curve similarities. To assure the reliability of the clusters, the

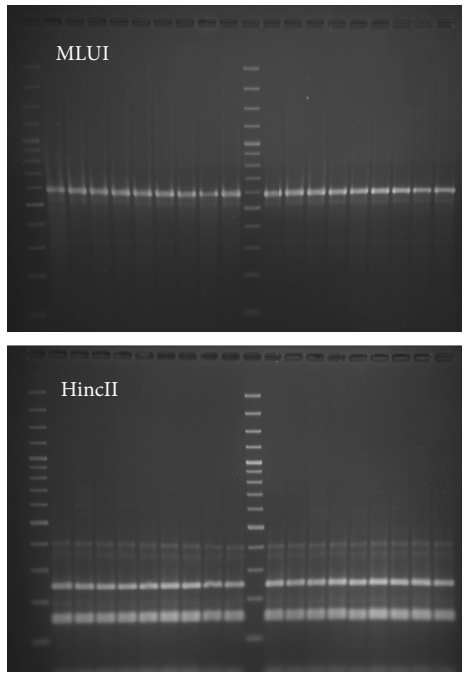


Figure 1: Gel picture of *hsp70* restriction digested products showing the isolates of *L. donovani* species.

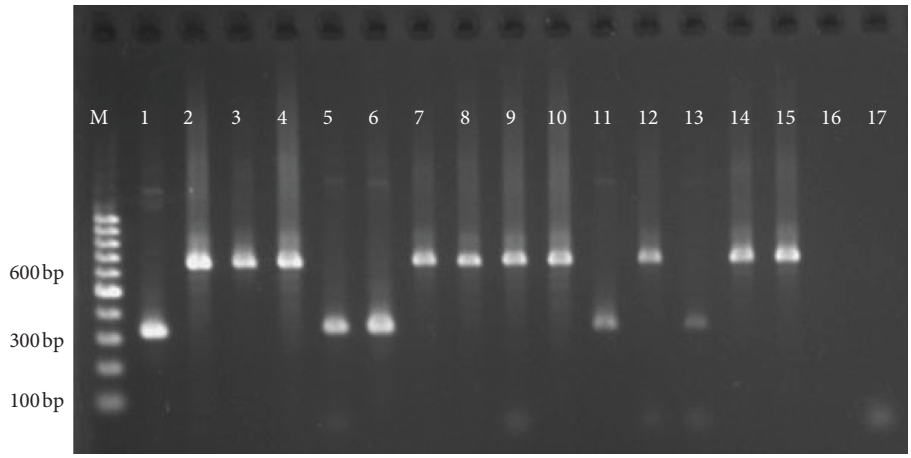


Figure 2: Gel picture of *haspB* PCR showing PCR products at 320 bp and 640 bp. Note: M: DNA ladder, 1: BPK806/0, 2: BPK811/0, 3: BPK814/0, 4: BPK813/0, 5: 63232-Fx, 6: 63233-Fx, 7: 63238-Fx, 8: 63241-Fx, 9: 63245-Fx, 10: 63256-Fx, 11: 63269-Fx, 12: BPK-PKN435, 13: 63277-Fx, 14: BPK-PKN467, 15: BPK-PKN468, 16: negative control N1, and 17: negative control N2.

duplicate experiments were done. Furthermore, four consecutive subcultures of two parasites 63291-Fx and BPK-PKN468 were examined to minimize the experimental variations.

The Bayesian clustering approach was also employed to estimate the kDNA population structure using Structure v2.3.4 [19]. $L(K)$, $L(K)'$, and $\Delta K$ were computed from 50 runs for $1 \leq K \leq 10$ using a burn-in of $10^4$ and run length of $10^5$ iterations. For each RFLP band, allelic diversity for each population was calculated for the number of individuals.

## 3. Result

All parasite isolates were confirmed as *L. donovani* species by *hsp70* as shown in Figure 1 and rRNA assay. *haspB assay* was classified into group A ($n = 6$) and group B ($n = 12$) as shown in Figure 2. Most of the group A parasites were originated from hilly districts, namely, Bhojpur, Khotang, and Okhaldhunga, except the one parasite from Sunsari (Figure 3). In contrast, the group B parasites were isolated from low-land districts (Terai) such as Jhapa, Morang, Sunsari, Saptari, and Siraha. In case of clinical presentation in

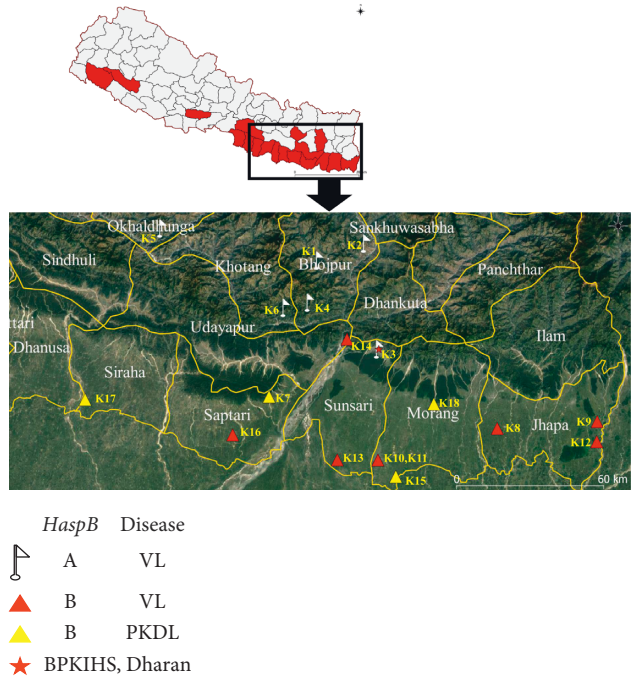


Figure 3: Spatial distribution of different genotypes and disease in Eastern Nepal.

Table 1: Genotypes of clinical isolates and their geographical origin.

| VL/PKDL | Isolates | Origins | | Genotypes | |
|---|---|---|---|---|---|
| | | District | VDC | *haspB* | kDNA RFLP |
| VL | BPK806/0 | Bhojpur | Pawala | A | K4 |
| VL | BPK811/0 | Saptari | Rajbiraj | B | K16 |
| VL | BPK813/0 | Morang | Biratnagar | B | K10 |
| VL | BPK814/0 | Jhapa | Chandragadhi | B | K9 |
| VL | 63232-Fx | Bhojpur | Mane Bhanjyang | A | K1 |
| VL | 63233-Fx | Bhojpur | Jarayotar | A | K2 |
| VL | 63238-Fx | Jhapa | Gauradaha | B | K8 |
| VL | 63241-Fx | Jhapa | Maheshpur | B | K12 |
| VL | 63245-Fx | Morang | Biratnagar | B | K11 |
| VL | 63256-Fx | Morang | Dewanganj | B | K13 |
| VL | 63269-Fx | Khotang | Wopung | A | K6 |
| VL | 63277-Fx | Sunsari | Dharan | A | K3 |
| VL | 63291-Fx | Sunsari | Chatara | B | K14 |
| VL | 63294-Fx | Okhaldhunga | Obu | A | K5 |
| PKDL | BPK-PKN435 | Morang | Jahada | B | K18 |
| PKDL | BPK-PKN466 | Morang | Majhare | B | K15 |
| PKDL | BPK-PKN467 | Siraha | Siraha | B | K17 |
| PKDL | BPK-PKN468 | Saptari | Rupnagar | B | K7 |

patients, group A parasites were isolated only from VL patients whereas group B parasites were isolated from both VL and PKDL patients as shown in Table 1.

kDNA minicircle PCR-RFLP identified 18 different genotypes which were distributed as follows: six genotypes (K1, K2, K3, K4, K5, and K6) were isolated from hilly districts and remaining 12 genotypes (K7 to K18) were isolated from low-land districts as depicted in Figure 3. The interexperimental variability was controlled by testing the duplicate samples of parasite isolates in different gels and included in the dendrogram analysis as shown in Figure 4, and gel image of restriction fragments is shown in Figures 5 and 6. The distribution of kDNA genotypes is also depicted in Table 1. The output from the structure also showed the two distinct populations of kDNA ($K = 2$) as shown in Figure 7. Hence, two distinctly different *L. donovani* parasite populations were identified with kDNA genotyping.

Among two different approaches of genotyping, six kDNA genotypes (K1, K2, K3, K4, K5, and K6) were sharing same characteristics with group A *haspB* genotype. Other 12

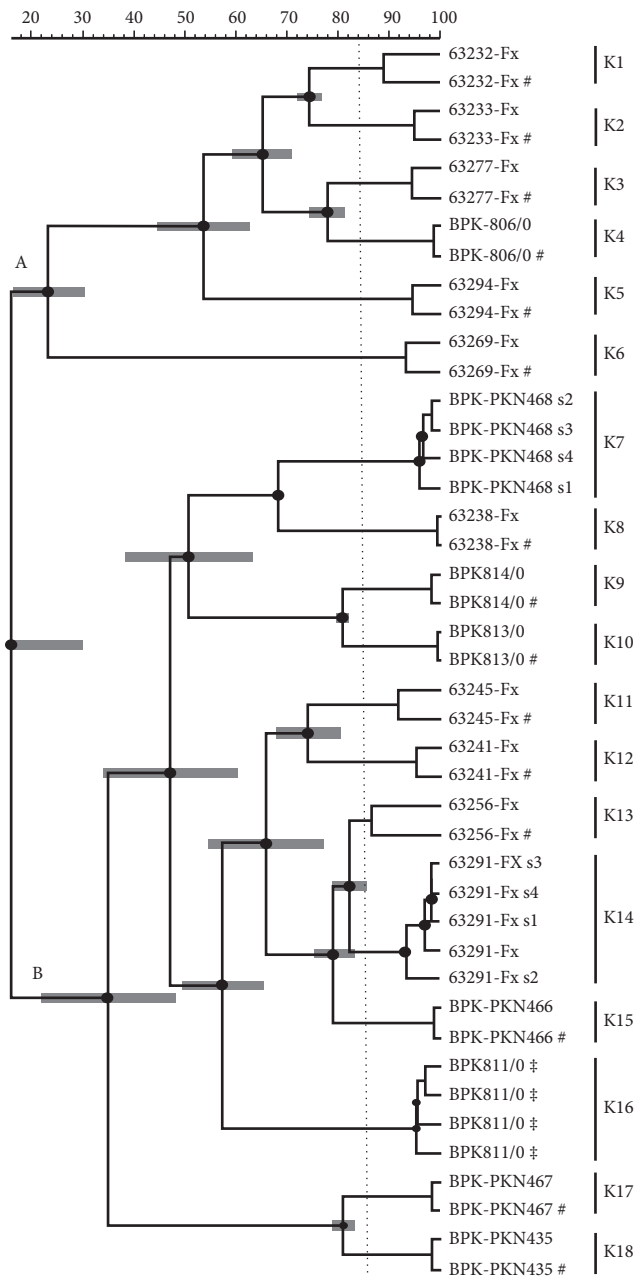


Figure 4: UPGMA dendrogram of all the 18 isolates obtained from kDNA PCR-RFLP (HaeIII) fingerprint data considering the densitometric curve. #: duplicate samples; s2–s4: four consecutive subcultures; ‡ control samples. A and B: groups separated according to *haspB* PCR product size.

kDNA genotypes (K7 to K18) had the same genetic characteristic with group B *haspB* genotype as shown in Figure 4.

## 4. Discussion

VL and PKDL are still considered as major public health problems in South Asian countries such as Nepal. PKDL cases are considered as reservoirs to maintain the endemicity during interepidemic period, but less attention has been given to explore the PKDL epidemiology. This may potentially jeopardize all the achievements of ongoing elimination programme. In fact, molecular epidemiology study has been limited to VL cases only [20, 21]. No such data are available in Nepalese PKDL cases. In this context, we aim to genetically characterize the *L. donovani* parasite causing VL and PKDL by the two assays (a) *haspB* PCR and (b) kDNA PCR-RFLP and explore the genetic similarity between these parasites with different clinical manifestations. This study differentiated the parasites into two different *haspB* genotypes, which is consistent with the finding of Bhattarai et al. We found that parasites isolated from hill districts had significantly different genotypes and PKDL were not identified in isolates from hill districts. The finding of this study indicates that the *L. donovani* genotypes have association

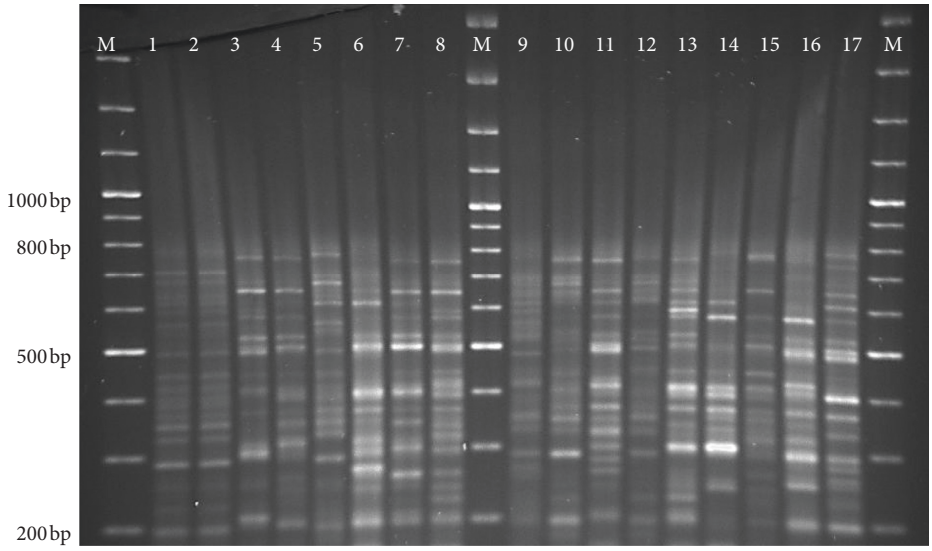


Figure 5: Gel picture of kDNA PCR-RFLP using HaeIII restriction digested products. Note: M: DNA ladder, Lane 1: BPK806, Lane 2: BPK806 (duplicate sample), Lane 3: BPK813, Lane 4: BPK814, Lane 5: 63233-Fx, Lane 6: 63241-Fx, Lane 7: 63245-Fx, Lane 8: 63256-Fx, Lane 9: 63269-Fx, Lane 10: 63277-Fx, Lane 11: 63291-Fx, Lane 12: 63294-Fx, Lane 13: BPK-PKN435, Lane 14: BPK-PKN467, Lane 15: BPK-PKN468, Lane 16: BPK811, and Lane 17: BPK-PKN466.

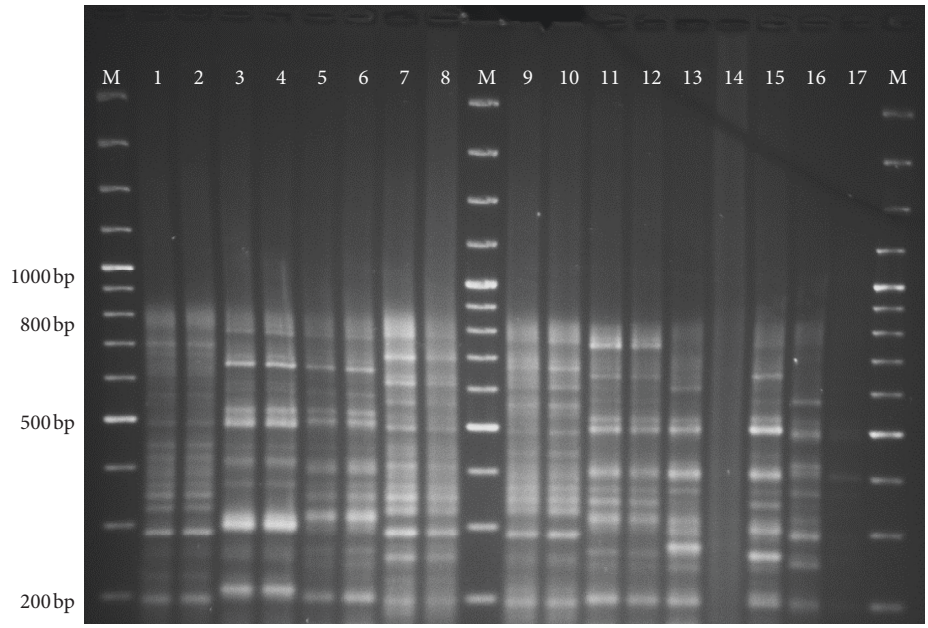


Figure 6: Gel picture of kDNA PCR-RFLP using HaeIII restriction digested products. Note: M: DNA ladder, Lane 1: BPK806, Lane 2: BPK813, Lane 3: BPK814, Lane 4: 63232-Fx, Lane 5: 63233-Fx, Lane 6: 63238-Fx, Lane 7: 63241-Fx, Lane 8: 63245-Fx, Lane 9: 63256-Fx, Lane 10: 63269-Fx, Lane 11: 63277-Fx, Lane 12: 63294-Fx, Lane 13: BPK-PKN435, Lane 14: BPK-PKN467, Lane 15: BPK-PKN468, Lane 16: BPK811, and Lane 17: BPK-PKN466.

with clinical features of leishmaniasis, and similar finding has also been demonstrated in Sri Lanka by Kariyaswami et al. [22]. This genotype diversity in these isolates needs further exploration to further confirm whether these clinical isolates are different, not only in their genetic makeup, but also in their clinical manifestation, epidemiology, antigenicity, and parasitic factor as well.

In addition, another molecular marker kDNA owing to its high amount of heterogeneity has been exploited by the molecular biologist for strain characterization in *Leishmania* to depict the microepidemiology of the parasite [20, 23, 24]. The kDNA RFLP is sensitive to interexperimental as well as interlaboratory variations, so robust protocol should be followed for reproducible result. To achieve reliable result, we used the standardized amount of DNA for PCR and RFLP assay, experimental control was included in each batch of RFLP, four consecutive subcultures of same isolates were studied, and for further robustness, all the samples were

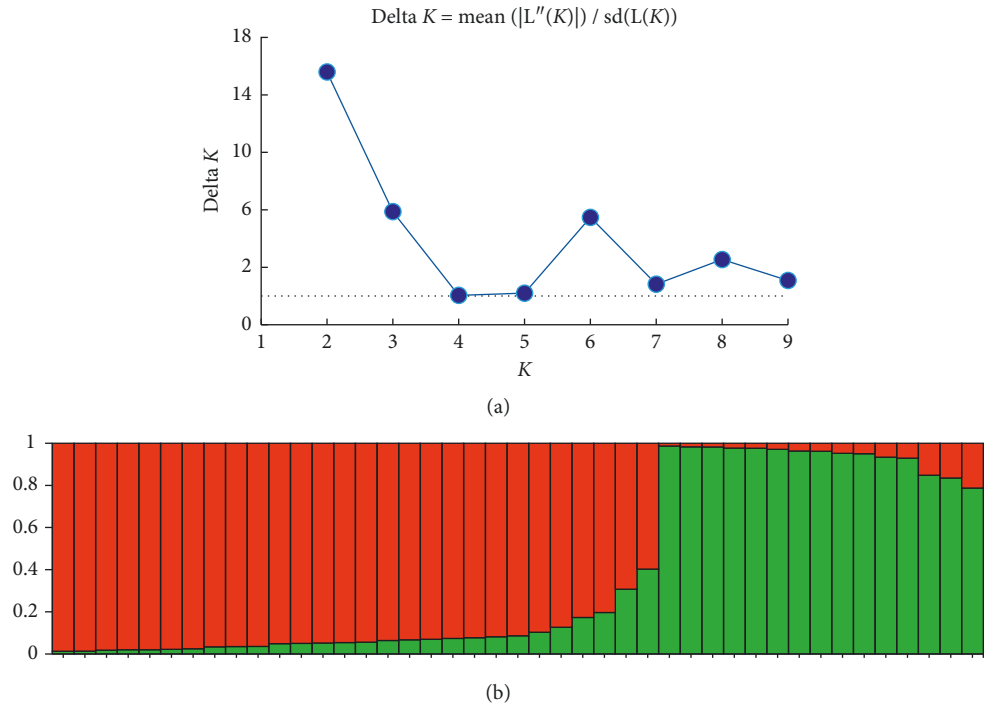


Figure 7: *L. donovani* kDNA genotypes determined by Structure v2.3.4. (a) Structure Harvester output for the determination of $K$ (http://taylor0.biology.ucla.edu/structureHarvester/). Two distinct populations of kDNA genotypes are determined ($k = 2$). (b) Summary plot of estimates of $Q$ value. Each individual data is represented by a single vertical line broken into $K$ coloured segments, with length proportional to each of the $K$ inferred clusters.

studied in duplicates. In this study, kDNA fingerprint showed the distinct clusters of two separate genotypes which were consistent with group A and group B, as determined by *haspB* PCR. This indicates further proof of principle that these isolates had genetically separate entity that influences the different clinical manifestations such as visceral or dermal manifestation in patients. Similar findings have been reported from the Indian subcontinent using $\beta$-tubulin gene as a probe where parasites from VL and PKDL were randomly clustered in between different assigned genotypes [9]. Another study using probe Ldp13 also showed genetic heterogeneity among VL and PKDL isolates from the Indian subcontinent [10]. This is particularly interesting because the Sudanese isolates were found to have similar genetic makeup by various PCR fingerprinting methods [25]. The mechanism of parasite diversification between VL and PKDL is still a matter of research, but some evidence points towards the contributory role of immune response of patient [2].

Ostyn et al. demonstrated that the VL infections at hilly districts were locally transmitted, and in this study, we also found the different *L. donovani* genotypes circulating in hilly districts. Hence, Ostyn et al. documented the expansion of VL in new endemic hilly areas of Nepal which is verified by the evidence obtained from the study of epidemiology, microbiology, clinical, and entomology [16]. Moreover, *Phlebotomus argentipes* sandfly infected with *L. donovani* were identified, and hence, the asymptomatic infections were also reported in hilly districts by Ostyn et al. This might be the influence of recent increasing trends of temperature in hills due to the global warming that favours the breeding of sandfly vector populations. Therefore, it is an urgent need to explore the role of PKDL as a probable reservoir for VL in order to understand the transmission dynamic of VL together with global impact of climate change.

## 5. Conclusions

This study concludes that PKDL and VL clinical parasite isolates were genetically separated and most of them confined to particular geographic location of Nepal. However, different molecular tools are developed elsewhere [26]; the high discriminatory power of kDNA PCR-RFLP tool could be useful in the analysis of molecular epidemiology of VL and PKDL in future.

## Data Availability

This is a hospital-based study. Samples were collected during the routine diagnostic and genotyping procedure. Therefore, the data of the analysis are available upon request from the corresponding author or Head, Department of Microbiology (hod.microbiology@bpkihs.edu), B. P. Koirala Institute of Health Sciences, Dharan, Nepal.

## Conflicts of Interest

The authors declare that there are no conflicts of interest regarding the publication of this paper.

## Acknowledgments

We wish to express our kind gratitude to Ganesh Sah and Iccha Ghale from the Kala-Azar Laboratory (B. P. Koirala Institute of Health Sciences) for their cooperation and kind support for this study. The department fund from B. P. Koirala Institute of Health Sciences was used to complete this study.

## References

[1] S. Ganguly, N. K. Das, J. N. Barbhuiya, and M. Chatterjee, "Post-kala-azar dermal leishmaniasis—an overview," *International Journal of Dermatology*, vol. 49, no. 8, pp. 921–931, 2010.

[2] E. E. Zijlstra, A. M. Musa, E. A. Khalil, I. M. El Hassan, and A. M. El-Hassan, "Post-kala-azar dermal leishmaniasis," *The Lancet Infectious Diseases*, vol. 3, no. 2, pp. 87–98, 2003.

[3] S. Uranw, B. Ostyn, A. Rijal et al., "Post-kala-azar dermal leishmaniasis in Nepal: a retrospective cohort study (2000–2010)," *PLoS Neglected Tropical Diseases*, vol. 5, no. 12, article e1433, 2011.

[4] S. Singh, U. Sharma, and J. Mishra, "Post-kala-azar dermal leishmaniasis: recent developments," *International Journal of Dermatology*, vol. 50, no. 9, pp. 1099–1108, 2011.

[5] M. R. Banjara, M. L. Das, C. K. Gurung et al., "Integrating case detection of visceral leishmaniasis and other febrile illness with vector control in the post-elimination phase in Nepal," *The American Journal of Tropical Medicine and Hygiene*, vol. 100, no. 1, pp. 108–114, 2019.

[6] D. Mondal, C. Bern, D. Ghosh et al., "Quantifying the infectiousness of post-kala-azar dermal leishmaniasis towards sandflies," *Clinical Infectious Diseases*, vol. 69, no. 2, pp. 251–258, 2019.

[7] D. Mukhopadhyay, J. E. Dalton, P. M. Kaye, and M. Chatterjee, "Post kala-azar dermal leishmaniasis: an unresolved mystery," *Trends in Parasitology*, vol. 30, no. 2, pp. 65–74, 2014.

[8] A. Picado, B. Ostyn, S. P. Singh et al., "Risk factors for visceral leishmaniasis and asymptomatic *Leishmania donovani* infection in India and Nepal," *PLoS One*, vol. 9, no. 1, Article ID e87641, 2014.

[9] A. Dey and S. Singh, "Genetic heterogeneity among visceral and post-kala-azar dermal leishmaniasis strains from eastern India," *Infection, Genetics and Evolution*, vol. 7, no. 2, pp. 219–222, 2007.

[10] G. Sreenivas, B. V. Subba Raju, R. Singh et al., "DNA polymorphism assay distinguishes isolates of *Leishmania donovani* that cause kala-azar from those that cause post-kala-azar dermal Leishmaniasis in humans," *Journal of Clinical Microbiology*, vol. 42, no. 4, pp. 1739–1741, 2004.

[11] E. J. Tobie, T. von Brand, and B. Mehiman, "Cultural and physiological observations on *Trypanosoma rhodesiense* and *Trypanosoma gambiense*," *Journal of Parasitology*, vol. 87, no. 4, pp. 714–717, 1949-2001.

[12] A. M. Montalvo, J. Fraga, I. Maes, J.-C. Dujardin, and G. Van der Auwera, "Three new sensitive and specific heat-shock protein 70 PCRs for global *Leishmania* species identification," *European Journal of Clinical Microbiology & Infectious Diseases*, vol. 31, no. 7, pp. 1453–1461, 2012.

[13] K. Rai, N. R. Bhattarai, M. Vanaerschot et al., "Single locus genotyping to track *Leishmania donovani* in the Indian subcontinent: application in Nepal," *PLOS Neglected Tropical Diseases*, vol. 11, no. 3, article e0005420, 2017.

[14] J. Fraga, A. M. Montalvo, L. Maes, J.-C. Dujardin, and G. Van der Auwera, "HindII and SduI digests of heat-shock protein 70 PCR for *Leishmania* typing," *Diagnostic Microbiology and Infectious Disease*, vol. 77, no. 3, pp. 245–247, 2013.

[15] S. Deborggraeve, M. Boelaert, S. Rijal et al., "Diagnostic accuracy of a new *Leishmania* PCR for clinical visceral leishmaniasis in Nepal and its role in diagnosis of disease," *Tropical Medicine & International Health*, vol. 13, no. 11, pp. 1378–1383, 2008.

[16] B. Ostyn, S. Uranw, N. R. Bhattarai et al., "Transmission of *Leishmania donovani* in the hills of Eastern Nepal, an outbreak investigation in Okhaldhunga and Bhojpur districts," *PLOS Neglected Tropical Diseases*, vol. 9, no. 8, article e0003966, 2015.

[17] S. Odiwuor, A. Muia, C. Magiri et al., "Identification of *Leishmania tropica* from micro-foci of cutaneous leishmaniasis in the Kenyan Rift Valley," *Pathogens and Global Health*, vol. 106, no. 3, pp. 159–165, 2012.

[18] C. Haralambous, M. Antoniou, F. Pratlong, J.-P. Dedet, and K. Soteriadou, "Development of a molecular assay specific for the *Leishmania donovani* complex that discriminates *L. donovani*/*Leishmania* infantum zymodemes: a useful tool for typing MON-1," *Diagnostic Microbiology and Infectious Disease*, vol. 60, no. 1, pp. 33–42, 2008.

[19] J. K. Pritchard, M. Stephens, and P. Donnelly, "Inference of population structure using multilocus genotype data," *Genetics*, vol. 155, no. 2, pp. 945–959, 2000.

[20] N. R. Bhattarai, J. C. Dujardin, S. Rijal, S. De Doncker, M. Boelaert, and G. Van Der Auwera, "Development and evaluation of different PCR-based typing methods for discrimination of *Leishmania donovani* isolates from Nepal," *Parasitology*, vol. 137, no. 6, pp. 947–957, 2010.

[21] S. Rijal, B. Ostyn, S. Uranw et al., "Increasing failure of miltefosine in the treatment of kala-azar in Nepal and the potential role of parasite drug resistance, reinfection, or noncompliance," *Clinical Infectious Diseases*, vol. 56, no. 11, pp. 1530–1538, 2013.

[22] U. L. Kariyawasam, A. Selvapandiyan, K. Rai et al., "Genetic diversity of *Leishmania donovani* that causes cutaneous leishmaniasis in Sri Lanka: a cross sectional study with regional comparisons," *BMC Infectious Diseases*, vol. 17, no. 1, p. 791, 2017.

[23] M. A. Morales, C. Chicharro, M. Ares, C. Cañavate, D. G. Barker, and J. Alvar, "Molecular tracking of infections by *Leishmania infantum*," *Transactions of the Royal Society of Tropical Medicine and Hygiene*, vol. 95, no. 1, pp. 104–107, 2001.

[24] Y. Botilde, T. Laurent, W. Quispe Tintaya et al., "Comparison of molecular markers for strain typing of *Leishmania infantum*," *Infection, Genetics and Evolution*, vol. 6, no. 6, pp. 440–446, 2006.

[25] N. O. El Tai, M. El Fari, I. Mauricio et al., "*Leishmania donovani*: intraspecific polymorphisms of Sudanese isolates revealed by PCR-based analyses and DNA sequencing," *Experimental Parasitology*, vol. 97, no. 1, pp. 35–44, 2001.

[26] S. Khanra, S. Datta, D. Mondal et al., "RFLPs of ITS, ITS1 and *hsp70* amplicons and sequencing of ITS1 of recent clinical isolates of kala-azar from India and Bangladesh confirms the association of *L. tropica* with the disease," *Acta Tropica*, vol. 124, no. 3, pp. 229–234, 2012.

Hindawi
Canadian Journal of Infectious Diseases and Medical Microbiology
Volume 2019, Article ID 3840563, 6 pages
https://doi.org/10.1155/2019/3840563

*Research Article*

# Genome Sequence of Colistin-Resistant Bacteremic *Shewanella algae* Carrying the Beta-Lactamase Gene $bla_{\text{OXA-55}}$

**Ying-Ju Chen,[1] Kwong-Chung Tung,[2] Yu-Kai Hong,[3] Shi-Yu Chen,[3] Yao-Ting Huang,[3] and Po-Yu Liu[4,5,6]**

[1]*Department of Food and Nutrition, Providence University, Taichung 43301, Taiwan*
[2]*Department of Veterinary Medicine, National Chung Hsing University, Taichung 40227, Taiwan*
[3]*Department of Computer Science and Information Engineering, National Chung Cheng University, Chiayi 62102, Taiwan*
[4]*Division of Infectious Diseases, Department of Internal Medicine, Taichung Veterans General Hospital, Taichung 40705, Taiwan*
[5]*Rong Hsing Research Center for Translational Medicine, National Chung Hsing University, Taichung 40227, Taiwan*
[6]*Ph.D. Program in Translational Medicine, National Chung Hsing University, Taichung 40227, Taiwan*

Correspondence should be addressed to Yao-Ting Huang; ythuang@cs.ccu.edu.tw and Po-Yu Liu; liupoyu@gmail.com

Received 21 February 2019; Revised 6 April 2019; Accepted 22 May 2019; Published 10 June 2019

Guest Editor: Alberto Antonelli



*Shewanella algae* is an emerging pathogen widely distributed in aquatic environment. Bacteremia is a major manifestation of *S. algae* infections, and there are increasing reports of antibiotic-resistant strains. However, little is known about the genomic characteristics of human bacteremic *S. algae*. Here, we report the results of the whole-genome sequencing of colistin-resistant *S. algae* TYL, a blood isolate. Chromosome-encoded *pmrC* associated with colistin resistance and $bla_{\text{OXA-55}}$ gene intrinsic to *S. algae* was identified. Continuous surveillance for the emergence of *S. algae* is needed.

## 1. Introduction

*Shewanella algae* is a nonfermenting Gram-negative bacterium and autochthonous inhabitant of aquatic environments [1]. The organism could tolerate a wide range of physiological conditions [2] and has been documented as an emerging zoonotic pathogen [3]. It has been reported to cause ulcerative disease in marine fish [4] and shellfish [5]. The clinical spectrum in human infection is broad, including bacteremia, biliary tract infection, pneumonia, and soft tissue infections [6]. Bacteremia is one of the most common presentations of *S. algae* infections, which is associated with considerable morbidity and mortality [7].

The emergence of colistin resistance has become a major public heath challenge. The major advances of sequencing technology in past decades have enabled improved understanding of the genomic background of many important pathogens and resistance determinants. High-quality genomic data have become critical for the study of pathogenesis and therapeutic intervention of infectious diseases.

Although there are increasing reports of colistin-resistant *S. algae* bloodstream infections worldwide [8], little is known about the genomic characteristics of human bacteremic *S. algae*. Moreover, the widespread environmental nature of *S. algae* raises concern for its role as a resistance reservoir. In this study, we determined the whole-genome sequence of a colistin-resistant *S. algae* strain isolated from blood.

## 2. Materials and Methods

*S. algae* strain TYL was isolated on trypticase soy agar supplemented with 5% sheep blood (Becton Dickinson, San Jose, CA, USA) from the blood of a septic patient. The strain was identified by matrix-assisted laser desorption/ionization time-of-flight mass spectrometry (MALDI-TOF MS, bioMérieux, Marcy-l'Etoile, France) and 16S ribosomal RNA gene sequencing. In brief, a PCR amplicon of the 16S ribosomal RNA gene was obtained with primers B27F (5′-AGAGTTTGATCCTGGCTCAG-3′) and U1492R (5′-

GGTTACCTTGTTACGACTT-3′) and subjected to Sanger sequencing. Sequences obtained were blasted against the bacterial 16S ribosomal RNA gene sequences in the GenBank database (http://www.ncbi.nlm.nih.gov/) using the BLASTn (optimized for MegaBLAST) algorithm. Antibacterial susceptibility testing was performed by the Vitek 2 system (bioMérieux, Marcy-l′Etoile, France) according to the manufacturer's instructions. The reference strains *Escherichia coli* ATCC 25922 and *Pseudomonas aeruginosa* ATCC 27853 were used as quality controls. The broth microdilution method was used to determine the minimum inhibitory concentration (MIC) of colistin.

Genomic DNA was extracted by using the QIAGEN Genomic-tip 100/G kit and the Genomic DNA Buffer Set (QIAGEN, Paisley, UK) then quantified by using the Qubit dsDNA HS Assay kit and the Qubit 2.0 fluorometer (Life 3 Technologies, Carlsbad, CA, USA). The indexed PCR-free library preparation was constructed using a multiplexed high-throughput sequencing TruSeq DNA Sample Preparation kit (Illumina, San Diego, CA, USA) following the standard protocol provided by the manufacturer with minor modification. Low-quality reads and bases were removed and trimmed using the Kmer-based tool DUK (http://duk.sourceforge.net/) and FASTQ Trimmer (https://github.com/agordon/fastx_toolkit), respectively. The reads were assembled using Velvet version 1.2.07 [9]. Wgsim 0.3.0 (https://github.com/lh3/wgsim) was then used to generate 1–3 kb simulated paired-end reads. The genome was assembled using the ALLPATHS-LG v. R46652 [10] and annotated using the Prokaryotic Genomes Automatic Annotation Pipeline (PGAAP) (https://www.ncbi.nlm.nih.gov/genome/annotation_prok/). Protein family analysis is performed by RPSBLAST v. 2.2.15 [11] against COGs (Clusters of Orthologous Groups of proteins) databases (*E*-value cutoff 0.001) (https://warwick.ac.uk/fac/sci/moac/people/students/peter_cock/python/rpsblast/). Homologs of the *S. algae* TYL genes were BLAST searched against the Integrated Microbial Genomes and Microbiomes database v.5.0 [12], the Virulence Factor Database [13], and the Comprehensive Antibiotic Resistance Database [14] to identify candidate virulence genes and antibiotic-resistant genes.

## 3. Results and Discussion

Whole-genome sequencing was performed using the Illumina MiSeq platform which generated 4,270,654 reads (mean read length of 301 bp) and a gross amount of 1,285,466,854 bp. The assembly of the draft genome sequence consists of 100 scaffolds amounting to 4,821,720 bp (total read depth of 267-fold coverage), and the $G+C$ content is 52.95%. An illustration of the genomic contents in the genome of TYL is shown in Figure 1. The maximum contig size was 234,074 bp, and the N50 size was 96,168 bp. Of the 4,304 genes predicted, 4,112 were protein-coding genes, 13 RNAs, 90 tRNAs, and 6 noncoding RNAs. The distribution of genes into COGs functional categories is presented in Table 1. This Whole Genome Shotgun project has been deposited at DDBJ/ENA/GenBank under the accession number: LVDB01000000. The version described in this paper is version LVDB01000000.

To measure the nucleotide-level genomic similarity between TYL and the other *Shewanella* genomes, the Average Nucleotide Identity was calculated using a modified algorithm [15]. Results from this analysis showed an Average Nucleotide Identity (ANI) value higher than 98% with both the C6G3 (NCBI accession number: NZ_JPMA00000000.1) and MARS 14 strains (NCBI accession number: NZ_CDQH00000000.1), confirming the identification at the species level (Figure 2).

The TYL strain is resistant to colistin (MIC = 32 $\mu$g/ml) and susceptible to imipenem (MIC ≤ 0.25 $\mu$g/ml), piperacillin/tazobactam (MIC ≤ 4 $\mu$g/ml), ceftriaxone (MIC ≤ 1 $\mu$g/ml), ceftazidime (MIC ≤ 1 $\mu$g/ml), cefepime (MIC ≤ 1 $\mu$g/ml), gentamicin (MIC ≤ 1 $\mu$g/ml), and amikacin (MIC ≤ 2 $\mu$g/ml).

Over the past decade, the emergence of multidrug-resistant Gram-negative microorganisms increased the use of colistin as the remaining therapeutic option [17]. Nevertheless, the reports of colistin resistance globally are of great concern. The two most studied nonfermentative Gram-negative bacteria with acquired resistance to colistin are *Acinetobacter baumannii* and *Pseudomonas aeruginosa* [18]. Lipid A modification is a common mode of colistin resistance in clinical isolates belonging to these two species [19, 20]. We identified the homolog of *pmrC* gene associated with colistin resistance [21]. Analysis of the upstream and downstream of *pmrC* gene was performed. We found *pmrA* and *pmrE* genes located downstream of *pmrC* gene. We noted a similar arrangement in colistin-resistant *S. algae* MARS 14 (Figure S1). Functional genomic study on *S. algae* MARS 14 demonstrated that the colistin resistance in *S. algae* is associated with phosphoethanolamine transferase EptA-encoding *pmrC* gene [21]. EptA adds phosphoethanolamine to lipid A, resulting in structural modification of lipopolysaccharide and colistin resistance [21]. Studies of colistin resistance patterns of *S. algae* are limited to case series and case reports [22, 23]. It was suggested that all *S. algae* are resistant to colistin [24]. However, there are also reports of colistin-susceptible strains [25]. Large-scale comparative genomics focus on *pmr* genes, and colistin resistance phenotype are needed to fully exploit mechanisms of colistin resistance in *S. algae*.

The emergence of carbapenem-resistant *S. algae* is a growing concern worldwide. Carbapenemase producers are of major concern. In this study, we detected a chromosome-encoded $bla_{\text{OXA-55}}$ ß-lactamase gene. OXA-type carbapenemases are members of class D ß-lactamases with carbapenem-hydrolysing activities. The mechanisms of carbapenem resistance in *S. algae* are suggested to be caused by beta-lactamase gene $bla_{\text{OXA-55}}$ [23]. Various $bla_{\text{OXA}}$-type genes have been reported in different *Shewanella* species [26]. In addition, there are increasing numbers of studies on horizontal gene transfer in *Shewanella* that demonstrate the organism is a potential reservoir of antimicrobial resistance [27, 28]. However, the OXA-55 ß-lactamase is also present in carbapenem-susceptible *S. algae* [29]. The resistance of carbapenems in *S. algae* may involve a combination of OXA-

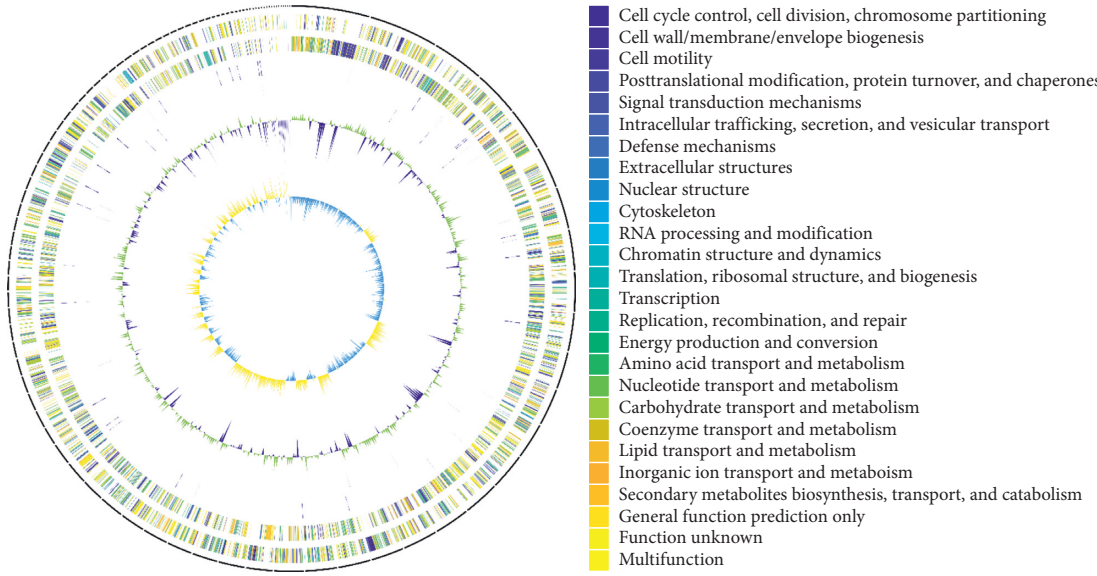


Figure 1: Circular genome map of *Shewanella algae* TYL. Circles from the outside to inside: (1) DNA coordinates; (2, 3) function-based color-coded mapping of the CDSs predicted on the forward and reverse strands. Functions are color-coded; (4) tRNA genes; (5) rRNA genes; (6) GC plot showing regions above the average (green) and below (violet); (7) GC skew showing regions above average (yellow) and below (light blue).

Table 1: COG functional categories of *Shewanella algae* TYL genome.

| COG class | Description | Count | % |
|---|---|---|---|
| D | Cell cycle control, cell division, chromosome partitioning | 37 | 0.88 |
| M | Cell wall/membrane/envelope biogenesis | 223 | 5.16 |
| N | Cell motility | 69 | 1.73 |
| O | Posttranslational modification, protein turnover, and chaperones | 193 | 4.50 |
| T | Signal transduction mechanisms | 223 | 5.35 |
| U | Intracellular trafficking, secretion, and vesicular transport | 76 | 1.80 |
| V | Defense mechanisms | 91 | 2.18 |
| W | Extracellular structures | 0 | 0.00 |
| A | RNA processing and modification | 2 | 0.05 |
| J | Translation, ribosomal structure, and biogenesis | 193 | 4.64 |
| K | Transcription | 248 | 5.49 |
| L | Replication, recombination, and repair | 183 | 6.30 |
| C | Energy production and conversion | 277 | 6.61 |
| E | Amino acid transport and metabolism | 258 | 5.99 |
| F | Nucleotide transport and metabolism | 89 | 2.01 |
| G | Carbohydrate transport and metabolism | 109 | 2.60 |
| H | Coenzyme transport and metabolism | 135 | 3.20 |
| I | Lipid transport and metabolism | 111 | 2.51 |
| P | Inorganic ion transport and metabolism | 257 | 5.99 |
| Q | Secondary metabolites biosynthesis, transport, and catabolism | 52 | 1.23 |
| R | General function prediction only | 0 | 0.00 |
| S | Function unknown | 1,288 | 29.79 |
| — | Multifunction | 80 | 1.99 |

55 *ß*-lactamase and another mechanism. Routine surveillance and further investigation are needed for the resistance emergence.

*S. algae* causes diseases in both humans and marine animals. The organism has been reported to cause various diseases in shrimp, marine fish, and shellfish [4, 5, 30]. In humans, *S. algae* infections have been associated with seafood ingestion and water exposure [6]. Severe bacteremic illness complicated with human shewanellosis is not uncommon [31]. Pathogenicity test showed the $LD_{50}$ of *S. algae* was $1.8 \times 10^4$ CFU/mL for 20-day-old abalone postlarvae [4]. Hemolysis was demonstrated in the pathogenic strains of *S. algae* [30].

Hemolytic activity has long been suspected as a virulence factor of *S. algae* [32]. The *S. algae* TYL genome carries genes encoding hemolysin A (*hlyA*) and hemolysin

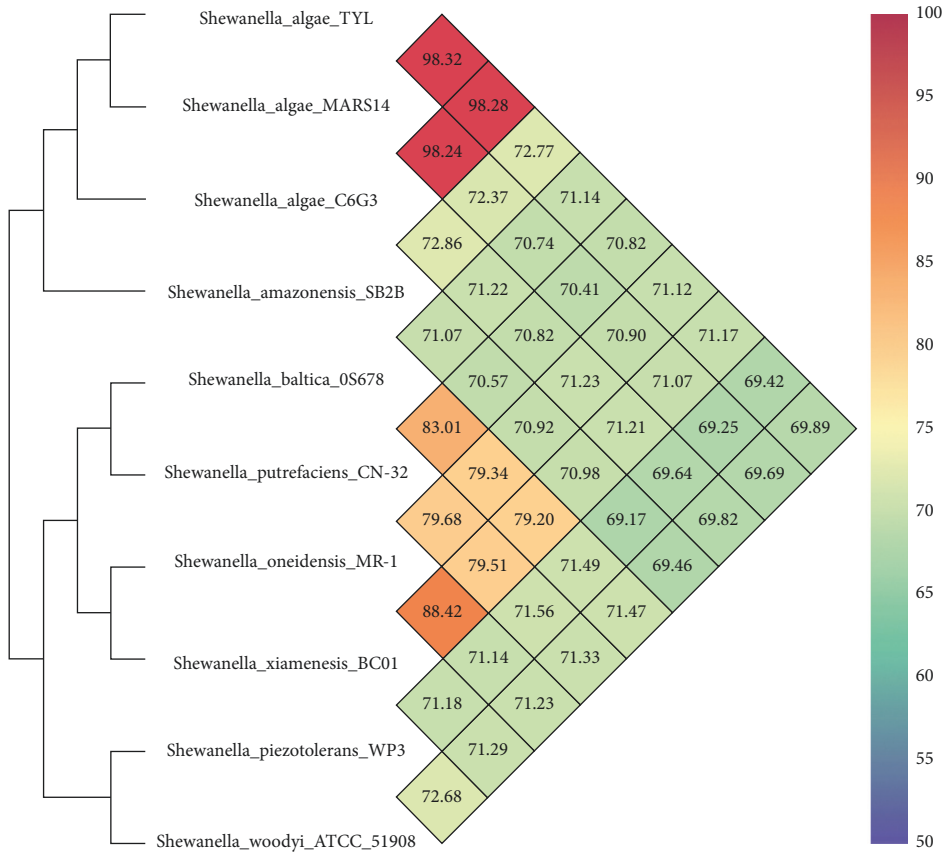


Figure 2: Heat-map and phylogenetic trees based on Average Nucleotide Identity values determined for *Shewanella algae* TYL and related strains. The values between two strains are given in the junction point of the diagonals departing from each strain. Figure two is reproduced from the study of Tseng et al. [16] (under the Creative Commons Attribution License/public domain).

III (*hly*III). Hemolysin A belongs to RTX pore-forming toxin $\alpha$-hemolysin, which rearranges membrane permeability and causes cell lysis. Genomic analysis of *S. algae* TYL in this report supports the previous study, which demonstrated the hemolytic activity of environmental *S. algae* and thus suggested it as a possible virulence determinant [33].

Biliary tract infection is one of the major presentations and possible ports of entry in shewanellosis [34]. Bile salts possess antimicrobial activity, causing damage to lipids in the cell membrane and DNA. Hence, *S. algae* must be able to survive the deleterious action of bile salts. A previous study demonstrated bile resistance in *S. algae* [24]. In this study, we identified genes associated with bile tolerance (*htpB*, *exbBD*, and *galU*). The results support the earlier genomic study, suggesting a common mechanism of bile resistance in *Shewanella* [16].

## 4. Conclusions

In summary, multiple resistance and virulence determinants in *S. algae* TYL were identified by whole-genome sequencing. To the best of our knowledge, this report describes the first *S. algae* blood isolate. Our data provide the impetus for further research on the zoonotic potential of *S. algae*.

## Data Availability

This Whole Genome Shotgun project has been deposited at DDBJ/ENA/GenBank under the accession LVDB01000000. The version described in this paper is version LVDB01000000.

## Conflicts of Interest

The authors declare that there are no conflicts of interest regarding the publication of this article.

## Acknowledgments

We would like to thank Dr. Lee Pan for his help in Kyoto and Osaka. YTH was supported in part by a grant (106-2221-E-194-056-MY3 and 107-2221-E-194 -030 -MY2) from Taiwan's Ministry of Science and Technology. YJC and PYL were supported by grants (TCVGH-PU1088101) from Taichung Veterans General Hospital.

## Supplementary Materials

Figure S1: genetic context of pmrC in *Shewanella algae* MARS 14 and *Shewanella algae* TYL. The arrows indicate the positions and directions of transcription for each gene. (*Supplementary Materials*)

## References


[1] Z. Han, J. Sun, A. Lv et al., "Isolation, identification and characterization of *Shewanella algae* from reared tongue sole, *Cynoglossus semilaevis* Günther," *Aquaculture*, vol. 468, pp. 356–362, 2017.

[2] S. Y. Tseng, P. Y. Liu, Y. H. Lee et al., "The pathogenicity of *Shewanella algae* and ability to tolerate a wide range of temperatures and salinities," *Canadian Journal of Infectious Diseases and Medical Microbiology*, vol. 2018, Article ID 6976897, 9 pages, 2018.

[3] Z. Y. Wu, P. Y. Liu, S. Y. Tseng, Y. H. Lee, and S. P. Ho, "Characteristics and phylogeny of *Shewanella haliotis* isolated from cultivated shellfish in taiwan," *Canadian Journal of Infectious Diseases and Medical Microbiology*, vol. 2018, Article ID 9895148, 6 pages, 2018.

[4] C. Chen, C. Hu, X. Chen, and L. Zhang, "Identification and characterization of *Shewanella algae* as a novel pathogen of ulcer disease of fish *Scinenops ocellata*," *Oceanologia Et Limnologia Sinica*, vol. 34, no. 1, pp. 1–8, 2003.

[5] J. Cai, H. Chen, K. D. Thompson, and C. Li, "Isolation and identification of *Shewanella alga* and its pathogenic effects on post-larvae of abalone *Haliotis diversicolor supertexta*," *Journal of Fish Diseases*, vol. 29, no. 8, pp. 505–508, 2006.

[6] P.-Y. Liu, C.-F. Lin, K.-C. Tung et al., "Clinical and microbiological features of *Shewanella* bacteremia in patients with hepatobiliary disease," *Internal Medicine*, vol. 52, no. 4, pp. 431–438, 2013.

[7] A. J. Martin-Rodriguez, O. Martin-Pujol, F. Artiles-Campelo, M. Bolanos-Rivero, and U. Romling, "*Shewanella* spp. infections in Gran Canaria, Spain: retrospective analysis of 31 cases and a literature review," *JMM Case Reports*, vol. 4, no. 12, article e005131, 2017.

[8] T. Takata, H. Chikumi, S. Morishita et al., "*Shewanella algae* bacteremia in an end-stage renal disease patient: a case report and review of the literature," *Internal Medicine*, vol. 56, no. 6, pp. 729–732, 2017.

[9] D. R. Isomoto and E. Birney, "Velvet: algorithms for de novo short read assembly using de Bruijn graphs," *Genome Research*, vol. 18, no. 5, pp. 821–829, 2008.

[10] S. Gnerre, I. Maccallum, D. Przybylski et al., "High-quality draft assemblies of mammalian genomes from massively parallel sequence data," *Proceedings of the National Academy of Sciences*, vol. 108, no. 4, pp. 1513–1518, 2011.

[11] S. Altschul, W. Gish, W. Miller, E. W. Myers, and D. J. Lipman, "Basic local alignment search tool," *Journal of Molecular Biology*, vol. 215, no. 3, pp. 403–410, 1990.

[12] I. A. Chen, K. Chu, K. Palaniappan et al., "IMG/M v.5.0: an integrated data management and comparative analysis system for microbial genomes and microbiomes," *Nucleic Acids Research*, vol. 47, no. 1, pp. D666–D677, 2018.

[13] L. Chen, D. Zheng, B. Liu, J. Yang, and Q. Jin, "VFDB 2016: hierarchical and refined dataset for big data analysis-10 years on," *Nucleic Acids Research*, vol. 44, no. 1, pp. D694–D697, 2016.

[14] B. Jia, A. R. Raphenya, B. Alcock et al., "CARD 2017: expansion and model-centric curation of the comprehensive antibiotic resistance database," *Nucleic Acids Research*, vol. 45, no. 1, pp. D566–D573, 2017.

[15] I. Doshi, Y. Ouk Kim, S.-C. Park, and J. Chun, "OrthoANI: an improved algorithm and software for calculating average nucleotide identity," *International Journal of Systematic and Evolutionary Microbiology*, vol. 66, no. 2, pp. 1100–1103, 2016.

[16] S. Y. Tseng, K. C. Tung, J. F. Cheng et al., "Genome characterization of bile-isolated *Shewanella algae* ACCC," *Gut Pathogens*, vol. 10, no. 1, p. 38, 2018.

[17] J. Li, R. L. Nation, J. D. Turnidge et al., "Colistin: the re-emerging antibiotic for multidrug-resistant gram-negative bacterial infections," *The Lancet Infectious Diseases*, vol. 6, no. 9, pp. 589–601, 2006.

[18] A. O. Olaitan, S. Morand, and J. M. Rolain, "Mechanisms of polymyxin resistance: acquired and intrinsic resistance in bacteria," *Frontiers in Microbiology*, vol. 5, p. 643, 2014.

[19] Y. Cai, D. Chai, R. Wang, B. Liang, and N. Bai, "Colistin resistance of *Acinetobacter baumannii*: clinical reports, mechanisms and antimicrobial strategies," *Journal of Antimicrobial Chemotherapy*, vol. 67, no. 7, pp. 1607–1615, 2012.

[20] N. Martis, S. Leroy, and V. Blanc, "Colistin in multi-drug resistant *Pseudomonas aeruginosa* blood-stream infections," *Journal of Infection*, vol. 69, no. 1, pp. 1–12, 2014.

[21] A. A. Telke and J.-M. Rolain, "Functional genomics to discover antibiotic resistance genes: the paradigm of resistance to colistin mediated by ethanolamine phosphotransferase in *Shewanella algae* MARS 14," *International Journal of Antimicrobial Agents*, vol. 46, no. 6, pp. 648–652, 2015.

[22] J. M. Janda and S. L. Abbott, "The genus *Shewanella*: from the briny depths below to human pathogen," *Critical Reviews in Microbiology*, vol. 40, no. 4, pp. 293–312, 2014.

[23] K. Yousfi, S. Bekal, V. Usongo, and A. Touati, "Current trends of human infections and antibiotic resistance of the genus *Shewanella*," *European Journal of Clinical Microbiology & Infectious Diseases*, vol. 36, no. 8, pp. 1353–1362, 2017.

[24] H. M. Holt, B. Gahrn-Hansen, and B. Bruun, "*Shewanella algae* and *Shewanella putrefaciens*: clinical and microbiological characteristics," *Clinical Microbiology and Infection*, vol. 11, no. 5, pp. 347–352, 2005.

[25] M. Gressier, D. Mbayo, H. Deramond, F. Grados, F. Eb, and B. Canarelli, "First case of human spondylodiscitis due to *Shewanella algae*," *International Journal of Infectious Diseases*, vol. 14, no. 3, pp. e261–e264, 2010.

[26] A. Antonelli, D. M. Di Palo, A. Galano et al., "Intestinal carriage of *Shewanella xiamenensis* simulating carriage of OXA-48–producing Enterobacteriaceae," *Diagnostic Microbiology and Infectious Disease*, vol. 82, no. 1, pp. 1–3, 2015.

[27] Y. Fang, Y. Wang, Z. Li et al., "Distribution and genetic characteristics of SXT/R391 integrative conjugative elements in *Shewanella* spp. from China," *Frontiers in Microbiology*, vol. 9, p. 920, 2018.

[28] A. B. Jousset, L. Dabos, R. A. Bonnin et al., "CTX-M-15-Producing *Shewanella* species clinical isolate expressing OXA-535, a chromosome-encoded OXA-48 variant, putative progenitor of the plasmid-encoded OXA-436," *Antimicrobial Agents and Chemotherapy*, vol. 62, no. 1, 2018.

[29] J. Walther-Rasmussen and N. Høiby, "OXA-type carbapenemases," *Journal of Antimicrobial Chemotherapy*, vol. 57, no. 3, pp. 373–383, 2006.

[30] L. Shufang, J. Zhang, Q. Dequan, Y. Shiping, and Z. Huang, "Biological characteristics and pathogenicities of *Shewanella algae* and *Shewanella abalone* from babylonia," *Agricultural Science & Technology*, vol. 16, no. 9, pp. 1845–1859, 2015.

[31] F. Zhang, Y. Fang, F. Pang et al., "Rare *Shewanella* spp. associated with pulmonary and bloodstream infections of cancer patients, China: a case report," *BMC Infectious Diseases*, vol. 18, no. 1, p. 454, 2018.

[32] G. P. Richards, M. A. Watson, E. J. Crane 3rd, I. G. Burt, and D. Bushek, "*Shewanella* and *photobacterium* spp. in oysters

and seawater from the Delaware Bay," *Applied and Environmental Microbiology*, vol. 74, no. 11, pp. 3323–3327, 2008.

[33] Z. Y. Wu, S. P. Ho, J. F. Cheng et al., "Whole-genome characterization of *Shewanella algae* strain SYT3 isolated from seawater reveals insight into hemolysis," *Future Microbiology*, vol. 13, no. 16, pp. 1709–1717, 2018.

[34] J.-H. Byun, H. Park, and S. Kim, "The phantom menace for patients with hepatobiliary diseases: *Shewanella haliotis*, often misidentified as *Shewanella algae* in biochemical tests and MALDI-TOF analysis," *Japanese Journal of Infectious Diseases*, vol. 70, no. 2, pp. 177–180, 2017.

Hindawi
Canadian Journal of Infectious Diseases and Medical Microbiology
Volume 2019, Article ID 9464768, 11 pages
https://doi.org/10.1155/2019/9464768

*Research Article*

# The Importance of Coordinated Actions in Preventing the Spread of Yellow Fever to Human Populations: The Experience from the 2016-2017 Yellow Fever Outbreak in the Northeastern Region of São Paulo State

**Márcio Junio Lima Siconelli**,[1] **Danillo Lucas Alves Espósito**,[1] **Nathália Cristina Moraes**,[2] **Julia Maria Ribeiro**,[3] **Lívia Perles**,[3] **Maria Angélica Dias**,[4] **Adolorata Aparecida Bianco Carvalho**,[2] **Karin Werther**,[3] **Natália Coelho Couto de Azevedo Fernandes**,[5] **Silvia D'Andretta Iglezias**,[5] **Karina Paes Bürger**,[2] **and Benedito Antonio Lopes da Fonseca**[1]

[1]*Department of Internal Medicine, Ribeirão Preto Medical School, University of São Paulo FMRP/USP, Av. Bandeirantes, 3900, Vila Monte Alegre, Ribeirão Preto, 14049-900 São Paulo, Brazil*
[2]*Veterinary Preventive Medicine and Animal Reproduction Department, Faculty of Agricultural and Veterinary Sciences, Universidade Estadual Paulista "Júlio de Mesquita Filho" (FCAV/Unesp), Access Way Prof. Paulo Donato Castellane s/n, Jaboticabal, 14884-900 São Paulo, Brazil*
[3]*Animal Pathology Department, Faculty of Agricultural and Veterinary Sciences, Universidade Estadual Paulista "Júlio de Mesquita Filho" (FCAV/Unesp), Access Way Prof. Paulo Donato Castellane s/n, Jaboticabal, 14884-900 São Paulo, Brazil*
[4]*Municipal Health Secretary, Av. General Glicério, 569, Center, Jaboticabal, 14870-520 São Paulo, Brazil*
[5]*Nucleus of Pathological Anatomy, Pathology Center, Adolfo Lutz Institute of São Paulo, State Secretary of Health, Av. Dr. Arnaldo, 351, 7° Floor, 01246-902 São Paulo, Brazil*

Correspondence should be addressed to Benedito Antonio Lopes da Fonseca; baldfons@fmrp.usp.br

Received 10 January 2019; Revised 12 March 2019; Accepted 28 March 2019; Published 19 May 2019

Guest Editor: Dimosthenis Chochlakis



Yellow fever (YF) is a zoonotic arthropod-borne disease that is caused by the yellow fever virus (YFV) and characterized by a sylvatic and urban cycle. Its most severe presentation is manifested as a hemorrhagic disease, and it has been responsible for thousands of deaths in the last decades. This study describes the public health approaches taken to control the 2016-2017 YF outbreak in nonhuman primates (NHPs) that took place in the northeastern region of São Paulo state, Brazil. NHPs recovered from the field were necropsied, and YF diagnoses were made at the Laboratory of Molecular Virology, Ribeirão Preto Medical School and the Center of Pathology, Adolfo Lutz Institute of São Paulo. NHP samples were inoculated into Vero cells for YFV isolation. RNA extraction was performed directly from NHP tissues and tested by RT-qPCR. YFV-positive samples were confirmed by sequencing. Based on the rapid RT-qPCR results, surveillance actions were implemented in the entire region. Confirmatory histopathology and immunohistochemistry for YFV were also performed. Among nine NHPs, gross hepatic involvement was observed in six animals, five of which were YFV-RT-qPCR-positive. One YFV was isolated from the serum of an infant NHP. YFV RNA sequences diverged from the virus responsible for the last epizootic that occurred in São Paulo state, but it was similar to the current Brazilian epizootic. Public health actions included dissemination of information on YF transmission, investigation of the probable location of NHP infection, characterization of the environment, and subsequent creation of the blueprint from which prevention and control measures were implemented. The YFV sylvatic cycle occurred in the periurban areas of the northeastern region of São Paulo state, but no human cases were reported during this period, showing that integrated actions between human, animal, and environmental health professionals were critical to restrain the virus to the sylvatic cycle.

## 1. Introduction

It is estimated that 60% of disease-causing pathogens in humans are zoonotic, and most of them are maintained in the wild through enzootic cycles [1, 2]. One example of these pathogens is the yellow fever virus (YFV), which causes yellow fever (YF), an acute and noncontagious infectious disease that affects animals and humans. YF is characterized by fever, jaundice, and hemorrhage, and it is responsible for the death of hundreds of people. YF remains enzootic in the tropical forests of America and Africa causing epizootics with known periodicity or epidemics of greater or lesser impact on public health [3–6]. Its reemergence in the areas outside of the Amazon region is concerning for public health authorities in the Americas and throughout the world.

In the Americas, transmission occurs through the bite of infected female hematophagous mosquitoes from the *Culicidae* family, especially by the *Aedes aegypti* species, in the urban area, and *Haemagogus* and *Sabethes* genera in the wild environment, characterizing two cycles of transmission: an urban and a sylvatic cycle [6–9]. However, the existence of a possible new vector in Brazil, *Aedes albopictus*, has been suggested as susceptible to infection by YFV [10–14].

The sylvatic cycle of YF transmission involves nonhuman primates (NHP) and sylvatic mosquitoes [15, 16]. The NHP species that are present in South America are mostly susceptible to YFV infection [6]. Among neotropical monkeys, the disease occurs in an epizootic manner, especially with the genus *Alouatta*, in which a high mortality rate is observed, and this represents a concern regarding species conservation and ecological balance in the area affected by YFV [6, 17–21]. Many other primates are severely affected, such as those of the genera *Ateles*, *Aotus*, *Saguinus*, *Cebus*, *Sapajus*, *Callithrix*, and *Callicebus*. Although monkeys of the genera *Cebus* and *Sapajus* are easily infected, they usually have a subclinical infection with low lethality, and they generally develop protective immunity, as shown by the presence of neutralizing antibodies, which indicates probable infection and survival [6, 22, 23].

The YFV is the prototype of the *Flavivirus* genus from the *Flaviviridae* family, which has genetic material that consists of a positive-sense, single stranded RNA [24]. Its genome encodes three structural (C, *pr*M, and E) and seven nonstructural (NS1, NS2A, NS2B, NS3, NS4A, NS4B, and NS5) proteins [25, 26]. Although only one serotype of the YFV has been described, there are seven genotypes that carry small genetic changes, two from the Americas (South America 1 and South America 2) and five from Africa (West Africa 1, West Africa 2, East Africa 1, East Africa 2, and Angola), but no difference in the disease presentation is observed among them [27–29].

In Brazil, the most frequent genotype is South America 1 (SA1), although five other lineages that derived from SA1 has been identified (SA1A to SA1E), with SA1E previously recorded in the 2008 epidemic in São Paulo state [9, 24, 30–32]. Recently, a YFV genome from a virus that was isolated in Espirito Santo state during the 2017 outbreak was sequenced in its entirety, and changes were found to eight amino acids that were located in the C, NS3, and NS5 proteins [32].

The last case of urban YF in Brazil was reported in 1942 in the Amazon region, and since then, no records of urban transmission have been confirmed [8, 24]. However, the risk of YF reurbanization exists because *Ae. aegypti* is widely distributed in the country.

In the recent history of São Paulo state, three major sylvatic outbreaks have been recorded. In 2008, two human deaths, from autochthonous cases, were reported in the northeastern region of the state [33–35], and in 2016, Brazil reported six confirmed human cases of YF to the World Health Organization (WHO), with two deaths occurring in São Paulo state [36–38]. According to the São Paulo State Health Department, 227 animals with suspected YFV infection were reported in the state up to December 2016, and among those, 24 were positive for YFV in the northern region of the state [36]. In 2017, 21 autochthonous human cases were confirmed up to June, and nine patients died. During this period, 110 of 643 NHP were also infected with YFV [36].

In the last two years, Brazil has experienced the largest outbreak of YF in the last 70 years, a situation that has alarmed the population and health authorities mainly because of the virus dissemination, which reached areas that were previously classified as free of YFV circulation [21, 32, 39, 40].

Because of the absence of records on YFV infections in NHP since 1935 [39] in the northeast-central region of São Paulo state, the objective of this manuscript is to report the features of the recent YF outbreak in NHPs in this region of Brazil, the molecular characterization of a YFV isolated during this period, and the importance of these findings to initiate coordinated measures among all public health services to prevent the occurrence of human cases.

## 2. Materials and Methods

*2.1. Description of the Study Site.* The study site described here is located in the northeastern region of São Paulo state, at the coordinates 21°15′18.00″ south and 48°19′19.20″ west (Figure 1). The area is characterized by long green corridors, extending from rural to the urban areas. The vegetation in the region is characterized by the Brazilian cerrado biome (regarded as the Brazilian Savanna), which is mostly residual ciliary forest including areas of permanent preservation. The intense exploitation of sugarcane cultures left fragments ("islands") of forested areas and in some parts without direct communication between them, forming true mosaics of vegetation. The average annual rainfall is approximately 1423.7 mm, accumulating in the months of January, February, March, October, November, and December. In addition to the high precipitation, the average temperature is also high, reaching an average of 29.1°C. The month of October stands out with the highest temperatures, with an average of 30.9°C [41].

*2.2. Necropsy and Collection of Biological Material.* Necropsy and collection of biological samples were performed at the Service of Pathology of Wild Animals, School


Figure 1: (a) Map from the study site. In the smaller image, São Paulo state is in red inside Brazil's map and the larger image is the São Paulo state map, including the study site (Jaboticabal/SP) that is highlighted in red. (b) Aerial satellite view of the urban and rural areas of the municipality of Jaboticabal/SP. Sources: (a) http://www.skyscrapercity.com/showthread.php?t=1513060; (b) Google Earth, 2017.

of Veterinary Medicine, São Paulo State University (FCAV/Unesp), following an established protocol for necroscopic examination of NHPs [42, 43]. Most of the necroscopic examinations were performed as soon as the NHP arrived at the Pathology Service to avoid organ degradation. However, some animals were either refrigerated (between 2°C and 8°C) or frozen (−20°C) before the necroscopic examination.

Concomitantly, biological samples were collected according to the "Guide for the Surveillance of Epizootics in Nonhuman Primates and Entomology Applied to Yellow Fever" [42, 43] and subsequently stored. The samples were sent to the Laboratory of Molecular Virology, Ribeirão Preto Medical School, University of São Paulo, Ribeirão Preto, São Paulo, for virologic and molecular testing and to the Center of Pathology of Adolfo Lutz Institute of São Paulo for histopathological and immunohistochemical testing. These test results were required to make a diagnosis of YF.

Tissue fragments of approximately 0.5 cm by 2.0 cm were collected and divided in two sections. One section was placed in 10% buffered formaldehyde solution and kept at room temperature for subsequent encasement in paraffin blocks and histopathological testing. The other section of the sample was frozen at −20°C and subsequently stored at −70°C. The main organs sampled were the liver, spleen, lung, brain, heart, and kidneys. Based on the viability of the carcass, other tissues were harvested, such as the stomach, lymph nodes, adrenal glands, intestines, blood, bladder, and gonads.

*2.3. Histopathological and Immunohistochemical Diagnosis.* Slides that were 3 $\mu$m thick were made from formalin-fixed and paraffin-embedded tissues and were stained with hematoxylin and eosin (H&E) before microscopic examination. The main lesions were described and classified according to intensity and distribution. Additional slides were deparaffinized, followed by antigen retrieval under pressure and incubation with primary anti-FA polyclonal antibody (produced in the Arthropod-borne Virus Laboratory at the Adolfo Lutz institute). Signal amplification was achieved using a polymer conjugated with an enzyme (MACH4 universal AP Polymer and Polymer MACH4™ universal AP, Biocare, Pike Lane, Concord, CA, USA) that was visualized using chromogen (Warp red™, Biocare, Pike Lane, Concord, CA, USA).

*2.4. Molecular and Virologic Diagnosis.* To optimize virus recovery, liver samples were chosen to be tested first because of the YFV tropism to the liver. RNA was extracted using the phenol-chloroform technique, and it was subjected to YFV-specific RT-qPCR. If the result was positive, other harvested tissues were subjected to RT-qPCR (TaqMan® Fast Virus 1-Step Master Mix, Applied Biosystems, Woodward St., Austin, TX, USA) to verify the tissues in which the virus was located. Primers used in both experiments were specifically designed for this study and are shown in Table 1. Samples with a positive result were subjected to Sanger sequencing (BigDye™, Applied Biosystems, Woodward St., Austin, TX, USA).

*2.5. Surveillance.* When the first cases were confirmed in October 2016, the Municipal Health Department was notified, and prevention and control strategies were implemented by public health officials. Strategic actions were based on selective house-to-house immunization throughout the rural areas in the region, mainly in the areas neighboring the location of the YFV-positive cases, to verify the population's vaccination status, control mosquito breeding sites in all constructed areas where animals were found, intensify surveillance for NHP death, implement

Table 1: Primers used in RNA detection by RT-qPCR and sequencing.

| Name | Use | Sequence |
|---|---|---|
| YF.For | qPCR | GTGACAGCCTTGGCCATT |
| YF.Rev | qPCR | AGGCTGGGCCAACAGCCA |
| YF.FAM | qPCR | 6FAM-GAAGCAACATGACGCAACGA-TAMRA |
| YF.Seq.For | Sequencing | ATCGTTCGTTGAGCGATTAGC |
| YF.Seq.Rev | Sequencing | CCAGTGCTGGGGCACTTGTCATT |

georeferencing in the affected area, and conduct health education for local health professionals and the population. The coordinates of the NHPs were georeferenced with the help of the native GPS application iOS 10 (Apple, Cupertino, CA, USA). The data were then entered into the Google Earth 7.1.7.2602 software. All occurrences received at the local surveillance unit were recorded, including live or dead animals and carcasses.

*2.6. Ethics.* This study was approved by the FCAV/Unesp Ethics Committee on the Use of Animals (process no. 010001/17). The reported cases followed the guidelines for research, diagnosis, prevention, and control measures, according to the "Guide to Surveillance of Epizootics in Nonhuman Primates and Entomology Applied to Yellow Fever" [42, 43] and the "Health Surveillance Guide" [42]. Additionally, all the cases investigated were entered into the Notification of Injury Information System (SINAN) from the Ministry of Health of Brazil.

## 3. Results

*3.1. Cases.* In late October 2016, an infant male howler monkey (*Alouatta caraya*) (monkey #1) was found separated from his group in a country club located on the outskirts of the main city and within the study site, and it was sent to the Veterinary Medical Service of Wild Animals of FCAV/Unesp. After a thorough physical examination, it looked healthy, and it was kept under quarantine. Three days later, the monkey developed apathy, anorexia, weight loss, pale mucosae, and loss of consciousness. In the following days, there was an intense deterioration of its clinical status, and the veterinarians chose to perform euthanasia. During this period, the Environmental Military Police reported that another young male howler monkey, from the same region drowned in the lake at the same country club (monkey #2). It was removed from the water and taken to the FCAV/Unesp but subsequently died.

After these cases, other reports were received, and nine animals were sent to FCAV/Unesp. All animals were necropsied, including five howler monkeys (monkeys #3 to #7), one capuchin monkey (*Sapajus nigritus*; monkey #8), and a white-tufted marmoset (*Callithrix jacchus*; monkey #9). Monkey #9 had been kept as a pet by authorized owners (Table 2). The reporting areas are presented in the map below (Figure 2).

The first positive YF cases (monkeys #1 and #2) were found in the western part of the study site. All other animals were found in the eastern region (monkeys #3 to #8), including those from which we could not collect any samples because of the advanced stage of decomposition. Although monkey #3 had no evidence of YFV infection, it was considered positive for YFV infection based on epidemiologic criteria. In addition to the monkey deaths, area residents reported that NHP deaths had probably been happening throughout August and September.

Other reports were made in addition to the reported cases, for a total of nine animals, comprising eight howler monkeys and a black-tufted marmoset (*Callithrix penicillata*). It was not possible to perform a necropsy on these animals because only bones or carcasses that were in an advanced stage of decomposition were found. These animals were included in this study because they were found near the sites where the other monkeys that were infected with YFV were found. Additionally, previous ongoing animal surveillance had shown that it was unusual to find so many dead animals in such small area and in a short time period.

*3.2. Necropsy Findings and Histopathological and Immunohistochemical Diagnosis.* Of the nine necropsied animals, five of them, all *Alouatta caraya*, had alterations that were suggestive of an acute infectious disease. External examination detected animals with a body weight within normal limits for the species and mucosa with intense yellowish color (ocular, oral, anal, and vaginal/preputial). An internal examination showed that the main organs affected were the liver, which was a normal size and had an evident reticular pattern with the color varying from pale yellow to intense yellowish; the kidneys were uniformly yellowish, in both the cortical and medullar regions, and without any change in size; and in some of these animals, the color of the omentum varied from yellow to intense orange. Two of the animals had hemorrhagic fluid and coagulated blood in the abdominal cavity (Figure 3).

Other findings, such as petechiae on the cardiac musculature, cerebral hemorrhage, splenomegaly, and yellowish staining on the walls of the gastrointestinal tract were also found. No similar gross pathological features were found in the livers of the other four necropsied animals, with the exception of a white-tufted marmoset that had yellowish regions on its liver.

All five confirmed cases showed intense panlobular necrosis with acidophilic bodies (Councilman-Rocha Lima bodies), mild to moderate fat degeneration, and mild to moderate inflammatory infiltrate, mainly in portal tract, that rarely had neutrophils associated (Figure 4). Multifocal hemorrhage was present in one of the cases. Most of them presented lymphoid necrosis in the white pulp of the spleen and proteinosis in the renal tubules. The brain, lungs, and heart did not present remarkable findings. On

Table 2: Nonhuman primate epizootics with collected samples and laboratory results, from November 2016 to April 2017.

| Sequence number of notifications | Animal ID | Date of necropsy | Species | Results RT-qPCR |
|---|---|---|---|---|
| 01 | Monkey #1 | 04/11/16 | *Alouatta caraya* | Positive |
| 02 | Monkey #2 | 04/11/16 | *Alouatta caraya* | Positive* |
| 04 | Monkey #3 | 30/11/16 | *Alouatta caraya* | Negative |
| 09 | Monkey #4 | 07/12/16 | *Alouatta caraya* | Positive |
| 10 | Monkey #5 | 11/12/16 | *Alouatta caraya* | Positive |
| 11 | Monkey #7 | 08/01/17 | *Sapajus nigritus* | Negative |
| 13 | Monkey #9 | 13/01/17 | *Alouatta caraya* | Positive |
| 14 | Monkey #6 | 13/03/17 | *Alouatta caraya* | Negative |
| 15 | Monkey #8 | 26/04/17 | *Callithrix jacchus* | Negative |

*RT-qPCR performed by Adolfo Lutz Institute of São Paulo.


Figure 2: Satellite image of the study site with georeferenced notifications, between October 2016 and April 2017. Numbers 01 to 15 correspond to the sequence of notifications received during the period. Red dots represent animals that recently died, carcasses, or bones (*Alouatta caraya* species). The green dot represents an animal that recently died (*Sapajus nigritus* species). A purple dot represents a carcass of the *Callithrix penicillatta* (12) and *C. jacchus* (15) species. Source: Google Earth, 2019.

immunohistochemistry, all cases showed a strong red immunolabeling that was limited to the hepatocyte cytoplasm, indicating a severe infection.

*3.3. Molecular Diagnosis and Epidemiology.* Eight samples were tested at the LMV-FMRP/USP (Laboratory of Molecular Virology, Ribeirão Preto Medical School at the University of São Paulo). Hepatic tissue from all NHPs was tested, except for monkey #1, from which it was only possible to collect and extract RNA from serum. RT-qPCR detected YFV in five samples (monkeys #1, #2, #4, #5, and #9), confirming infection by YFV. The other samples were negative (Table 2). The samples from monkey #2 were tested at the Adolfo Lutz Institute of São Paulo, and YFV infection was also confirmed. Several other tissues for monkeys #4, #5, and #9 were also RT-qPCR-positive for YFV. A summary of YFV detection in these samples is presented in Table 3.

After a positive RT-qPCR result, 1,000-bp fragments including the capsid, prM, and E protein regions of the genome were sequenced. Sequences were submitted to the GenBank database (accession numbers: MF443184, strain JabSPM01; MF443185, strain JabSPM02; MF443186, strain JabSPM03; and MF443187, strain JabSPM04). A YFV from one of the monkey samples (4283912, strain JabSPM02) was isolated in Vero cells.

*3.4. Surveillance.* Based on the positive laboratory results, strategies were implemented to avoid the virus spreading into the population in the adjacent rural areas and especially into the urban area.

(a) (b) (c) (d)

Figure 3: A female of *Alouatta caraya* species (monkey #4). (a) Record of the place where the animal was found. (b) Kidney midsagittal section, showing yellowish coloration. (c) Liver with yellowish coloration and reticular pattern evidenced. (d) Mesentery with yellowish coloration and intense hemorrhage.

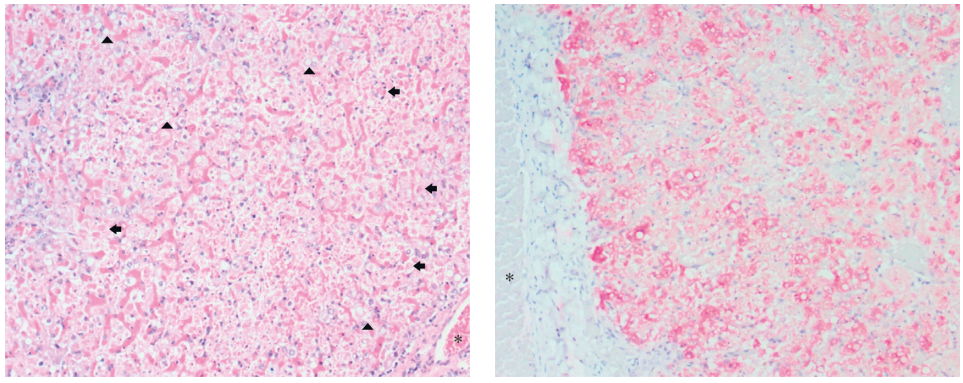

(a) (b)

Figure 4: Histopathologic and immunohistochemical findings in the liver of a neotropical nonhuman primate, *Alouatta caraya* species (monkey #5), that died of YF in Jaboticabal, São Paulo, Brazil, 2016. Asterisks (*) indicate the portal vein. (a) Moderate (diffuse) lytic necrosis with some Councilman-Rocha Lima (apoptotic) bodies (arrows), mild macrovacuolar steatosis (arrow head). Original magnification ×100, H&E staining. (b) Positive granular and massive intracytoplasmic immunolabeling for the yellow fever virus antigen, with panlobular distribution. Original magnification ×100; anti-YF virus (NDTV/IAL), Warp red™, counter staining with Harrys hematoxylin.

An intensive house-to-house vaccination program was conducted in the rural area of the epizootic region, initially targeting the locale where the first positive cases were found. During vaccination, health education was also provided for the area residents using a personal approach, and information leaflets about the disease were handed out. Control measures were then extended into neighboring areas.

To evaluate the vaccination status of the population and, if necessary, to perform mass vaccination, state and city governments established a vaccination "*D*" day, which was about 10 days after beginning of the house-to-house vaccination. On that day, approximately 3,000 doses of the vaccine were administered to the population. Combining the vaccination campaign that started about 2 weeks before the "*D*" day and the vaccinations performed on "*D*" day, more than 10,000 doses of YF vaccine were used to immunize people living in high-risk areas, either for the first time or to boost the immune response against YF. House-to-house vaccination in the rural area of the epizootic location lasted for 33 days and was completed in early 2017.

In addition to these actions, surveillance of NHP health status within the study site was intensified. Monkey groups

Table 3: Real-time RT-PCR results for yellow fever virus in several biological tissues of nonhuman primates of the *Alouatta caraya* species found dead in study sites between November 2016 and April 2017.

| Tissue/organs | Monkey #1 | Monkey #4 | Monkey #5 | Monkey #9 |
|---|---|---|---|---|
| Blood | N/A | N | P | P |
| Serum | P | N/A | N/A | N/A |
| Brain | N/A | P | P | P |
| Heart | N/A | P | P | P |
| Lung | N/A | P | P | P |
| Liver | N/A | P | P | P |
| Stomach | N/A | N/A | N/A | P |
| Spleen | N/A | P | P | P |
| Large intestine | N/A | N/A | N/A | P |
| Mesenteric lymph node | N/A | N/A | N/A | P |
| Adrenal | N/A | N/A | P | P |
| Kidneys | N/A | P | P | P |
| Urinary vesicle | N/A | N/A | N/A | P |
| Gonads (testicle) | N/A | N/A | N | P |

P, positive; N, negative; N/A, no available samples.

living in small forested areas in urban and periurban environments were tracked and monitored, looking for the presence of either diseased or dead animals during the epizootic period.

## 4. Discussion

Since the 1990s, the northeastern portion of São Paulo state has been considered a high-risk area for YF transmission, and vaccination of people in this area has been recommended since that time [17]. In Brazil, a high-risk area is defined as a location where the YFV circulates either continuously or intermittently. After approximately 7 years without YF cases in São Paulo state [31], the first human death was reported in March 2016, in a wooden area located about 100 miles from the area described in this study. After that case in July 2016, *C. penicillata* was found in a city near our study site, which was later confirmed as YFV positive. In October of the same year, an epizootic broke out within the site described here, and samples were collected from nine of 18 NHP found, and YFV infections were confirmed in five of them. Samples were not collected from 9 NHP because of the advanced stage of decomposition. However, there was no other evidence for their cause of death besides inhabiting the area where the YFV-infected monkeys were found. During that time, the study site was one of the areas that had the highest number of reported YF cases in *A. caraya* (13/15; 86.7%), which was similar to numbers reported in the 2009 outbreak [6, 17, 34]. This is directly related to the susceptibility of this species, which is considered to be the main sentinel for the disease [6]. All NHP cases, except for the white-tufted marmoset, were located in periurban or rural areas.

The study site described here was characterized as small areas of remaining forest that had been either destroyed or preserved with changes in the native vegetation. Additionally, field investigations demonstrated that all animals were found near the riverbanks or streams. The first two YF-positive cases were found in the western part of the study site in October, and soon thereafter, other animal deaths were reported in the eastern region. During epidemiologic investigations, several NHPs' bones were found, mainly in the eastern region. However, it is not possible to establish a direct connection between the two regions, which are separated from each other by approximately 5 to 6 miles, a space that is occupied by a city of about 75,000 inhabitants, and there had been no record of free-living NHPs in that urban area. Additionally, people living in the rural areas reported that NHP deaths had been happening since August or September. Although some animals were found between late November and early December 2016, it is possible that the virus had been circulating already for months. The detection of a YFV-infected howler monkey in January 2017 (monkey #9), which was found dead between September and November 2016 but kept frozen for teaching purposes, reinforces this assumption.

Although improbable, human activity may have contributed to the spread of the virus to several areas, suggesting that this is of central importance in epizootic/epidemic outbreaks and it can act directly as a source of infection. This hypothesis is based on the fact that a transiently infected person in their viremic or incubation period can introduce the virus to areas with high vector population densities and increase the availability of vertebrate hosts, such as NHPs [6, 31, 39]. However, there has been no evidence for human infections in the study area, which is an observation that goes against the possibility of humans taking a central role in YFV transmission.

In Brazil, most of the municipalities have an infestation by the *Ae. aegypti*, *Ae. albopictus*, or both and show high levels of infestation, with R0 (basic reproduction number) >1, which indicates an initial phase of a dengue epidemic. The R0 for urban YFV transmission is 43% lower than that of the initial phase of dengue [44, 45]. To lower the risk of transmission, all mosquito control measures must be improved in urban areas, where people and the health authorities can act directly against the vector (i.e., drain accumulated water from containers and eliminate all mosquito breeding sites). In the sylvatic cycle, it is not possible to introduce any control measures for the mosquitoes because there is no way to

remove all breeding sites from the trees due to their location in the canopy and that all mosquito species that can transmit the YFV have different habitats. Additionally, it is not acceptable to control these mosquitoes using insecticides. Because controlling the sylvatic mosquito population is difficult, and YFV vaccination is the only strategy for effective prevention that is available for people living in the rural or sylvatic areas.

Indirectly, destroying forested areas to construct human dwellings resulted in a stronger interaction between humans and the sylvatic environment (wild animals and many vector species). Because of this, NHPs and other animals started to move out of their natural habitat in search for food, water, and shelter, creating the opportunity for translocation of various pathogens that can potentially cause zoonotic diseases, such as YFV, between NHPs and humans [31, 46]. Although reurbanization of the disease has been speculated, because urban yellow fever is transmitted by *Ae. aegypti*, a mosquito that is highly prevalent in Brazil, YF reurbanization has not happened. However, many other hypotheses may try to explain the lack of reurbanization, such as genetic differences from the 1942 *Ae. aegypti* population, when it was eliminated, and the current *Ae. aegypti* population. Mutations in the YFV genome that occurred throughout the years may have changed the transmission patterns through acquisition of several new hosts in the sylvatic cycle. Furthermore, it is important to investigate the presence of the virus in populations of *Ae. aegypti* during seasonal period [14].

Other explanations besides the above hypothesis have been suggested for the emergence of apparently unprecedented NHP cases, such as maintenance of the virus in animal species other than NHP so that transmission is kept at low levels, and after 5 to 8 years of low activity, the virus can replicate in epizootic proportions [6, 47, 48]. The absence of YFV circulation during this period is due to the time that the monkey populations take to recover, and new susceptible animals are born. Additionally, YF-infected mosquito eggs remain viable in the environment by resisting harsh weather conditions and hatching under suitable climate conditions, which may contribute to the permanence of the virus in the wild [24, 39, 49]. Finally, illegal trafficking of wild animals can move the virus out of its sylvatic cycle and introduce it into virus-free areas [21, 42].

Thus, to control the sylvatic cycle of YFV and prevent dissemination from the area with confirmed cases, working perimeters of the investigation were defined from the places of probable infection. For places where laboratory-confirmed YF cases were found and those with the presence of either rivers or streams, there was a recommendation that house-to-house vaccination should take place within a 30-kilometer radius from the reported case. However, because of limited operational capacity of healthcare personnel, a radius of 15 kilometers was used, including the study site. This intervention was based on the observations made during previous outbreaks, such as the epizootic of Minas Gerais (2002/2003), which included the banks of the Rio Doce, and the epizootics in São Paulo, which occurred from 2000 to 2010 and involved other rivers (Rio Grande, Rio Cubatão, Rio Mogi-Guaçu, and Rio Paranapanema) [33]. The presence of forested areas bordering on rivers that often pass through urban areas may constitute a relevant risk factor for the disease. Thus, the presence of susceptible NHP and competent vectors in these places were considered to be the ideal scenario for the emergence of an epizootic, and control measures were readily instituted on these areas.

The conclusive diagnosis of the YF can be performed using different techniques such as viral isolation, molecular techniques (RT-PCR or RT-qPCR), and identification of the YFV antigen in the tissues (immunochemistry) [21]. As described by many studies, it was possible to observe some histopathological findings that are characteristic of a classic injury caused by the YFV, which is usually associated with the disease in humans (midzonal lytic necrosis, apoptotic bodies such as Councilman-Rocha Lima bodies, steatosis, and scarce paucicellular inflammation) [7, 21, 50–55].

Histopathological analysis by H&E staining in the liver cannot confirm the disease, as it may only suggest that an YFV infection is present. Immunohistochemistry can detect the presence of the virus in the tissues, and it is considered to be a confirmatory test for this virus. Before the advent of molecular techniques, this approach was considered to be the method of choice to diagnose YF [56, 57]. Thus, immunochemistry is considered to be part of the official surveillance and diagnosis for YF disease in humans and NHPs. Additionally, this technique assumes greater importance in a postmortem diagnosis, when much time has passed from death until sample collection, because these postmortem tissues are not suitable for use in molecular biology techniques. Immunohistochemistry is an important tool for the surveillance service, and it contributes to early detection of YFV in a region that is undergoing an outbreak [42].

Histopathological tests are important to make the correct diagnosis; however, the molecular techniques have improved and provided agility to the diagnosis and surveillance of the YFV. Molecular investigations performed in this study showed that four YFV RNA sequences, which were amplified from four different animals, were identical to each other and indicated that the same strain was circulating in the region during the study period. Similarly, all four RNA sequences were identical to the viruses detected in Espirito Santo state, KY885000 (strain ES-504/BRA/2017) and KY885001 (strain ES-505/BRA/2017), which were isolated in February 2017 [32]. This result showed that the same YFV was circulating in most of the southern part of Brazil.

According to surveillance studies by the Ministry of Health between 2014 and 2016, YFV has been spreading into the Amazon region and to other areas of the country in a southeastern direction, and it arrived in the central, western, and southeastern parts of the country between 2015 and 2016 [21, 38, 40]. In São Paulo state, YFV was first detected in the northwestern region and moved eastward, to the northeastern region of the state, where the study site was located. In this area, human YFV transmission was avoided because of the rapid implementation of the control measures described above, aiming to quickly detect the presence of the virus in the NHP population and consequently stop virus amplification. This was

accomplished by the combined efforts of epidemiologists, veterinarians, field workers, and a solid infrastructure of virology laboratories and lab personnel. However, in the northern part of São Paulo state, especially in the area in which epizootics originated in the southern part of Minas Gerais state, prevention of YF in the human population was not as efficient, probably because it took too long to implement strategies such as the ones described above for this study site. The presence of islands of preserved forested areas, susceptible NHP, and an abundance of vectors resulted in a rapid southward dissemination of this virus in epizootic proportions, starting in Minas Gerais state and reaching the metropolitan region of São Paulo city in October 2017, when cases of NHP were detected in municipal parks [36]. Human cases detected in this region were associated with a low level of vaccine coverage. This type of epidemiological situation, where the YFV circulated within the Atlantic Forest biome and spread up to the coast of São Paulo state, had not been recorded since the 1930s [21, 39].

The recent YF outbreak that occurred in Brazil shows that a clear change in the pattern of the YFV sylvatic transmission cycle has recently emerged, showing a possible adaptation of this virus to areas that are in close proximity to urban environments where sylvatic cycle vectors and NHPs are increasingly found in association with humans. This allows for total conditions to perpetuate the YFV sylvatic cycle, as observed in the epizootic in 2016/2017. Additionally, environmental policies must be implemented in green protected areas and places with large NHP populations where the YFV circulated, and new public health policies must be formulated, such as new surveillance strategies (permanent active surveillance and monitoring of NHPs, vectors, and others animals in hot spot areas) because of the changing patterns that have been recently established for YFV. Ultimately, all these policies must take into consideration the possible reurbanization of YF in Brazil, and widespread vaccination should be advised. However, YF reurbanization has not happened, and all current YF human cases had a significant interaction with rural areas.

Although Brazilian health authorities have implemented surveillance actions for YF, our study shows the vulnerability of the available Health System to the occurrence of diseases that were previously considered to be controlled. Additionally, it underscores the requirement for integrated and multiprofessional actions between humans, animals, and environmental interfaces, and most importantly, the control actions must be rapidly implemented to avoid virus dissemination to disease-free areas.

## Data Availability

The data used to support the findings of this study are included within the article.

## Conflicts of Interest

The authors declare that they have no conflicts of interest.

## Acknowledgments

The authors thank the staff from the Nucleus of Pathological (NAP), Center of Pathology and Nucleus of Diseases Transmitted by Vectors (NDTV), and Center of Virology from Adolfo Lutz Institute of São Paulo for YF diagnosis and antibody production and for their help in diagnosing some samples. This work was supported, in part, by a grant from the São Paulo State Health Department (FESIMA—Oficio CAF no. 003/2016).

## References

[1] D. E. Norris, "Mosquito-borne diseases as a consequence of land use change," *EcoHealth*, vol. 1, no. 1, pp. 19–24, 2004.

[2] OIE, World Organization for animal health. One World, One Health, 2019, http://www.oie.int/en/for-the-media/press-releases/detail/article/one-world-one-health/.

[3] P. L. Brès, "A century of progress in combating yellow fever," *Bull World Health Organ*, vol. 64, pp. 775–786, 1986.

[4] S. A. Thompson, J. K. Hilliard, D Kittel et al., "Retrospective analysis of an outbreak of B virus infection in a colony of DeBrazza's monkeys (*Cercopithecus neglectus*)," *Comparative Medicine*, vol. 50, pp. 648–657, 2000.

[5] F. P. Câmara, A. L. B. B. Gomes, L. M. F. D. Carvalho, and L. G. V. Castello, "Dynamic behavior of sylvatic yellow fever in Brazil (1954–2008)," *Revista da Sociedade Brasileira de Medicina Tropical*, vol. 44, no. 3, pp. 297–299, 2011.

[6] E. S. Moreno, R. Spinola, C. H Tengan et al., "Yellow fever epizootics in non-human primates, São Paulo State, Brazil, 2008-2009," *Revista do Instituto de Medicina Tropical de São Paulo*, vol. 55, no. 1, pp. 45–50, 2013.

[7] G. K. Strode, *Yellow Fever*, McGraw-Hill Book Company, New York, NY, USA, 1951.

[8] T. P. Monath, "Yellow fever," in *The Arboviruses: Ecology and Epidemiology*, T. P. Monath, Ed., pp. 139–231, CRC Press, Boca Raton, FL, USA, 1988.

[9] P. F. C. Vasconcelos, J. E. Bryant, A. P. A. Travassos da Rosa, R. B. Tesh, S. G. Rodrigues, and A. D. T. Barrett, "Genetic divergence and dispersal of yellow fever virus, Brazil," *Emerging Infectious Diseases*, vol. 10, no. 9, pp. 1578–1584, 2004.

[10] B. R. Miller and M. E. Ballinger, "*Aedes albopictus* mosquitoes introduced into Brazil: vector competence for yellow fever and dengue viruses," *Transactions of the Royal Society of Tropical Medicine and Hygiene*, vol. 82, no. 3, pp. 476-477, 1988.

[11] R. L. De Oliveira, A. M. B. De Filippis, M. Vazeille, and A.-B. Failloux, "Large genetic differentiation and low variation in vector competence for dengue and yellow fever viruses of *Aedes albopictus* from Brazil, the United States, and the Cayman islands," *The American Journal of Tropical Medicine and Hygiene*, vol. 69, no. 1, pp. 105–114, 2003.

[12] R. Maciel-de-Freitas, R. B. Neto, J. M. Gonçalves, C. T. Codeco, and R. Lourenço-de-Oliveira, "Movement of dengue vectors between the human modified environment and an urban forest in Rio de Janeiro," *Journal of Medical Entomology*, vol. 43, no. 6, pp. 1112–1120, 2006.

[13] J. R. Saraiva, A. Maitra, A. K. R. Galardo, and V. M. Scarpassa, "First record of Aedes (Stegomyia) albopictus in the state of Amapá northern Brazil," *Acta Amazonica*, vol. 49, no. 1, pp. 36–40, 2018.

[14] R. Klitting, E. Gould, C. Paupy, and X. de Lamballerie, "What does the future hold for yellow fever virus? (I)," *Genes*, vol. 9, no. 6, p. 291, 2018.

[15] W. D. Tigertt, T. O. Berge, W. S. Gochenour et al., "Section of biological and medical sciences: experimental yellow fever," *Transactions of the New York Academy of Sciences*, vol. 22, no. 5, pp. 323–333, 1960.

[16] T. P. Monath, K. R. Brinker, C. B. Cropp, F. W. Chandler, and G. E. Kemp, "Pathophysiologic correlations in a rhesus monkey model of yellow fever," *The American Journal of Tropical Medicine and Hygiene*, vol. 30, no. 2, pp. 431–443, 1981.

[17] A. P. M. Romano, Z. G. A. Costa, D. G. Ramos et al., "Yellow fever outbreaks in unvaccinated populations, Brazil, 2008-2009," *PLoS Neglected Tropical Diseases*, vol. 8, no. 3, article e2740, 2014.

[18] I. Holzmann, I. Agostini, H. Areta, P. Ferreyra, M. Beldomenico, and M. S. D. Bitetti, "Impact of yellow fever outbreaks on two howler monkey species (*Alouatta guariba clamitans* and *A. caraya*) in misiones, Argentina," *American Journal of Primatology*, vol. 72, no. 6, pp. 475–480, 2010.

[19] M. M. Kowalewski, J. S. Salzer, J. C. Deutsch, M. Raño, M. S. Kuhlenschmidt, and T. R. Gillespie, "Black and gold howler monkeys (*Alouatta caraya*) as sentinels of ecosystem health: patterns of zoonotic protozoa infection relative to degree of human-primate contact," *American Journal of Primatology*, vol. 73, no. 1, pp. 75–83, 2011.

[20] M. A. B. Almeida, E. Santos, J. C Cardoso et al., "Yellow fever outbreak affecting *Alouatta* populations in southern Brazil (Rio Grande do Sul State), 2008-2009," *American Journal of Primatology*, no. 1, p. 74, 2012.

[21] N. C. C. A. Fernandes, M. S. Cunha, J. M Guerra et al., "Outbreak of yellow fever among nonhuman primates, Espirito Santo, Brazil, 2017," *Emerging Infectious Diseases*, vol. 23, no. 12, 2017.

[22] T. C. Rocha, P. M. Batista, R Andreotti et al., "Evaluation of arboviruses in non-human primates," *Revista da Sociedade Brasileira de Medicina Tropical*, vol. 48, no. 2, pp. 143–148, 2015.

[23] M. A. Lima, N. S. Romano-Lieber, and A. M. R. D. C. Duarte, "Circulation of antibodies against yellow fever virus in a simian population in the area of Porto Primavera Hydroelectric Plant, São Paulo, Brazil," *Revista do Instituto de Medicina Tropical de São Paulo*, vol. 52, no. 1, pp. 11–16, 2010.

[24] T. P. Monath and P. F. C. Vasconcelos, "Yellow fever," *Journal of Clinical Virology*, vol. 64, pp. 160–173, 2015.

[25] C. M. Rice, E. M. Lenches, S. R. Eddy, S. J. Shin, R. L. Sheets, and J. H. Strauss, "Nucleotide sequence of yellow fever virus: implications for *Flavivirus* gene expression and evolution," *Science*, vol. 4715, no. 229, pp. 726–733, 1985.

[26] T. J. Chambers, C. S. Hahn, R. Galler, and C. M. Rice, "*Flavivirus* genome organization, expression, and replication," *Annual Review of Microbiology*, vol. 44, no. 1, pp. 649–688, 1990.

[27] S. E. Robertson, B. P. Hull, O. Tomori, O. Bele, J. W. Leduc, and K. Esteves, "Yellow fever: a decade of reemergence," *JAMA: The Journal of the American Medical Association*, vol. 276, no. 14, pp. 1157–1162, 1996.

[28] E. Wang, S. C. Weaver, R. E. Shope, R. B. Tesh, D. M. Watts, and A. D. T. Barrett, "Genetic variation in yellow fever virus: duplication in the 3′ noncoding region of strains from Africa," *Virology*, vol. 225, no. 2, pp. 274–281, 1996.

[29] J. E. Staples and T. P. Monath, "Yellow fever: 100 years of discovery," *JAMA*, vol. 300, no. 8, pp. 960–962, 2008.

[30] M. R. T. Nunes, G. Palacios, K. N. B Nunes et al., "Evaluation of two molecular methods for the detection of yellow fever virus genome," *Journal of Virological Methods*, vol. 174, no. 1-2, pp. 29–34, 2011.

[31] R. P. de Souza, P. G. Foster, M. A Sallum et al., "Detection of a new yellow fever virus lineage within the South American genotype I in Brazil," *Journal of Medical Virology*, vol. 82, no. 1, pp. 175–185, 2010.

[32] M. C. Bonaldo, M. M. Gómez, A. A. C Santos et al., "Genome analysis of yellow fever virus of the ongoing outbreak in Brazil reveals polymorphisms," *Memórias do Instituto Oswaldo Cruz*, vol. 112, no. 6, pp. 1–5, 2017.

[33] L. D. C. Saad, R. B. Barata, L. D. C. Saad, and R. B. Barata, "Surtos de febre amarela no estado de São Paulo, 2000–2010," *Epidemiologia e Serviços de Saúde*, vol. 25, no. 3, pp. 531–540, 2016.

[34] M. Mascheretti, C. H. Tengan, H. K. Sato et al., "Febre amarela silvestre: reemergência de transmissão no estado de São Paulo, Brasil, 2009," *Revista de Saúde Pública*, vol. 47, no. 5, pp. 881–889, 2013.

[35] E. S. Moreno, I. M. Rocco, E. S. Bergo et al., "Reemergence of yellow fever: detection of transmission in the State of São Paulo, Brazil, 2008," *Revista da Sociedade Brasileira de Medicina Tropical*, vol. 44, no. 3, pp. 290–296, 2011.

[36] São Paulo (Estado). Secretaria de Estado de Saúde. Centro de Vigilância Epidemiológica Professor Alexandre Vranjac. Coordenadoria de Controle de Doenças. Divisão de Zoonoses. Febre Amarela, http://www.saude.sp.gov.br/cve-centro-de-vigilancia-epidemiologica-prof.-alexandre-vranjac/areas-de-vigilancia/doencas-de-transmissao-por-vetores-e-zoonoses/agravos/febre-amarela.

[37] PAHO. Organización Panamericana de la Salud, *Alerta Epidemiológica Fiebre amarilla—9 de enero de 2017*, PAHO. Organización Panamericana de la Salud, Washington, DC, USA, 2017.

[38] World Health Organization, *Yellow fever—Brazil, Disease Outbreak News*, World Health Organization, Geneva, Switzerland, 2017, http://www.who.int/csr/don/04-april-2017-yellow-fever-brazil/en/.

[39] P. F. D. C. Vasconcelos, "Yellow fever in Brazil: thoughts and hypotheses on the em0ergence in previously free areas," *Revista de Saúde Pública*, vol. 44, no. 6, pp. 1144–1149, 2010.

[40] C. Possas, R. Lourenço-de-Oliveira, P. L Tauil et al., "Yellow fever outbreak in Brazil: the puzzle of rapid viral spread and challenges for immunization," *Memórias do Instituto Oswaldo Cruz*, vol. 113, no. 10, article e180278, 2018.

[41] G. S. Rolim, V. R. Hinojosa, C. A. S. Capita, and V. S. N. C. Souza, *Resenha Meteorológica do Período 1971–2010*, Faculdade de Ciências Agrárias e Veterinárias, São Paulo, Brazil, 2014, http://www.fcav.unesp.br/#!/estacaoagroclimatologica/resenha/periodo-1971-2010.

[42] Brasil. Ministério da Saúde. Febre amarela: sintomas, tratamento, diagnóstico e prevenção. http://portalms.saude.gov.br/saude-de-a-z/febre-amarela-sintomas-transmissao-e-prevencao.

[43] M. A. B. Almeida, J. C. Cardoso, E. dos Santos et al., "Surveillance for yellow fever virus in non-human primates in southern Brazil, 2001–2011: a tool for prioritizing human populations for vaccination," *PLoS Neglected Tropical Diseases*, vol. 8, no. 3, article e2741, 2014.

[44] E. Massad, M. N. Burattini, F. A. B. Coutinho, and L. F. Lopez, "Dengue and the risk of urban yellow fever reintroduction in São Paulo State, Brazil," *Revista de Saúde Pública*, vol. 37, no. 4, pp. 477–484, 2003.

[45] C. B. Marcondes and M. F. F. M. Ximenes, "Zika virus in Brazil and the danger of infestation by *Aedes* (Stegomyia) mosquitoes," *Revista da Sociedade Brasileira de Medicina Tropical*, vol. 49, no. 1, pp. 4–10, 2016.

[46] J. E. Bryant, E. C. Holmes, and A. D. T. Barrett, "Out of Africa: a molecular perspective on the introduction of yellow fever virus into the Americas," *PLoS Pathogens*, vol. 3, no. 5, p. e75, 2007.

[47] T. P. Monath, "Yellow fever," in *Zoonoses*, S. R. Palmer, L. Soulsby, and D. I. H. Simpson, Eds., pp. 487–498, University Press, Oxford, UK, 1998.

[48] B. de Thoisy, P. Dussart, and M. Kazanji, "Wild terrestrial rainforest mammals as potential reservoirs for flaviviruses (yellow fever, dengue 2 and St. Louis encephalitis viruses) in French Guiana," *Transactions of the Royal Society of Tropical Medicine and Hygiene*, vol. 98, no. 7, pp. 409–412, 2004.

[49] B. J. Beaty, R. B. Tesh, and T. H. G. Aitken, "Transovarial transmission of yellow fever virus in stegomyia mosquitoes," *The American Journal of Tropical Medicine and Hygiene*, vol. 29, no. 1, pp. 125–132, 1980.

[50] W. T. Vieira, L. C. Gayotto, C. P. Lima, and T. Brito, "Histopathology of the human liver in yellow fever with special emphasis on the diagnostic role of the councilman body," *Histopathology*, vol. 7, no. 2, pp. 195–208, 1983.

[51] J. A. S. Quaresma, V. L. R. S. Barros, E. R. Fernandes et al., "Reconsideration of histopathology and ultrastructural aspects of the human liver in yellow fever," *Acta Tropica*, vol. 94, no. 2, pp. 116–127, 2005.

[52] J. A. S. Quaresma, M. I. S. Duarte, and P. F. C. Vasconcelos, "Midzonal lesions in yellow fever: a specific pattern of liver injury caused by direct virus action and in situ inflammatory response," *Medical Hypotheses*, vol. 67, no. 3, pp. 618–621, 2006.

[53] J. A. S. Quaresma, V. L. R. S. Barros, C. Pagliari et al., "Hepatocyte lesions and cellular immune response in yellow fever infection," *Transactions of the Royal Society of Tropical Medicine and Hygiene*, vol. 101, no. 2, pp. 161–168, 2007.

[54] J. A. S. Quaresma, C. Pagliari, D. B. A. Medeiros, M. I. S. Duarte, and P. F. C. Vasconcelos, "Immunity and immune response, pathology and pathologic changes: progress and challenges in the immunopathology of yellow fever," *Reviews in Medical Virology*, vol. 23, no. 5, pp. 305–318, 2013.

[55] S. G. Leal, A. P. M. Romano, R. V. Monteiro, C. B. D. Melo, P. F. D. C. Vasconcelos, and M. B. D. Castro, "Frequency of histopathological changes in howler monkeys (*Alouatta* sp.) naturally infected with yellow fever virus in Brazil," *Revista da Sociedade Brasileira de Medicina Tropical*, vol. 49, no. 1, pp. 29–33, 2016.

[56] W. C. Hall, H. Kruger, F. Pinheiro et al., "Demonstration of yellow fever and dengue antigens in formalin-fixed paraffin-embedded human liver by immunohistochemical analysis," *The American Journal of Tropical Medicine and Hygiene*, vol. 45, no. 4, pp. 408–417, 1991.

[57] E. J. Ezyaguirre, D. H. Walker, and S. R. Zaki, "Immunohistology of infectious diseases," in *Diagnostic Immunohistochemistry*, D. J. Dabbs, Ed., pp. 58–82, Saunders, Elsevier Health Sciences, Philadelphia, PA, USA, 2013.

Hindawi
Canadian Journal of Infectious Diseases and Medical Microbiology
Volume 2019, Article ID 8543460, 5 pages
https://doi.org/10.1155/2019/8543460

*Research Article*

# Seasonal and Gender Differences in Presence of *Rickettsia felis* and Blood meals Provide Additional Evidence of a Vector Role for Mosquitoes

**Jilei Zhang**,[1,2] **Guangwu Lu**,[1] **Patrick John Kelly**,[3] **and Chengming Wang**[1,4]

[1]*College of Veterinary Medicine, Yangzhou University, Yangzhou, Jiangsu, China*
[2]*Division of Gastroenterology and Hepatology, Department of Medicine, University of Illinois at Chicago, Chicago, Illinois, USA*
[3]*Ross University School of Veterinary Medicine, Basseterre, Saint Kitts and Nevis*
[4]*College of Veterinary Medicine, Auburn University, Auburn, AL, USA*

Correspondence should be addressed to Jilei Zhang; jileiz@uic.edu and Chengming Wang; wangche@auburn.edu

Received 1 February 2019; Accepted 24 March 2019; Published 10 April 2019

Guest Editor: Snezana Tomanovic



*Rickettsia felis* belongs to spotted fever group *Rickettsia* and is an emerging human pathogen most commonly transmitted by a range of fleas and ticks. While recent evidence has suggested mosquitoes are infected with *R. felis*, there is little information about the role of mosquitoes in the organism's transmission. In this study, around 100 mosquitoes were collected monthly between 2013 and 2014 from the same residential dwelling at Yangzhou, China. The collected mosquitoes were identified for their species and gender, followed by *gltA*-based PCR and hydroxymethylbilane synthase-based PCR to determine the prevalence of *Rickettsia* and blood meal. Three mosquito species (*Culex pipiens*: 76%, 996/1,304; *C. tritaeniorhynchus*: 17%, 216/1,304; *Aedes albopictus*: 7%, 92/1,304) were identified. For 1,088 female mosquitoes, 31% of them ($n = 336$) were positive for blood meal and 7% ($n = 77$) carried *R. felis* DNA. In a strong contrast, none of the 216 male mosquitoes were positive for blood meal but two males were positive for *Rickettsia*. Interestingly, 63% of *R. felis*-positive mosquitoes (50/79) were negative for blood meal, being significantly higher than 37% of mosquitoes and being positive for both *R. felis* and blood meal ($P = 0.008$). Furthermore, we compared the prevalence of *Rickettsia* and blood meal in the mosquitoes collected in the months with temperature below and above 23°C, the minimum temperature required for mosquito egg hatching. Mosquitoes captured in the months below 23°C showed significant higher positivity of *R. felis*(71/936, 7.6% vs. 8/368, 2.2%; $P = 0.002$) and blood meal (294/936, 31.4% vs. 36/368, 9.8%; $P < 10^{-4}$) than in the months above 23°C. Collectively, the seasonal and gender differences of *R. felis* and blood meal in mosquitoes add to the existing evidence, supporting a potential vector role of mosquitoes in the transmission of *R. felis*. Studies with a *R. felis* infection model covering the full life cycle of mosquitoes is necessary to unambiguously prove the transstadial and transovarial transmission of *R. felis* in mosquitoes.

## 1. Introduction

*Rickettsia felis* is an obligate intracellular Gram-negative bacterium belonging to the family *Rickettsiaceae* [1] and the agent of flea-borne spotted fever in people [2]. Except the primary vector of fleas, *R. felis* was detected in mosquitoes by a growing number of recent reports, paralleling the increasing implication of *R. felis* as a human pathogen [3–9]. Additionally, it was suggested that *Rickettsia* may be maintained in mosquitoes through both transstadial and transovarial transmission [4, 7, 8]. *R. felis* can grow in some mosquito cell lines, such as *Aedes albopictus* and *Anopheles gambiae* [10], indicating the possibility of the transmission and evolution of *Rickettsia* in the mosquito.

Mosquitoes are cosmopolitan in every land region with huge numbers except for Antarctica and a few islands [11]. Feeding on blood is a behavioral trait of female mosquitoes that allows them to obtain the nutrients necessary for reproduction [12]. Male mosquitoes mainly feed on nectar and plant juices, but not blood meal. However, the number and

abundance of mosquito species and the blood-sucking activities are variable due to the vectors of climatic circumstances, animals, and human activities. Investigation on the seasonal differences of *R. felis* and blood meal in female and male mosquitoes will lead to a better understanding of this organism's transmission.

Here, molecular approaches were used to determine the positivity of *Rickettsia* and blood meal of the mosquitoes captured from the same residential dwelling between September 2013 and August 2014. The findings of this study were described as below.

## 2. Materials and Methods

*2.1. Sample Collection.* Between September 2013 and August 2014, mosquitoes ($n$ = 1,304) were captured monthly with hand nets in the same residential dwelling of Yangzhou, Jiangsu, China (Table 1, Figure 1). The collection of mosquitoes was not performed in January and February of 2014 when the university was closed for the holiday. After washing in PBS to exclude the possibility of environmental contamination with *R. felis*, the species and gender of the collected mosquitoes were identified using standard morphological criteria [15] and PCR before putting into 400 $\mu$l (individual)/600 $\mu$l (pool) of RNA/DNA Stabilization Reagent (Roche Molecular Biochemicals, Indianapolis) and then stored at −80°C freezer until DNA extraction as described below. The average monthly temperatures in the Yangzhou were obtained from the local weather station.

*2.2. DNA Extraction.* After thawing and triturating with the shaker (Precellys 24 sysis and homogenization, France) at 5800 × rpm, 15 s × 2 (times), and 20 s (interrupt) at room temperature, mosquitoes were used for DNA extraction with QIAamp DNA Mini Kit (QIAGEN, Valencia, USA) according to the manufacturer's descriptions.Then, the extracted DNAs were kept in −80°C freezer until performance of PCR assay detection.

*2.3. PCR Assays.* HMBS gene (hydroxymethylbilane synthase gene) is a single-copy gene of the heme synthesis pathway in mammalians but not plants and prokaryotes (Table 1). The HMBS-basedFRET-qPCR targeting for a 286 bp amplicon was used for blood meal detection in mosquitoes as described before [4, 13]. The HMBS-basedFRET-qPCR was proved to be highly sensitive and specific and was confirmed to detect 13 mammalian species of blood meals in mosquitoes [13].

The *gltA*-based FRET-qPCR targeting for a 170 bp amplicon of *Rickettsia* spp. and nested-PCR targeting for 446 bp and 353 bp amplicon *gltA* gene were used in this study to detect *Rickettsia* infections as described before [4, 5]. The *gltA* gene encodes one type of citrate synthase which plays a key role in energy production and providing biosynthetic precursors. The *gltA*-based PCRs were established with high sensitivity and specificity and applied in variety of samples including mosquitoes [4, 5].

The species of mosquitoes were also verified by the PCR assay with amplicon of 710 bp cytochrome c oxidase subunit 1 gene (*CO1* gene) as described before [14, 16]. *CO1* gene is one of three mitochondrial DNA-encoded subunits of cytochrome c oxidase which is a key enzyme in aerobic metabolism. It is proposed as the DNA barcoding system for animal life [17] and had been used as the DNA barcodes for the common mosquito species in China [16].

*2.4. Statistical Analysis.* The chi-squared test (Statistica, StatSoft, Tulsa, USA) was used to compare the prevalence of *Rickettsia* and blood meal between different groups of mosquitoes. $P < 0.05$ was considered significantly different.

## 3. Results and Discussion

According to the morphological criteria and PCR followed by DNA sequencing, three mosquito species were identified in this study, including *Culex pipiens* (76%, 996/1,304), *C. tritaeniorhynchus* (17%, 216/1,304), and *Aedes albopictus* (7%, 92/1,304), in both female (83%, 1088/1,304) and male (17%, 216/1,304) (Table 1, Figure 1).

*R. felis* was detected in all the months with mosquito samples except in April and August of 2014 (6%, 79/1,304). We found that about one-third of the female mosquitoes (31%, 336/1,088) had taken a blood meal while 7% (77/1,088) carried *R. felis* DNA. In strong contrast, none of the 216 male mosquitoes were positive for a blood meal but two were *R. felis* positive. The absence of a blood meal in the males was anticipated as males do not feed on animals but obtain their nutrition from plants. Detection of *R. felis* DNA in male mosquitoes, however, suggests vertical (transovarial) transmission of *R. felis* in mosquitoes such that the organism could be maintained in the population without mosquitoes having to feed on rickettsemic hosts.

In this study, 79 *R. felis*-positive mosquitoes were identified. For these *Rickettsia*-positive samples, 63% of them (50/79) were free of a blood meal, being significantly higher than 37% being also positive for blood meal (29/79) ($P$ = 0.008) (Table 2, Figure 1). This further stipulates the possibility of vertical transmission of this organism in mosquitoes.

Yangzhou, located in the east of China with the coordinates of 32°24′N, 119°25′E, has a subtropical monsoon climate with humid changeable wind, longer winter (4 months) and summer (3 months), and shorter springs and autumns (2 months each). The annual average temperature is 15°C with the highest in July (40°C) and lowest in January (−15°C). The average atmosphere temperature for each of the four months (May, June, July, and August) of 2014 was above 23°C, the minimum temperature required for mosquito egg hatching [18, 19]. Species richness and number abundance of the mosquito were generally higher during the summer and fall [20]; for instance, *C. pipiens* appear around May, and the density slowly increased until a seasonal maximum in July-August [21] or sometimes later in September [22], which is confirmed by our findings in this study. The temperature is critical to key

Table 1: Primers and probes used in the PCR reactions in this study.

| PCR | Primer/probe nucleotides | Amplicon | Reference |
|---|---|---|---|
| HMBS FRET-qPCR | Forward primer: 5′-tacctgactggaggagtctggagtct-3′<br>Downstream primer: 5′-gccaggctgatgcccaggttct-3′<br>Anchor probe: 5′-agcahgaagatggyccwga-6-FAM-3′<br>Reporter probe: 5′-LCRed640-gatgayccacagctggtrg-phos-3′ | 286 bp | [13] |
| *Rickettsia gltA* FRET-qPCR | Up primer: 5′-ttrcaaatagcaatagaacttgaagct-3′<br>Reverse primer: 5′-agcaagaaccgtaggctggat-3′<br>Anchor probe: 5′-atcgctcttaaagatgaatattttattgag-6-FAM-3′<br>Reporter probe: 5′-LCRed640-gaaaattatatccaaatgttgatttttattc-phos-3′ | 170 bp | [5] |
| *Rickettsia gltA* nested-PCR | Out-up primer: 5′-agtaaatccaataataaaaaatgckcttaata-3′<br>Out-down primer: 5′-cttaaagatgaatattttattgagagaaaat-3′<br>In-up primer: 5′atgagcagaatgcttctacttcaaca-3′<br>In-down primer: 5′-ttrcaaatagcaatagaacttgaagct-3′ | 446 bp<br>353 bp | [5] |
| Mosquito *COI* PCR | LCO1490: 5′-ggtcaacaaatcataaagatattgg-3′<br>HC02198: 5′-taaacttcagggtgaccaaaaaatca-3′ | 710 bp | [14] |

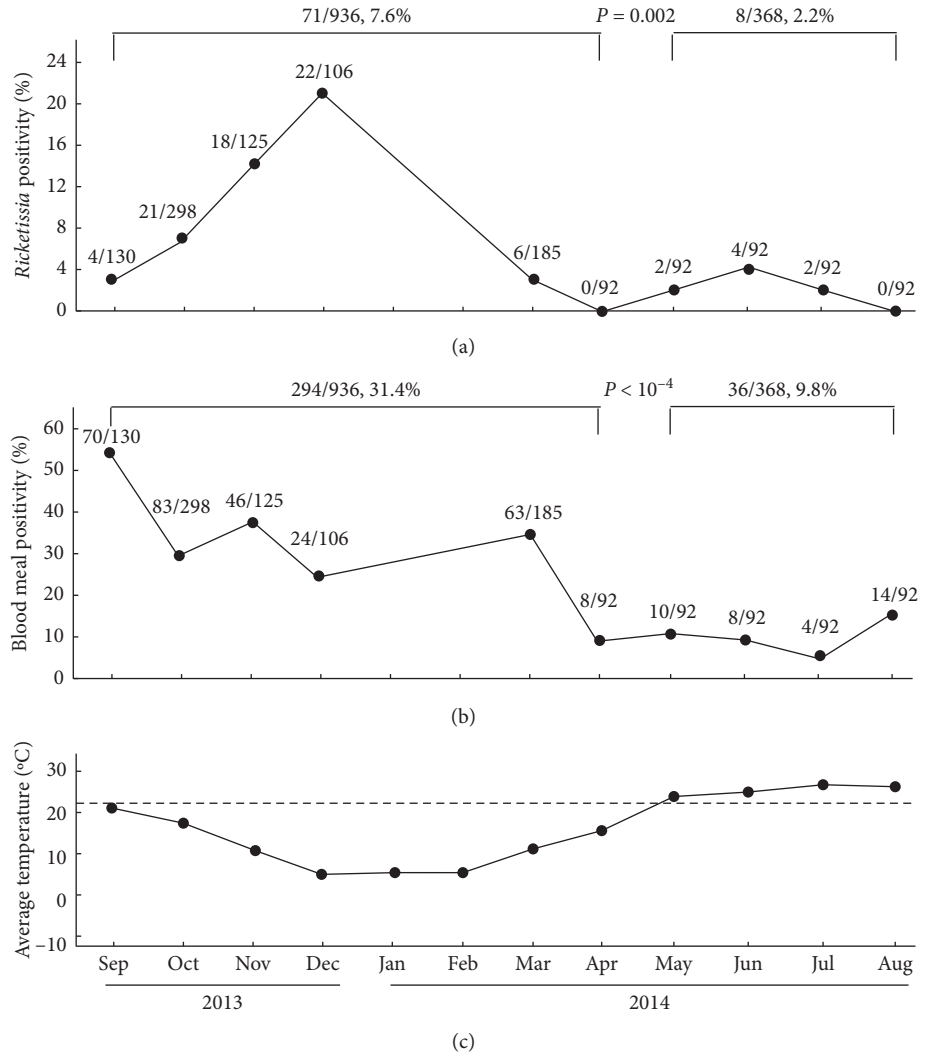


Figure 1: Significant higher *R. felis* and blood meal positivity in mosquitoes collected when the temperature was lower than 23°C than above 23°C. Mosquitoes collected in months with average temperatures below 23°C showed significant higher positivity of *R. felis* ((a); 71/936, 7.6% vs. 8/368, 2.2%; $P = 0.002$) and blood meal ((b); 294/936, 31.4% vs. 36/368, 9.8%; $P < 10^{-4}$) than collected between May and August with above 23°C temperature (c).

Table 2: Prevalence of *R. felis* and blood meal in mosquitoes in this study.

| Date | Sample # | Gender and species | *R. felis*+* | Blood meal+ | *R. felis* + blood meal+ | *R. felis* + blood meal− |
|---|---|---|---|---|---|---|
| Sep. 2013 | 130 | 70 ♀ *Culex pipiens*<br>60 ♀ *C. tritaeniorhynchus* | 3%, 2/70<br>3%, 2/60 | 54%, 38/70<br>55%, 33/60 | 100%, 2/2<br>100%, 2/2 | 0%, 0/2<br>0%, 0/2 |
| Oct. 2013 | 298 | 164 ♀ *C. pipiens*<br>134 ♀ *C. tritaeniorhynchus* | 7%, 12/164<br>7%, 9/134 | 29%, 48/164<br>28%, 37/134 | 42%, 5/12<br>11%, 1/9 | 58%, 7/12<br>89%, 8/9 |
| Nov. 2013 | 125 | 103 ♀ *C. pipiens*<br>22 ♀ *C. tritaeniorhynchus* | 15%, 15/103<br>14%, 3/22 | 38%, 39/103<br>36%, 8/22 | 47%, 7/15<br>67%, 2/3 | 53%, 8/15<br>33%, 1/3 |
| Dec. 2013 | 106 | 106 ♀ *C. pipiens* | 21%, 22/106 | 23%, 24/106 | 27, 6/22 | 73%, 16/22 |
| Mar. 2014 | 185 | 185 ♀ *C. pipiens* | 3%, 6/185 | 34%, 63/185 | 33%, 2/6 | 67%, 4/6 |
| April 2014 | 92 | 48 ♀ *C. pipiens*<br>44 ♂ *C. pipiens* | 0%, 0/48<br>0%, 0/44 | 17%, 8/48<br>0%, 0/44 | 0%, 0/0<br>0%, 0/0 | 0%, 0/0<br>0%, 0/0 |
| May 2014 | 92 | 52 ♀ *C. pipiens*<br>40 ♂ *C. pipiens* | 4%, 2/52<br>0%, 0/40 | 21%, 11/52<br>0%, 0/40 | 50%, 1/2<br>0%, 0/0 | 50%, 1/2<br>0%, 0/0 |
| June 2014 | 92 | 52 ♀ *C. pipiens*<br>40 ♂ *C. pipiens* | 4%, 2/52<br>5%, 2/40 | 17%, 9/52<br>0%, 0/40 | 50%, 1/2<br>0%, 0/0 | 50%, 1/2<br>100%, 2/2 |
| July 2014 | 92 | 40 ♀ *C. pipiens*<br>52 ♂ *C. pipiens* | 5%, 2/40<br>0%, 0/52 | 10%, 4/40<br>0%, 0/52 | 0%, 0/0<br>0%, 0/0 | 100%, 2/2<br>0%, 0/0 |
| Aug. 2014 | 92 | 52 ♀ *Aedes albopictus*<br>40 ♂ *Aedes albopictus* | 0%, 0/52<br>0%, 0/40 | 27%, 14/52<br>0%, 0/40 | 0%, 0/0<br>0%, 0/0 | 0%, 0/0<br>0%, 0/0 |
| Total | 1304 | 996 *C. pipiens*<br>216 *C. tritaeniorhynchus*<br>92 *Aedes albopictus* | 6%<br>79/1,304 | 31%<br>336/1,088 | 37%, 29/79 | 63%, 50/79 |

* *Rickettsia* positive/negative, blood meal positive/negative.

life-fitness parameter of the stages of many insect species [23], including mosquitoes. The development thermal threshold (23°C) (Figure 1(c), dash line) is the temperature below which immature stages would stop developing [18, 19]. The data in this study indicated that the positivity of *R. felis* (2%, 8/368 vs. 8%, 71/936, $P = 0.002$) and blood meal (10%, 36/368 vs. 31%, 294/936, $P < 10^{-4}$) in these four months above 23°C was significantly lower than those months below 23°C (Figure 1). Mosquitoes captured in the months without the possibility of mosquito egg hatching had significantly higher prevalence of *R. felis* than those in the months with constant egg hatching. This difference may add to the evidence suggesting the transstadial and transovarial transmission of *R. felis* in mosquitoes. In order to unambiguously prove the transstadial and transovarial transmission of this organism in mosquitoes, further studies with a *R. felis* infection model covering each life stage of mosquitoes is necessary.

## 4. Conclusions

In conclusion, the seasonal and gender differences of *R. felis* and blood meal in mosquitoes suggest the possible transstadial and transovarial transmission of *R. felis* in mosquitoes. Studies with the *R. felis* infection model within the full life cycle of mosquito are necessary to unambiguously prove the potential vector role of mosquitoes in transmission of this organism.

## Data Availability

The data used to support the findings of this study are included within the article.

## Conflicts of Interest

The authors declare that they have no conflicts of interest.

## Acknowledgments

This project was supported by grant from the National Natural Science Foundation of China (no. 31472225) and the Priority Academic Program Development of Jiangsu Higher Education Institutions, Yangzhou, Jiangsu Province, China.

## References

[1] C. E. Pérez-Osorio, J. E. Zavala-Velázquez, J. J. A. León, and J. E. Zavala-Castro, "*Rickettsia felis* as emergent global threat for humans," *Emerging Infectious Diseases*, vol. 14, no. 7, pp. 1019–1023, 2008.

[2] S. K. Sahni, H. P. Narra, A. Sahni, and D. H. Walker, "Recent molecular insights into rickettsial pathogenesis and immunity," *Future Microbiology*, vol. 8, no. 10, pp. 1265–1288, 2013.

[3] C. Socolovschi, F. Pagés, and D. Raoult, "*Rickettsia felis* in *Aedes albopictus* mosquitoes, Libreville, Gabon," *Emerging Infectious Diseases*, vol. 18, no. 10, pp. 1687–1689, 2012.

[4] J. Zhang, P. John Kelly, G. Lu, L. Cruz-Martinez, and C. Wang, "Rickettsia in mosquitoes, Yangzhou, China," *Emerging Microbes & Infections*, vol. 5, no. 10, pp. 1–7, 2016.

[5] J. Zhang, G. Lu, P. Kelly et al., "First report of *Rickettsia felis* in China," *BMC Infectious Diseases*, vol. 14, no. 1, p. 682, 2014.

[6] E. Angelakis, O. Mediannikov, P. Parola, and D. Raoult, "*Rickettsia felis*: the complex journey of an emergent human pathogen," *Trends in Parasitology*, vol. 32, no. 7, pp. 554–564, 2016.

[7] C. Dieme, Y. Bechah, C. Socolovschi et al., "Transmission potential of *Rickettsia felis* infection by *Anopheles gambiae*

mosquitoes," *Proceedings of the National Academy of Sciences*, vol. 112, no. 26, pp. 8088–8093, 2015.

[8] W.-P. Guo, J.-H. Tian, X.-D Lin et al., "Extensive genetic diversity of Rickettsiales bacteria in multiple mosquito species," *Scientific Reports*, vol. 6, no. 1, article 38770, 2016.

[9] P. Parola, O. Mediannikov, C. Dieme, and D. Raoult, "Reply to Slesak et al.: so much about *Rickettsia felis* infection to be discovered," *Proceedings of the National Academy of Sciences*, vol. 112, no. 48, pp. E6595–E6596, 2015.

[10] P. Parola, D. Musso, and D. Raoult, "*Rickettsia felis*: the next mosquito-borne outbreak?," *The Lancet Infectious Diseases*, vol. 16, no. 10, pp. 1112-1113, 2016.

[11] J. Fang, "Ecology: a world without mosquitoes," *Nature*, vol. 466, no. 7305, pp. 432–434, 2010.

[12] Y. Zhu, R. Zhang, B. Zhang et al., "Blood meal acquisition enhances arbovirus replication in mosquitoes through activation of the GABAergic system," *Nature Communications*, vol. 8, no. 1, p. 1262, 2017.

[13] L. Wei, P. Kelly, J. Zhang et al., "Use of a universal hydroxymethylbilane synthase (HMBS)-based PCR as an endogenous internal control and to enable typing of mammalian DNAs," *Applied Microbiology and Biotechnology*, vol. 98, no. 12, pp. 5579–5587, 2014.

[14] O. Folmer, M. Black, W. Hoeh, R. Lutz, and R. Vrijenhoek, "DNA primers for amplification of mitochondrial cytochrome c oxidase subunit I from diverse metazoan invertebrates," *Molecular Marine Biology and Biotechnology*, vol. 3, no. 5, pp. 294–299, 1994.

[15] Mosquito taxonomic inventory, http://mosquito-taxonomic-inventory.info/.

[16] G. Wang, C. Li, X. Guo et al., "Identifying the main mosquito species in China based on DNA barcoding," *PloS One*, vol. 7, no. 10, Article ID e47051, 2012.

[17] P. D. N. Hebert, A. Cywinska, S. L. Ball, and J. R. DeWaard, "Biological identifications through DNA barcodes," *Proceedings of the Royal Society of London. Series B: Biological Sciences*, vol. 270, no. 1512, pp. 313–321, 2003.

[18] C. Christiansen-Jucht, P. E. Parham, A. Saddler, J. C. Koella, and M.-G. Basáñez, "Temperature during larval development and adult maintenance influences the survival of *Anopheles gambiae* s.s," *Parasites & Vectors*, vol. 7, no. 1, p. 489, 2014.

[19] M. G. Grech, P. D. Sartor, W. R. Almirón, and F. F. Ludueña-Almeida, "Effect of temperature on life history traits during immature development of *Aedes aegypti* and *Culex quinquefasciatus* (*Diptera: Culicidae*) from Córdoba city, Argentina," *Acta tropica*, vol. 146, pp. 1–6, 2015.

[20] H. L. Zhang, Y. Z. Zhang, W. H. Yang et al., "Mosquitoes of Western Yunnan Province, China: seasonal abundance, diversity, and arbovirus associations," *PloS One*, vol. 8, no. 10, Article ID e77017, 2013.

[21] E. B. Vinogradova, *Culex Pipiens Pipiens Mosquitoes: Taxonomy, Distribution, Ecology, Physiology, Genetics, Applied Importance and Control*, Pensoft Publishers, Sofia, Bulgaria, 2000.

[22] B. T. Jackson and S. L. Paulson, "Seasonal abundance of culex restuans and culex pipiens in Southwestern Virginia through ovitrapping," *Journal of the American Mosquito Control Association*, vol. 22, no. 2, pp. 206–212, 2006.

[23] M. J. Kirby and S. W. Lindsay, "Effect of temperature and inter-specific competition on the development and survival of *Anopheles gambiae* sensu stricto and An. arabiensis larvae," *Acta Tropica*, vol. 109, no. 2, pp. 118–123, 2009.